PDMS SlipChip for Evaluation of Effective Drug Concentrations in Cancer Cells

（がん細胞での有効薬物濃度評価のための PDMS SlipChip の開発）

July, 2025

Doctor of Philosophy (Engineering)

Rafia Inaam

ラフィア イナム

Toyohashi University of Technology

Acknowledgements

I would like to express my heartfelt gratitude to the individuals and institutions whose invaluable support has guided me throughout my research journey.

First and foremost, I am deeply thankful to Professor Moeto Nagai for accepting me as his student and for his exceptional mentorship. This thesis would not have been possible without his continuous guidance and support. He is not only an outstanding researcher but also a remarkable human being, and I consider myself truly fortunate to have worked under his supervision.

I would also like to extend my sincere thanks to the members of my thesis committee, Professor Takayuki Shibata and Professor Tadaharu Adachi, for their insightful comments and constructive feedback during my graduation defense.

My heartfelt appreciation goes to my project advisors—Professor Moeto Nagai, Prof. Marcela Bolontrade, and Ms. Miyuki Okuda—as well as to all my current and former lab mates. Their assistance with experiments and the memorable experiences we shared have been invaluable to my time here. I would like to thank my colleagues, Dr. Shalini Nagabhooshanam, Mr. Aniket Mishra, and Mr. Pulasta Chakrabhorty, for their continued support and help.

I am grateful to Toyohashi University of Technology for providing me with the opportunity to pursue my research, and to the Amano Institution and other funding organizations for their generous financial support.

Lastly, I wish to thank my parents, Inaam ul Haq (late) and Rubina Inaam, along with my siblings and friends, for their unwavering emotional support throughout my research journey in Japan.

別紙４－１（課程博士（英文））

Date of Submission（month day, year）: July 10, 2025

Department of Mechanical Engineering	Student ID Number	D229102	Supervisors	Moeto Nagai Takayuki Shibata
Applicant's name	Rafia Inaam			

Abstract（Doctor）

Title of Thesis	PDMS SlipChip for Evaluation of Effective Drug Concentrations in Cancer Cells

Approx. 800 words

Osteosarcoma (OS) is the most common primary bone cancer, predominantly affecting children and young adults, with treatment efficacy often hampered by chemoresistance linked to the tumor microenvironment (TME) and the overexpression of multidrug resistance (MDR) transporters such as P-glycoprotein (P-gp). Hypoxia, a hallmark of the TME, further intensifies drug resistance, making the determination of minimum effective drug concentration (MEC) essential for advancing personalized cancer therapy. This study presents the development and optimization of a polydimethylsiloxane (PDMS)-based SlipChip microfluidic platform designed for high-throughput evaluation of drug efficacy in osteosarcoma cells. The SlipChip enables rapid and reproducible generation of concentration gradients at nanoliter scales, facilitating real-time assessment of drug responses under tumor microenvironment conditions.

Initially, the biocompatibility of the PDMS material was validated through the culture of SAOS-2 osteosarcoma cells under both normoxic and hypoxic conditions. The porous nature of PDMS facilitated efficient oxygen exchange, enabling accurate simulation of hypoxic TME. Cell viability, morphology, and proliferation were comparable to those observed in conventional tissue culture

platforms, with hypoxic conditions in the PDMS chips resulting in reduced proliferation and smaller cell size, consistent with physiological tumor behavior.

Technical advancements in device fabrication included the use of photolithography and soft lithography to produce PDMS SlipChips, with systematic modulation of curing temperatures to optimize surface energy and interlayer adhesion. The study found that lower curing temperatures increased surface energy, thereby enhancing adhesion and sealing, while higher temperatures resulted in stiffer, less adhesive PDMS. Lubrication with silicone oil, particularly 50 cSt at high spin speeds, was optimized to ensure reliable sealing and smooth slipping between layers. A custom 3D-printed stage with magnetic sealing and micro-gauges was developed to guarantee precise alignment, leak-free operation, and consistent microwell overlap. The design also addressed bubble formation by optimizing the width ratio (WR) of microwells to microchannels, with WR=5 achieving the lowest bubble coverage and most effective gradient formation.

Functional validation of the platform was demonstrated through gradient generation using Rhodamine 6G and green food dye, with fluorescence intensity measurements confirming the accuracy and reproducibility of concentration gradients.

The optimized SlipChip platform exhibited robust sealing, eliminated leakage and bubble-related inconsistencies, and supported healthy 3D cell culture. It enabled the study of ascorbic acid effects on osteosarcoma cell growth, with both SlipChip and traditional culture dishes showing similar cell death responses to the stimulus. These results confirm the platform's suitability for biological assays and its potential for high-throughput drug screening.

In conclusion, the PDMS SlipChip microfluidic platform developed in this research offers a reliable, high-throughput solution for evaluating drug efficacy in osteosarcoma cells. Innovations in fabrication, sealing, lubrication, and alignment have addressed key challenges in microfluidic gradient generation and cell-based assays. The platform successfully supports healthy cell culture and enables precise, reproducible drug screening, paving the way for personalized cancer therapy by facilitating rapid determination of MEC and real-time assessment of chemoresistance mechanisms. Future work will focus on applying the optimized SlipChip system for doxorubicin testing and further refining device performance for broader clinical applications.

Table of Contents

List of Figures

Chapter 1 Introduction

1.1 Cancer

Cancer remains one of the leading causes of death worldwide, posing a significant public health challenge across nations and age groups. According to statistics from the World Health Organization, cancer affects approximately 20 million people globally each year and is responsible for an estimated 9.7 million deaths annually, underscoring its profound impact on human health and society [1]. Among the various types of cancer, bone cancer stands out as a particularly aggressive and life-threatening malignancy that originates in the bones [2,3].

Bone cancer most commonly originates in the long bones, such as the femur, tibia, and humerus (Figure 1). What makes it especially dangerous is its tendency to develop drug resistance and its ability to spread to other organs, most frequently the lungs [3–5].

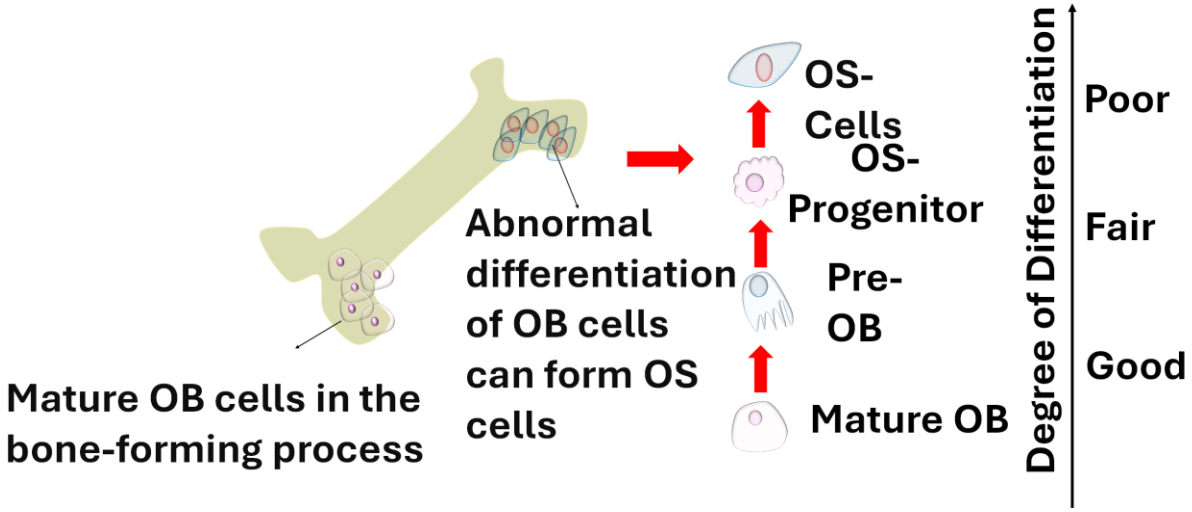

Figure 1 An abnormal degree of differentiation causes the development of osteosarcoma in the bone.

Bone cancer thrives in an oxygen-depleted environment, due to which certain proteins overexpress themselves, making the bone cancer tumor drug resistant. As a result of this, a very low concentration of drug molecules will not be allowed to enter the cells by being repelled by those overexpressed proteins (Figure 2(b)). If a very high concentration of drugs is made to enter the cells, it will not only kill cancer cells but will also damage healthy cells (Figure 2(a)). Hence, a minimum effective concentration of the drug is crucial to treat this cancer type.

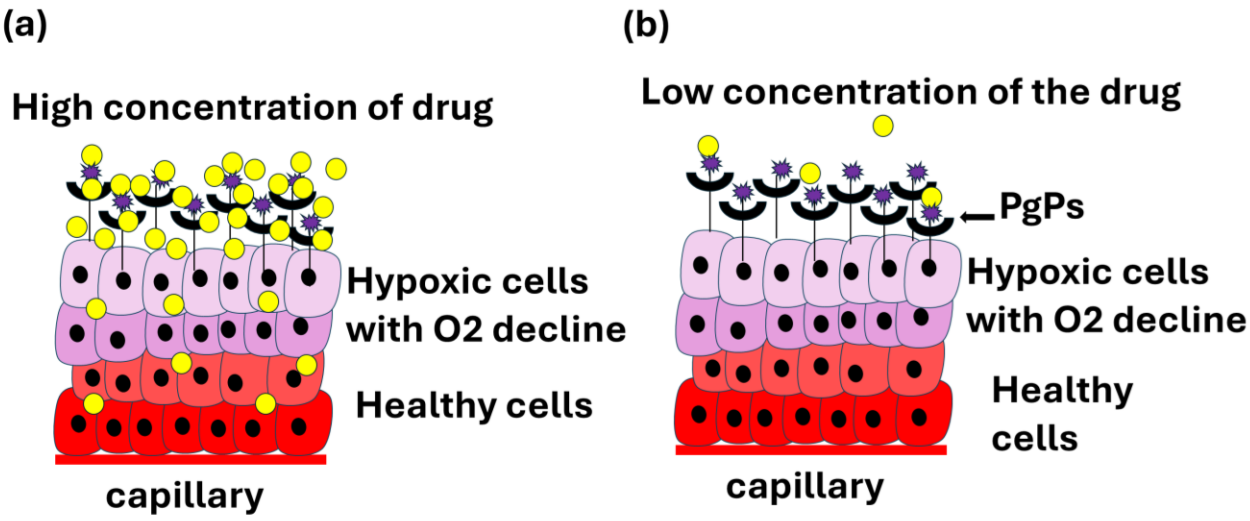

Figure 2 Drug resistance phenomenon in bone cancer cells (a), High concentration drug damages both cancer and healthy cells (b) Low concentration drug being pushed away by PgPs protein.

It primarily affects children, adolescents, and young adults, although it can occur at any age [2,4]. The overall incidence of osteosarcoma in the general population is relatively rare, estimated at 2 to 3 cases per million people per year. However, the incidence rises significantly among teenagers, reaching 8 to 11 cases per million annually in individuals aged 15 to 19 years. This age group is particularly vulnerable, likely due to the rapid bone growth that occurs during adolescence. Osteosarcoma accounts for approximately 3–6% of all childhood cancers and about 15% of childhood extra-cranial solid tumors, making it one of the most common bone cancers in the pediatric population [6,7]. In adults, osteosarcoma represents about 1% of all cancers, but its clinical presentation and prognosis can differ from those seen in younger patients.

Given its aggressive nature, high mortality rate, and the lack of a clear understanding regarding its origins, osteosarcoma remains a significant focus of medical research. The urgent need to uncover the underlying causes and develop more effective treatments for this malignancy drives ongoing studies in genetics, molecular biology, and innovative therapeutic approaches. Advancements in early detection, targeted therapies, and supportive care are crucial for improving survival rates and quality of life for patients affected by this challenging disease.

1.2 Personalized Drug Therapy and Microfluidics

Modern osteosarcoma treatment requires systematic evaluation across multiple therapeutic classes: traditional chemotherapeutics (doxorubicin ~580 Da, methotrexate ~454 Da), targeted small molecules (sorafenib ~465 Da), and emerging biologics including monoclonal antibodies (~150 kDa) and peptide-drug conjugates. Current screening platforms lack the technical versatility to handle this molecular diversity while maintaining physiologically relevant tumor conditions, creating a critical bottleneck in personalized therapy development. Precision medicine holds significant importance in the field of chemotherapy, as it enables clinicians to deliver the optimal drug dosage tailored to the specific characteristics of each cancer type [8]. This personalized approach not only enhances the effectiveness of treatment but also reduces the risk of adverse side effects, ultimately improving patient outcomes [9,10]. In recent years, microfluidics has emerged as a promising and versatile platform supporting the advancement of precision medicine and pharmaceutical analysis, particularly in drug discovery and the detection of various diseases and health conditions [11].

The microscale fluid dynamics characteristic allows for highly controlled manipulation of fluids within microchannels, facilitating sensitive and reproducible experiments with minimal sample volumes [12]. Such precision is especially valuable in the context of cancer diagnostics and its drug development, where even small variations in drug concentration can have a significant impact on therapeutic outcomes [13].

Microfluidic devices are commonly fabricated from polydimethylsiloxane (PDMS), a material favored for its biocompatibility, optical transparency, and ease of patterning [14]. These devices are widely employed as electrochemical sensors, colorimetric sensors, and magnetic sensors, enabling the detection of diseases through the identification of specific proteins or biomarkers[15] This versatility also contributes to making medical diagnostic methods more robust and reliable. Microfluidic devices can be broadly categorized into two types: active and passive systems. Active microfluidic devices utilize external energy sources or actuators, such as acoustic, centrifugal, electric, or magnetic fields, to manipulate fluids and particles within the device. For example, electrokinetic pumps are often used to achieve precise control over fluid movement in active systems [16]. However, these devices generally require more complex microfabrication techniques and additional instrumentation, which can increase both the cost and technical complexity of their operation.

On the other hand, passive microfluidic devices operate without the need for external energy sources. Instead, they rely on inherent fluid properties and channel geometry to drive fluid movement, utilizing mechanisms such as diffusive mixing, capillary forces, surface tension, and gravity-driven flows [17]. The fabrication of passive devices is typically simpler and more cost-effective compared to active devices, making them particularly attractive for applications in resource-limited settings or for high-throughput screening.

Numerous researchers have explored both active and passive microfluidic devices for a wide range of biological and medical assessments [18]. For instance, Natsuhara et al. developed a centrifugal-type microfluidic device that functions as a colorimetric sensor for the quantitative analysis of specific nucleic acid targets [19]. Similarly, M. Senel *et al.*, utilized a PDMS-based microfluidic device as an electrochemical sensor for the detection of dopamine, demonstrating the application of microfluidics in neurochemical sensing [20].

In summary, microfluidic devices—whether active or passive—are playing a pivotal role in advancing precision medicine. Their ability to perform highly sensitive, multiplexed biochemical analyses with minimal sample consumption is transforming the landscape of cancer therapy, pharmaceutical research, and disease diagnostics.

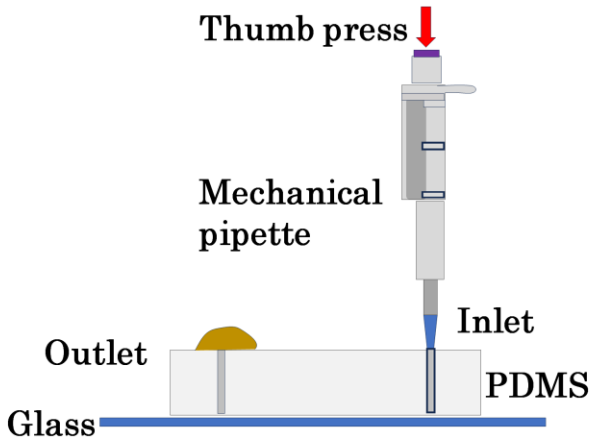

Figure 3 Schematics of the microfluidic SlipChip.

1.3 SlipChips and Their Role in Precision Drug Therapy

SlipChips represent a highly innovative and unconventional class of microfluidic devices that have revolutionized the way researchers perform multiplexed, high-throughput biochemical analyses [21]. Unlike traditional microfluidic systems that rely on continuous channels or external

pumps, SlipChips are ingeniously designed with two separate layers—a top and a bottom plate—each intricately patterned with maze-like arrays of microwells and disconnected microchannels. This unique architecture enables the creation of multiple isolated chambers within a single device, allowing for the simultaneous analysis of numerous samples while consuming only micro- or nano-scale volumes [21,22].One of the defining features of SlipChips is their classification as passive microfluidic devices. Rather than depending on external energy sources, pumps, or actuators, SlipChips operate based on the principle of diffusive mixing. The two layers are aligned so that their patterned surfaces face each other, but they are not permanently bonded. Instead, a non-permanent seal—often facilitated by a thin layer of lubricant—is used between the layers. This lubricant serves a dual purpose: it enables smooth slipping motion between the layers and also acts as a sealant to prevent leakage or cross-contamination between adjacent chambers [21].

The operation of a SlipChip is remarkably simple, typically consisting of three main steps. First, the top layer is carefully oriented and placed over the bottom layer, with both layers' microwells and microchannels aligned to create open pathways. This alignment allows for the easy loading of fluids into the device. Next, the top layer is slipped or slid relative to the bottom layer in a controlled manner. This slipping action disconnects the continuous pathways, causing the microwells of the two layers to overlap and form a series of isolated compartments. Finally, within these isolated chambers, diffusive mixing occurs between the fluids originally loaded into the microwells of each layer. This process enables multiple, independent reactions or analyses to take place simultaneously, all within a single, compact device [21–23].

The role of SlipChip in precision drug therapy can be attributed to its ability to easily manipulate the fluidic concentrations by diffusive mixing in isolated microenvironments and the development of various concentrations of fluids in multiple microwells, making it an invaluable tool for a variety of scientific applications, such as drug discovery. For instance, researchers have utilized SlipChips to determine the minimum effective concentration of antibiotics required to control bacterial infections, thereby supporting the development of more targeted and effective antimicrobial therapies [24]. The device's high throughput and minimal sample requirements also make it ideal for screening chemical compositions or performing combinatorial assays. Additionally, SlipChips have been successfully adapted for molecular biology applications, such as performing polymerase chain reaction (PCR) tests, which are essential for DNA amplification and genetic analysis [25]. In summary, PDMS SlipChips offer a versatile, user-friendly, and highly

efficient platform for conducting multiplexed biochemical analyses at the micro- and nanoscale. Their reliance on diffusive mixing, and development of gradient concentrations due to an innovative slip-based mechanism set them apart from conventional microfluidic devices. As a result, SlipChips continue to gain popularity among researchers seeking robust, high-throughput solutions for diagnostics, drug discovery, and molecular biology.

Glass SlipChips are commonly used due to their chemical resistance and precise fabrication. However, their complex manufacturing process and lack of gas permeability make them unsuitable for applications such as cell culture, where gas exchange is critical. Glass-based SlipChips have been widely used to determine effective antibiotic concentrations for bacteria such as *E. coli*; however, their limited gas permeability hinders their suitability for mammalian cell culture applications. In contrast, polydimethylsiloxane (PDMS) SlipChips present a more cost-effective, easily fabricated alternative with superior biocompatibility.

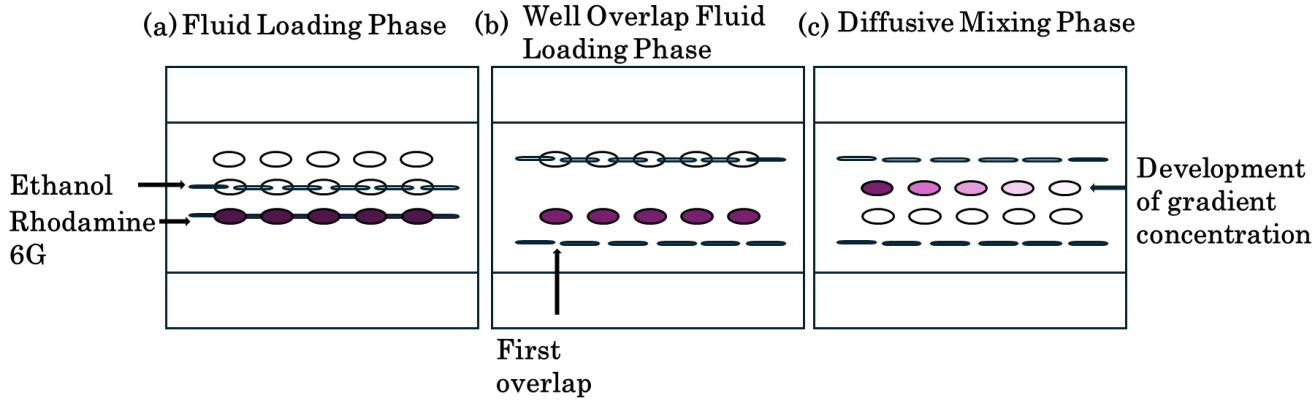

Figure 4 SlipChip functions. (a) Fluid loading phase. (b) 1st overlap of microwells. (c) 2nd overlap of microwells.

1.4 Research Objectives and Thesis Structure

1.4.1 Research Objective

Current osteosarcoma drug screening faces a critical limitation—no integrated system exists that can simultaneously reproduce the complex tumor microenvironment (including hypoxia and drug resistance mechanisms) AND systematically evaluate therapeutic efficacy across multiple drug modalities for minimum effective concentration (MEC) determination. Traditional 2D cultures fail to replicate physiologically relevant conditions, while existing microfluidic platforms cannot generate the precise concentration gradients necessary for personalized therapy

development across the molecular weight spectrum from small molecules (~500 Da) to large biologics (~150 kDa). Our goal is to develop a PDMS based leak and bubble free SlipChip to be used for therapeutic applications in determining the minimum effective concentration of drugs for bone cancer cells using SAOS-2 cell line[24] [26].

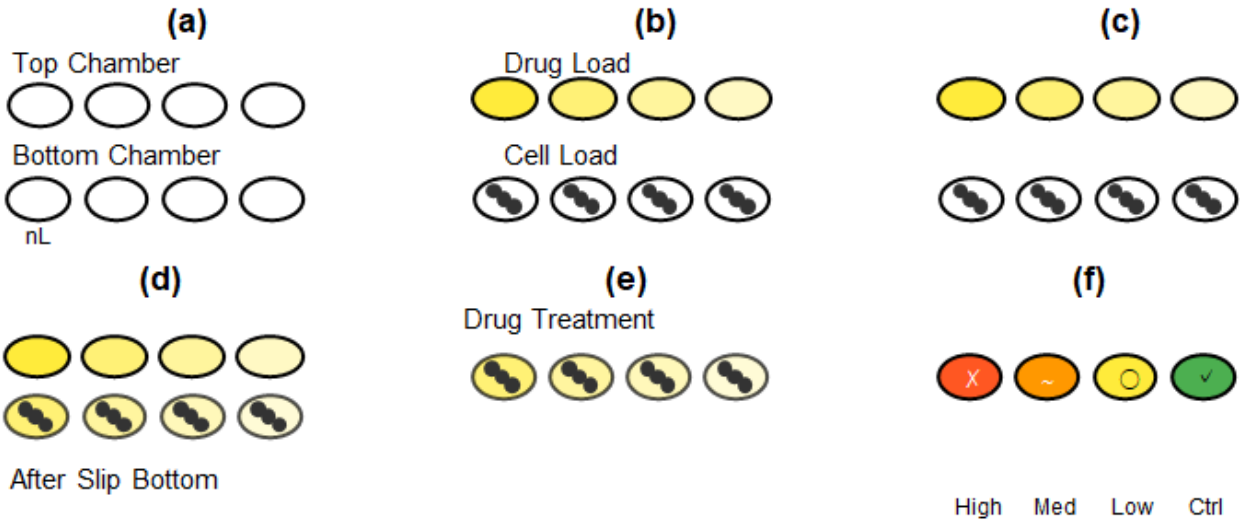

Figure 5 Osteosarcoma SlipChip drug screening system. Minimum effective concentration (MEC) determination using SlipChip.

Below is the brief introduction of each chapter and table 1 presents the brief analysis of thesis structure.

Chapter 1 highlights the urgency of studying osteosarcoma due to its aggressive nature, while introducing the SlipChip—an innovative BioMEMS device that enables high-throughput, micro-to-nanoscale analyses through a simple, two-layer slipping mechanism. It also outlines our goal to develop a PDMS-based, leak- and bubble-free SlipChip for efficient osteosarcoma drug testing.

Chapter 2 explores the development of a PDMS-based system to replicate hypoxic and normoxic tumor microenvironments for osteosarcoma research. It details the design and fabrication of the PDMS chip using CAD, photolithography, and soft lithography, along with the SAOS-2 cell culture techniques used. A novel method involving portable hypoxic bags was applied to create controlled environments, and experimental results compared these with standard petri dish cultures. Findings show that PDMS chips effectively generate hypoxic conditions, supporting cell growth and morphology comparable to traditional methods.

Chapter 3 optimizes PDMS SlipChip sealing and slipping by tuning curing temperatures and using low-viscosity silicone oils (50–100 cSt); adhesion and stiffness are quantified via contact angle, leakage, pneumatic and tensile tests; biocompatibility is confirmed; Rhodamine 6G validates reproducible gradient formation.

Chapter 4 introduces a magnetic aligner for precise x–y slipping, implements an oil-absorption lubrication method, and optimizes the width ratio (WR) to suppress bubbles, achieving leak- and bubble-free gradient formation with WR=5.

Chapter 5 demonstrates PDMS-based leak and bubble-free SlipChip-based 3D culture and evaluates ascorbic acid effects on osteosarcoma cells; cytotoxic responses are observed; gradient capability is not utilized here, serving as biological validation of the platform.

Chapter 6 presents conclusions and future work, outlining MEC studies (e.g., doxorubicin) under hypoxia with the leak- and bubble-free SlipChip (WR=5, 50 cSt, magnetic alignment).

Table 1. Brief analysis of thesis structure.

Chapter	Technical Achievement	Gradient Function Used?	Cell Culture Applied?	Integration Level	Critical Gap
Chapter 2	Hypoxic microenvironment	❌ No	✅ SAOS-2 (binary only)	Basic	No SlipChip, no gradient
Chapter 3	Separate demonstrations	✅ Rhodamine 6G only	✅ SAOS-2 only	Parallel but NOT integrated	No gradient + cells together
Chapter 4	Perfect gradient formation	✅ Optimized	❌ No cells	Technical perfection	No biological validation
Chapter 5	3D cell culture + AsA	❌ Not utilized	✅ SAOS-2 + AsA (binary only)	Single application	No gradient capability used
Chapter 6	Thesis Conclusion				

Chapter 2 Hypoxic Culture of Osteosarcoma Cells in PDMS Microfluidic Chamber and Plastic Bag

2.1 Introduction

The efficacy of anticancer therapies depends significantly on the ability of chemotherapeutic drugs to penetrate tumor cells. However, a major limitation to therapeutic success is the development of chemoresistance, wherein cancer cells become less responsive or unresponsive to drugs. One of the critical factors contributing to chemoresistance and tumor progression is hypoxia, a physiological condition characterized by oxygen deprivation. Hypoxia is commonly observed in solid tumors due to their rapid growth and inadequate vascularization, which limits oxygen diffusion to inner tumor regions. This oxygen-deprived environment not only drives malignant transformation and progression but also alters cellular behavior, enhancing resistance to chemotherapy and promoting metastasis [27].

Understanding the influence of hypoxia on cancer cell biology and drug response requires experimental models that can reliably replicate the tumor microenvironment. Traditional in vitro systems often fail to create physiologically relevant oxygen gradients and lack precision in maintaining hypoxic conditions. Additionally, techniques such as hypoxia chambers and oxygen-controlled incubators are often cost-intensive, laborious, and inefficient for routine or high-throughput use. Thus, there is a growing demand for user-friendly, reproducible, and cost-effective platforms that can simulate hypoxic tumor microenvironments with greater control and minimal manual intervention.

This study addresses this challenge by developing a microfluidic-based platform using polydimethylsiloxane (PDMS) chips in conjunction with a hypoxic plastic bag system. The PDMS-based microfluidic chip offers precise control over the microenvironment, while the plastic bag—containing an oxygen scavenger—enables the creation of a stable hypoxic condition in a closed system. To evaluate the effectiveness of this approach, osteosarcoma (SAOS-2) cells were cultured under both normoxic (normal oxygen) and hypoxic conditions using two configurations: the PDMS microfluidic chip and conventional glass-bottom culture dishes.

Quantitative assessments of cell health, morphology, and density were conducted to compare cellular responses under different conditions. The results demonstrated that SAOS-2 cells cultured under hypoxic conditions in the PDMS chip exhibited a markedly reduced average cell length of 18.6 μm, compared to approximately 80 μm in all other conditions. Additionally, cell density in the hypoxic PDMS chip was the lowest, with 30 cells/mm², indicating a significant influence of the hypoxic microenvironment on cell proliferation and morphology. These observations suggest that the PDMS chip, when used with the hypoxic bag system, successfully mimics the in vivo tumor microenvironment more accurately than traditional open-culture methods.

The findings validate the PDMS microfluidic platform as an effective tool for hypoxic cell culture, offering several advantages such as reduced sample volume, improved environmental control, and compatibility with high-throughput screening. Importantly, this study serves as a proof of concept for the integration of microfluidic technology with a simple hypoxia-inducing system, demonstrating its potential for broader applications in cancer research. By enabling the investigation of tumor growth, hypoxia-induced drug resistance, and metastatic behavior in a controlled setting, this platform represents a significant step forward in developing more physiologically relevant in vitro cancer models.

Cancer is a leading cause of death worldwide. Approximately 10 million people die from cancer every year [27]. Among various types of cancer, osteosarcoma is one of the malignant types of bone cancer. It occurs in both adults and adolescents. Its study is important because it has a high metastatic potential and a strong recurrence tendency even after extreme therapeutic treatments applied [28]. Since the 1970s, the 5-year survival rate for patients with metastatic OS disease has not shown significant improvement, remaining in the range of 15-30%. The emergence of micro metastases poses a significant challenge given their elusiveness to conventional methods and difficult clinical management, and the identification of mechanisms and differentially expressed genes associated with metastasis holds promise for the discovery of markers and targets for therapeutic intervention in OS metastasis.

We are working on the conditions that lead to metastasis development in osteosarcoma [28,29]. We aim to use microdevices to recreate the tumor microenvironment in our model, with the advantages of reproducing a controlled microenvironment, reducing sample and reagent volumes, and acquiring high-throughput screening. Hypoxia is a state of oxygen depletion or starvation and

is associated with tumor growth and resistance to therapeutic drugs. The state of oxygen depletion can be seen in Fig. 6 (a), where red cells above the capillary represent healthy cells, while cells further away from the capillary represent oxygen-depleted cells. A tumor grows blood vessels to meet its oxygen needs, a process called angiogenesis. The hypoxic environment of a tumor creates a state of emergency that initiates and/or enhances responses such as altered gene expression, suppression of apoptosis, chemoresistance, malignant progression, and distant tumor metastasis [27,30,31]. In vitro studies designed to mimic the in vivo environment have inherent limitations related to large sample consumption and the formation of macro-environments. The development of a cell culture platform that provides an in vitro environment that mimics physiological conditions is essential for the analysis of cellular responses.

Hypoxic conditions have been studied in microfluidic devices using hypoxic chambers [32], chemical methods [33], and oxygen-controlled incubators [34]. Hypoxic chambers are not capable of reproducing oxygen gradients as in the physiological situation [32]. The use of hypoxia incubators is rarely used because it require excessive consumption of nitrogen gas. This approach requires frequent replacement of nitrogen cylinders, which is not a budget-friendly approach. Chemical hypoxia depends on the use of different chemicals and not all chemicals are suitable for inducing hypoxia in certain cell types [27]. Identifying the right chemical for a particular cell type is time-consuming and expensive. There is a demand for a hypoxic system that is inexpensive, user-friendly, and helps replicate a near-physiological hypoxic tumor microenvironment condition. In contrast to the techniques, the use of hypoxic bags are a simpler approach to recreate hypoxic conditions. Hypoxic bag was used to develop variable oxygen tension throughout the device [34]. Combining the use of a bag with a microfluidic device would help replicate the tumor microenvironment like the physiological one [35]. However, microfluidic devices are prone to bubble formation. This bubble formation is hazardous for cell viability because it is related to high interfacial forces resulting in high shear stresses. These high shear stresses can rupture the cell membrane and damage the cells, or the bubble itself can impede the transfer of nutrients to the cells [36–38].

This chapter focused on the development of a suitable PDMS (Polydimethylsiloxane) platform to analyze tumor microenvironment conditions close to physiological phenomena with a hypoxic bag. Normoxic and hypoxic cultures of osteosarcoma cells were studied in a closed environment and an open chamber. The proposed device is inexpensive, user-friendly, and helps

to replicate near-physiological tumor microenvironment condition. An enclosed environment was developed using a microfluidic device and an open chamber was obtained using a glass-bottom (GB) culture dish. Oxygen removal was performed by using an oxygen scavenger contained in the hypoxic bag. The use of a PDMS microfluidic-based cell culture platform resulted in the creation of efficient hypoxic conditions.

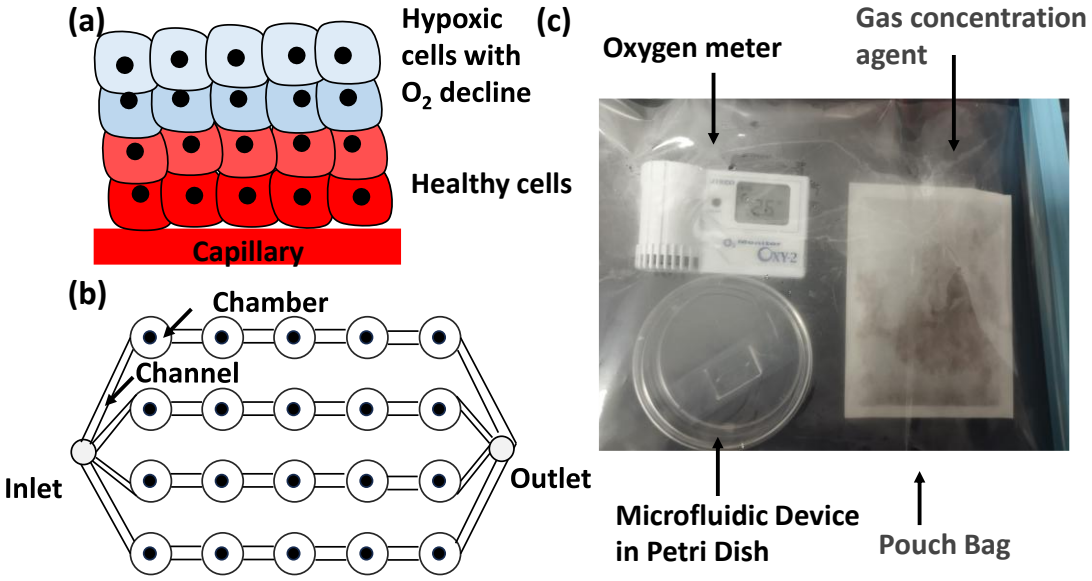

Figure 6 The experimental environment in this study. (a) Comparison of hypoxia and normoxia cells. (b) Microfluidic device. (c) Microfluidic device with oxygen scavenging system.

2.2 Methods

This section describes design and fabrication techniques and experimental approaches.

2.2.1 PDMS Microfluidic Chip

Smaller volumes with a high surface area ratio are more efficient in oxygen exchange as compared to large volumes. A microfluidic device would help to achieve a more efficient oxygen balance with this system as compared to the glass bottom (GB) culture dish [39]. As shown in Fig. 6(b) a microfluidic device was designed to have a continuous structure with microwells and cylindrical obstacles of different sizes. The white part in the image represents the channel whereas the gray part represents obstruction and surrounding areas. The outer diameter of each microwell was 2.0 mm with the variation of obstacle size from 0.5mm to 0.2mm, having an increment step size of 0.1mm. The device is designed to produce different concentrations of drugs, and obstacles of different sizes will be used for this purpose. Each had five wells with obstacles of the same size

throughout the row. This design is capable of exposing cells in culture to different concentrations of drugs in the future.

A negative photoresist, SU-8 3050 mold, with a height of 100 μm was fabricated on a silicon wafer by standard photolithography. The SU-8 was developed and silanized according to the method described in [40]. This was done because the patterned silicon wafer has a strong affinity for PDMS material. The affinity is strong enough to make it impossible for the PDMS to peel from the mold. Therefore, depositing a layer of silane over the mold surface prevents reaction between PDMS and silane, resulting in easy peeling of PDMS after curing. The mold was replicated in PDMS (Silpot 184) using soft lithography techniques at a ratio of PDMS base polymer to curing agent (10:1). We refer to PDMS chips that were assembled by permanent plasma treatment and bonding of the PDMS structure to a glass slide to obtain sealed PDMS microwells with a depth of 100 μm. Soft lithography and plasma bonding were performed according to the method described in [40,41].

2.2.2 Bubble Removal from PDMS chip

PDMS chips with multiple microwells and different sizes of obstacles were used for cell culture. Structures such as microwells with sharp edges are prone to bubble formation, hence, we had a large number of bubbles in our device. To eliminate bubbles in the microfluidic device, it was rinsed several times with a 70% ethanol solution until the PDMS channels were free of bubbles, as described in [42]. After this treatment, it was rinsed with a regular medium to prevent ethanol-induced cell damage. After this protocol, the cell suspensions could be flushed into the devices with a diminished probability of bubble formation.

2.2.3 Cell Culture in PDMS Chips and GB Dishes

The human Osteosarcoma (OS) cell line SAOS2 was obtained from Tohoku University, Sendai, Japan. Cells were cultured in Dulbecco's Modified Eagle Medium (DMEM) supplemented with 100 U/mL penicillin, 100 μg/mL streptomycin (Gibco, Thermo Fisher Scientist Co. Ltd), and 10% fetal bovine serum (FBS, COSMO BIO), at 37 °C and 5% CO_2. 15 μL of resuspended OS

cells (100 cells/μL culture medium) were introduced to the microfluidic chips. The initial cell density for all four devices was 100 cells/μL. The final volume introduced in each one of the microfluidic chips was 8.2 μL.

For comparison, cells were also cultured in non-coated GB culture dishes (35 mm, product code: D11140H, MATSUNAMI Co. Ltd.). These dishes were chosen to maintain the configuration of the conventional tissue culture approach and to observe the cells clearly. 100 μL of the resuspended cell solution was added to the dishes. All solutions were added by pipetting. The volume in each of the GB tissue culture dishes was 800 μL.

PDMS chips and GB dishes containing suspended cells were then incubated overnight, to allow the cells to adhere to the surface. One of the chips and one of the GB dishes were then placed in a hypoxia bag. An oxygen scavenger container was introduced in the bag until oxygen concentration was reduced to 1.4% [43] (Fig. 6c). The oxygen concentration was determined with an oxygen meter. When the hypoxic conditions were reached, the bag was sealed and returned into the incubator. The conditions of the incubator was set at 37°C with 5% CO_2 and air, and they were considered normoxic. The cultured cells contained in the hypoxic sealed bags were maintained at 37°C with 1.4% to 2.5% O_2. These were considered as hypoxic conditions. GB culture dish under normoxic conditions was used as a control.

2.2.4 Observation and Evaluation

To assess the effects of hypoxia on osteosarcoma cell viability and morphology, both qualitative and quantitative analyses were performed using fluorescence microscopy. As illustrated in Figure 7, the occurrence and subsequent removal of bubbles in the microwells, as well as morphological changes in cells before and after exposure to hypoxic conditions, were documented using an inverted fluorescence microscope (Nikon ECLIPSE Ti-E, Tokyo, Japan) at 4X magnification. Bubble formation is a critical consideration in microfluidic systems, as it can introduce high shear forces and disrupt nutrient flow, thereby compromising cell viability. These bubbles were monitored and managed to ensure optimal conditions for cell culture.

PDMS microfluidic chips and glass-bottom (GB) culture dishes were incubated under both hypoxic and normoxic conditions for a duration of 24 hours. Following incubation, cell viability was assessed through live/dead staining using Calcein-AM and propidium iodide (PI), both procured from DOJINDO Co. Ltd. Calcein-AM selectively stains live cells, which fluoresce green

due to intracellular esterase activity, while PI stains dead cells, emitting red fluorescence upon binding to nucleic acids in compromised cell membranes. This dual-staining approach enables a clear distinction between viable and non-viable cells [30].

Subsequent imaging was carried out at 10X magnification using the same fluorescence microscope, which was equipped with a high-resolution digital camera (DS-Fi3, Nikon). This setup enabled detailed visualization of cellular morphology and precise measurement of cell lengths under each experimental condition.

Stained images were analyzed to evaluate both cell viability and morphological characteristics. The assessment focused on four experimental groups: PDMS chips and GB dishes under normoxic and hypoxic conditions. Key parameters included the cell spreading area, cell density, and cell length. These metrics were used to determine the impact of oxygen availability on cell proliferation and overall health. Cells cultured under hypoxia, particularly in the PDMS chip, displayed marked reductions in spreading area and density, supporting the hypothesis that the microenvironment significantly influences cellular behavior and viability.

2.3 Results and Discussion

2.3.1 Bubble Removal from PDMS Chip

Figure 7(a,c,e,g) shows a PDMS chip with a considerable number of bubbles in it before it was subjected to the bubble removal procedure. Fig. 7(b,d,f,h) shows the appearance of bubbles after rinsing the chips with 70% ethanol and PBS, which helped in eliminating the bubble occurrence. Bubbles were completely removed in 89% of the 20 chambers.

2.3.2 Cell Health in PDMS Chip and GB-dishes

To evaluate the quality of cell culture in culture dishes and PDMS chips under normoxic and hypoxic conditions, we characterized cell health and cell morphology. Osteosarcoma cells adhered to both cell culture platforms. We found that rinsing the device with ethanol did not affect cell viability and it also prevented contamination in the device. An elongated, spreading typical epithelial-like morphology was observed in chips and GB dishes (Fig. 8a, Fig. 8b). Cells in PDMS chips were compared to those in GB dishes, and the lengths of the cells were measured. Cells in hypoxia shown in Fig. 8(a) were more rounded compared to cells in normoxia, where they show a typical epithelial morphology (cells are polygonal in shape and grow in discrete patches) (Fig. 8 b). These characteristics suggest that the stress condition induced by hypoxia is depicted by the

shape change [44]. As shown in calcein AM-stained image (Fig. 8(a)) and PI-stained image (Fig. 8(b)) it can be confirmed that cells in the PDMS chip detached under hypoxia, and they died earlier. Cells cultured under normoxia in GB dish and the microfluidic chip showed almost similar cell health. In both cases, the cells were more elongated and spread out with a typical SAOS-2 morphology, indicating a healthy cell morphology.

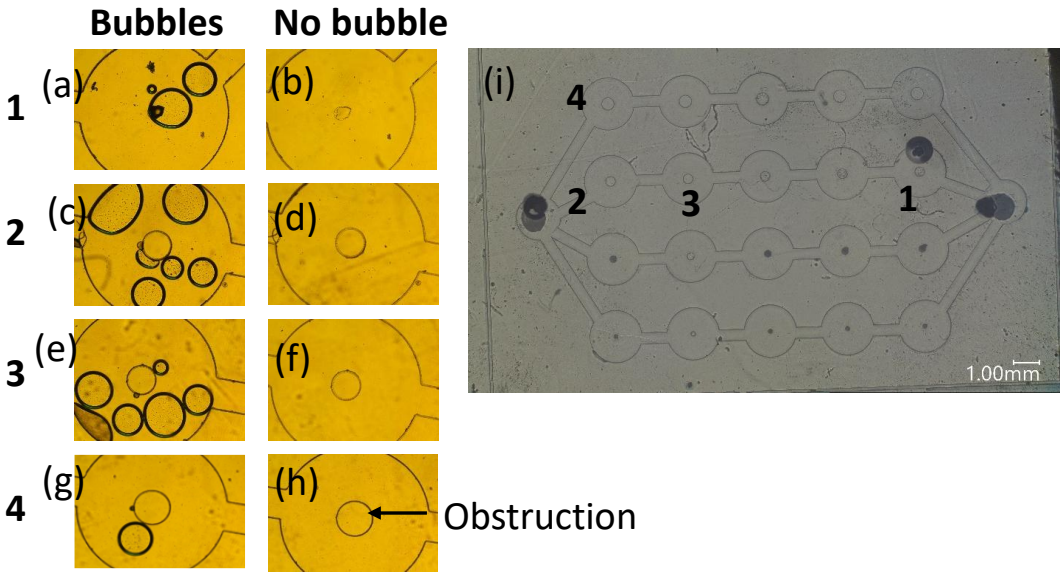

Figure 7 Bubble formation and removal from microfluidic device. Chamber diameters are 2.0 mm. Obstruction with diameters of (a), (b) 0.1mm (c), (d) 0.3 mm, (e), (f) 0.4 mm, and (g), (h) 0.5 mm. (i) Entire PDMS chip.

Fig. 8 shows Calcein-AM stained images of SAOS-2 cells. The cell morphology in the PDMS chip (Fig. 8a) changed under hypoxia, indicating a more stressed state due to lower oxygen levels [45,46]. A typical elongated cell morphology was found in PDMS chip under normoxia and in the GB dish under normoxia and hypoxia. This morphology indicated an overall similar state of cell health. GB dish with plastic material maintained healthy cell conditions even under hypoxia. Conventionally cell culture dishes are made with glass, plastic (mainly polystyrene material) or a combination of both. These materials are either non-porous or extremely finely porous in their nature and one of the reasons to choose them is to prevent the event of air borne contamination for cell cultures. In general, cell culture dishes are designed with a clearance to allow adequate oxygen exchange with the environment. However, it was found that this clearance was not sufficient for efficient oxygen removal to achieve hypoxic conditions. On the other hand, it was the porous

nature of PDMS material that made efficient oxygen removal possible [47]. Therefore, PDMS was able to maintain a hypoxic environment for tumor growth.

Previous studies have also reported the induction of hypoxia using glass bottom dishes, but with variable oxygen concentrations i.e. 21%, 5% and <0.1%. It also states that for long-term analysis oxygen levels further decreased, causing severe hypoxic induction in GB dish with <0.1% oxygen. This resulted in loss of cell proliferation and increased cell death. This suggests that in our study there was more oxygen scavenging and a gradual drop of oxygen level in PDMS chip than GB dish, resulting in severe hypoxic conditions, causing reduced cell proliferation and increased cell death. In addition, it was also found that ethanol rinsing was sufficient to protect the cell culture from airborne contamination.

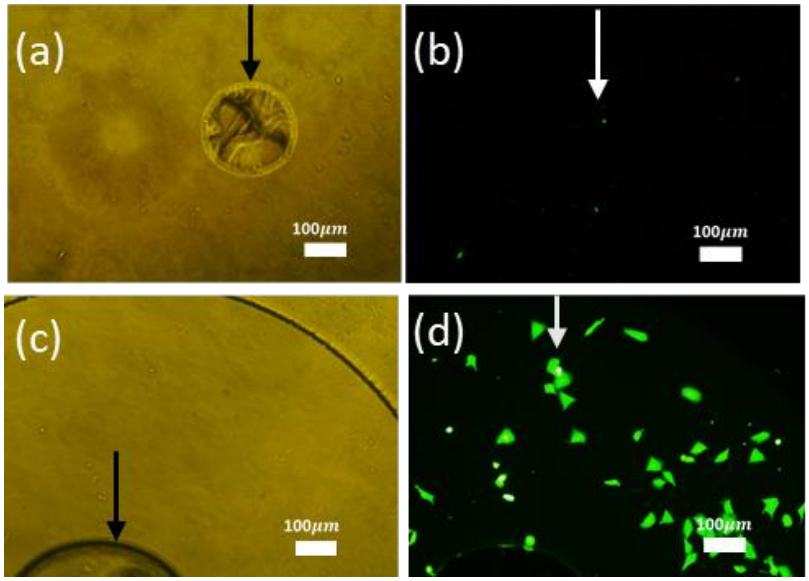

Figure 8 Microscope images of SAOS-2 cells in PDMS chip. (a) Bright-field image in hypoxia. (b) Calcein-AM stained image in hypoxia. (c) Bright-field image in normoxia. (d) Calcein-AM stained image in normoxia. Black and white arrows show obstruction and live cells.

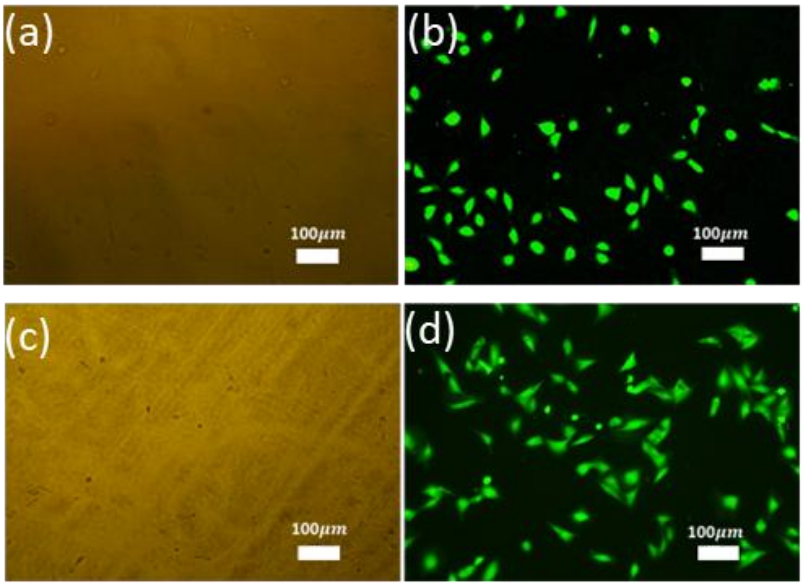

Figure 9 Microscope images of SAOS-2 cells in GB dish. (a) Bright field image and (b) Calcein-AM stained image in hypoxia. (c) Bright field image and (d) Calcein-AM stained image in normoxia.

2.3.3 Cell Density

To evaluate the quality of cell culture under normoxic and hypoxic conditions, the cell densities of the four devices were measured (Fig. 10). The cell density in a microfluidic chip under hypoxia was 30 cells/mm^2, which was significantly low compared to the normoxia conditions 348 cells/mm^2. hypoxia and normoxia were 334 and 362 cells/mm^2, respectively. 8% of live cells were present in the hypoxia-induced microfluidic chip. Cells were cultured in the microfluidic chip under normoxia, to maintain a healthy culture environment in the chip. The low viability of hypoxic cells in the PDMS chip indicates efficient hypoxia induction in the microfluidic device. Ideally number of live cells in the hypoxic-induced GB dish should be less than those in the normoxic-induced GB dish. However, calcein-stained images in GB dishes (Fig. 9(a) and (b)) under both hypoxia and normoxia have a total number of 75 cells. This suggests that traditional cell culture dishes may not be suitable for efficiently producing hypoxic tumor microenvironment conditions. Compared with the PI-stained images (Figure 10) after 24 h, the microfluidic chip in hypoxia had the highest number of dead cells. These results indicate that the PDMS-based microfluidic chip was the most suitable for hypoxia induction.

These results indicate that the hypoxic conditions induced in the PDMS chips hindered the cell growth or cell division process. The gas-permeable nature of PDMS allowed for efficient oxygen removal and maintained a hypoxic environment. This nature ultimately affected the cell division process and/ or induced cell death on PDMS chips [48].

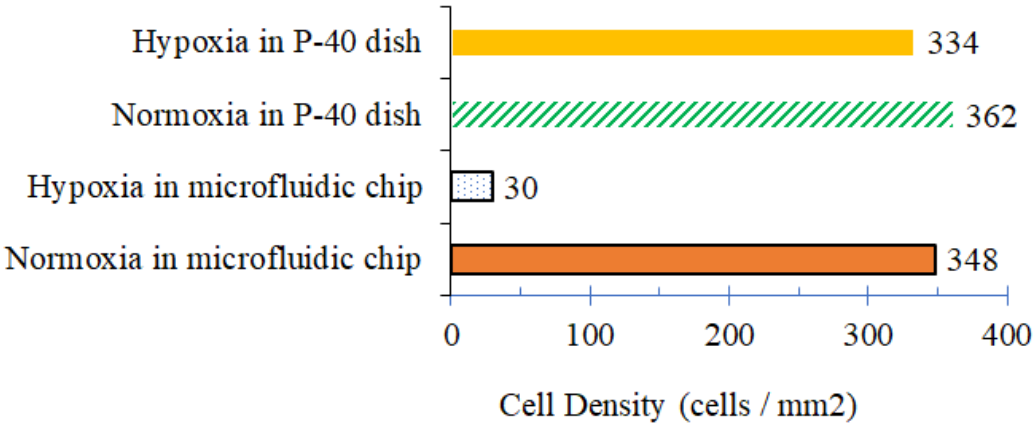

Figure 10 Cell density comparison of four cases of cell culture.

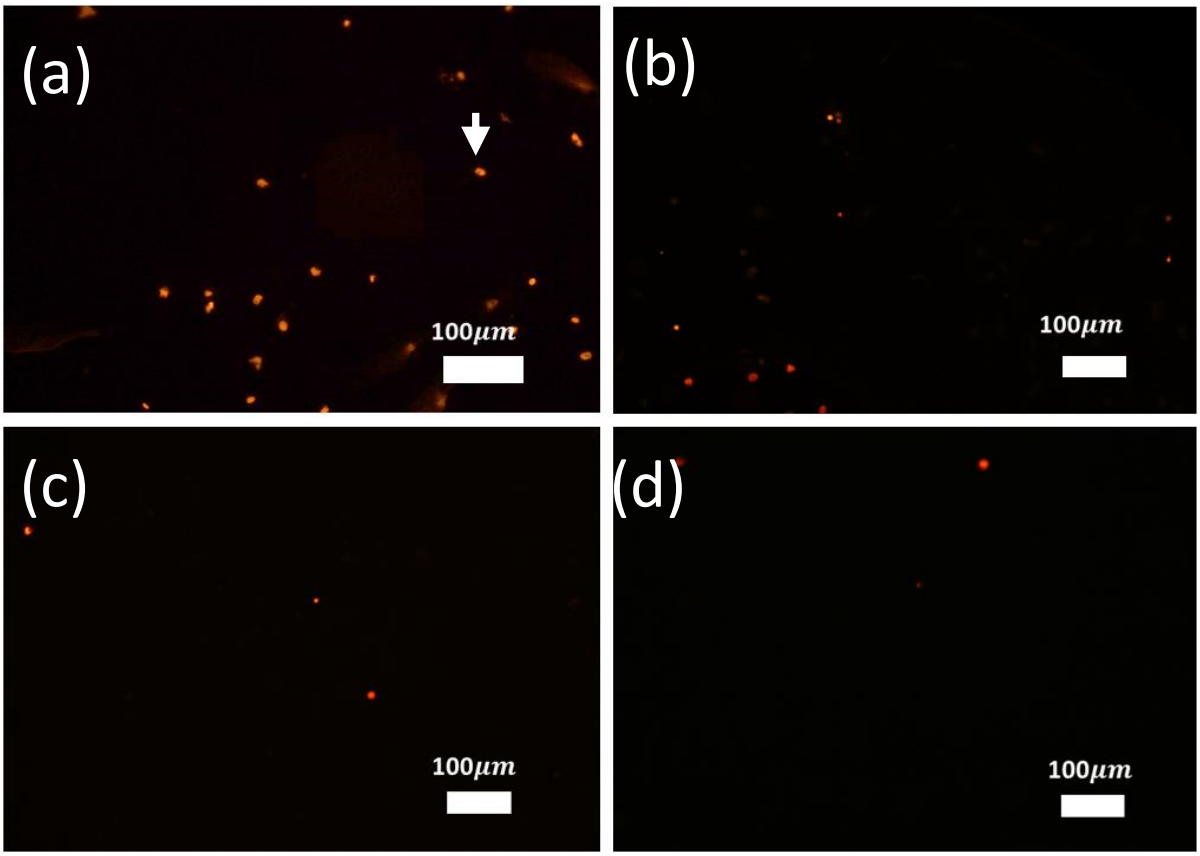

Figure 11 Microscope images of SAOS-2 cells stained with PI. PDMS chips under (a) hypoxia and(b) normoxia. (c) GB dishes cell culture under(c) hypoxia and (d) normoxia. White arrow shows an example of dead cells.

2.3.4 Cell Length

Cell length is an indicator of good or poor cell culture conditions. In healthy and favorable culture conditions, cells tend to adhere to the substrate surface and spread out, showing a good length. In unhealthy conditions, cells tend to squeeze together and show short lengths. Therefore, cell lengths were measured to evaluate the quality of the cell culture. The standard deviation of cell lengths was obtained for all four cases (n = 10) from Calcein-AM-stained images with the microscope. Figure 12 shows the averages and standard deviation of cell lengths. The minimum average length was 18.6 μm for a microfluidic chip under hypoxia. The small length of osteosarcoma cells in the microfluidic chip under hypoxic conditions suggests unhealthy conditions of indicating a highly stressed environment. Previous research work has also reported that cell morphology was rounded under severe hypoxic conditions [49]. This indicates reduced cell length under hypoxic conditions. It was attributed to efficient oxygen removal. The cell length in the hypoxic chip was relatively small and supports the conclusion that the PDMS material is good enough for cell culture to efficiently mimic the tumor microenvironment.

The maximum average length was 77.0 μm for the normoxia microfluidic chip. The average cell lengths under hypoxia and normoxia conditions in the GB dish were 76.9 μm and 78.1μm, respectively. These lengths in the three conditions were close to each other, indicating that there was no effective hypoxia induction in the GB tissue culture dish. The cell length in the microfluidic chip under normoxia was close to that in the GB tissue culture dish under normoxia, which was used as a control.

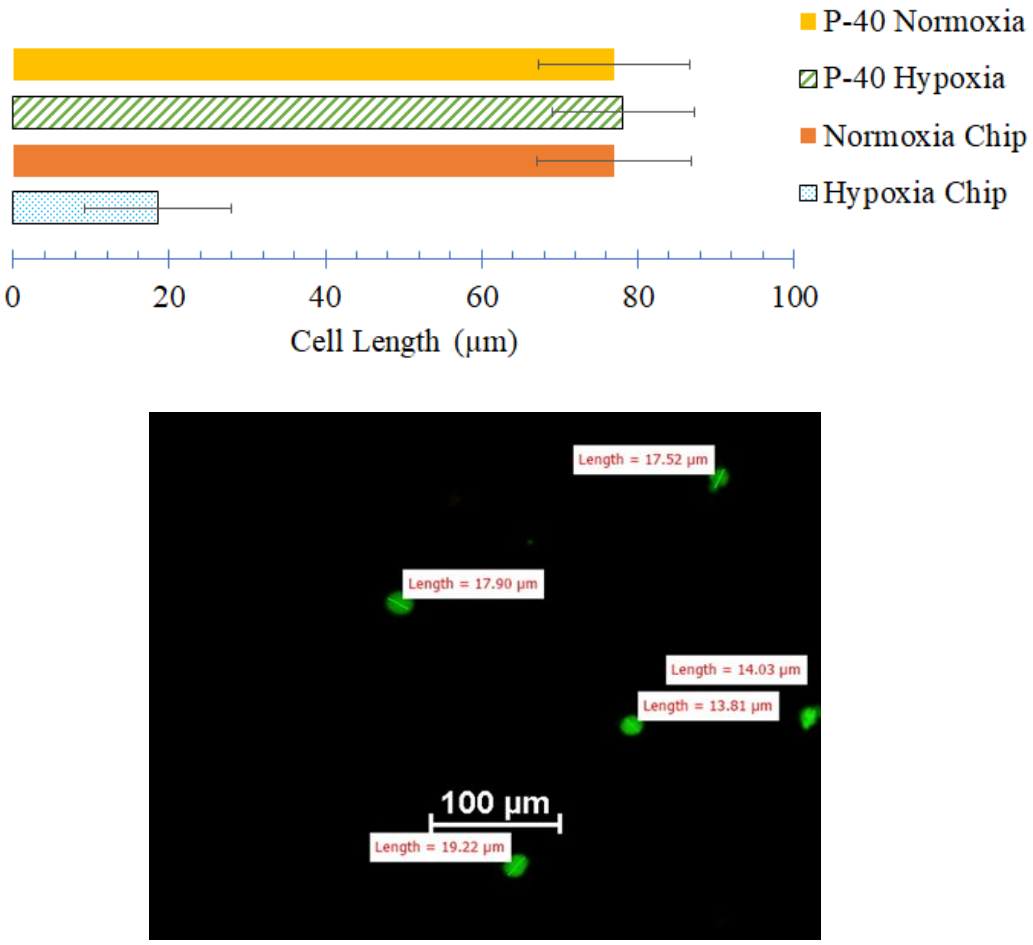

Figure 12 (a) Cell length comparison of four cases of cell culture (b) Measurement of cell length with the inverted fluorescence microscope (Nikon ECLIPSE Ti-E).

2.4 Conclusions

This study presents a simple, low-cost, and effective method to replicate hypoxic conditions representative of the tumor microenvironment using PDMS-sealed microfluidic chips and commercially available hypoxia-inducing plastic bags. One of the major technical challenges encountered during microfluidic culture—air bubble formation caused by direct pipetting into microchannels—was addressed through an optimized protocol involving a sequential rinse with 70% ethanol, followed by sterile saline and cell culture medium. This method efficiently removed bubbles without compromising cell viability, as the ethanol was promptly neutralized with physiological solution, ensuring that the cells were not exposed to cytotoxic conditions.

The use of hypoxia bags proved sufficient to create and maintain a hypoxic environment within PDMS microfluidic devices. The system's simplicity and user-friendliness—enabled by

easy sealing, straightforward insertion and removal of devices, and minimal spatial requirements within a standard incubator—highlight its practicality for routine laboratory use. Furthermore, the approach requires no specialized gas-handling equipment or complex infrastructure, making it a cost-effective alternative to traditional hypoxia chambers and oxygen-controlled incubators.

Experimental comparisons between cell cultures in glass-bottom (GB) dishes and PDMS microfluidic chips under normoxic and hypoxic conditions showed that the gas-permeable nature of PDMS enabled effective oxygen depletion, thereby replicating the hypoxic tumor environment more accurately than standard culture platforms. Hypoxic cultures in PDMS chips exhibited noticeable differences in cell length, density, and viability, confirming the platform's effectiveness in simulating in vivo-like stress conditions. Additionally, the small culture volumes required in the microfluidic channels facilitated faster oxygen equilibration, contributing to a more efficient induction of hypoxia.

Normoxic cell cultures in PDMS chips also produced results comparable to those in GB dishes, demonstrating that PDMS supports both hypoxic and normoxic conditions due to its oxygen permeability. This dual capability enhances the system's versatility for modeling a wide range of microenvironmental conditions.

Moving forward, this platform will be employed to explore drug resistance and stress-induced cellular responses in osteosarcoma models. The ability to apply dual drug or metabolite combinations and implement microchannel designs with varying obstruction geometries will allow for a deeper understanding of tumor behavior under physiologically relevant conditions. Overall, the integration of PDMS microfluidics with hypoxia bags provides a promising avenue for cancer-on-a-chip applications, advancing both basic cancer research and preclinical drug testing.

This hypoxic culture validation establishes the first critical component of our integrated drug screening platform — physiologically relevant microenvironment reproduction that accurately simulates osteosarcoma tumor conditions. This biological foundation will be systematically combined with precise gradient generation capabilities (Chapters 3-4) and optimized device performance (Chapter 4) to create the first complete system capable of MEC determination under tumor-relevant conditions.

Chapter 3 PDMS SlipChip: Optimizing Sealing, Slipping, and Biocompatibility Using Low-Viscosity Silicone Oils

3.1 Introduction

The PDMS SlipChip is a microfluidic platform enabling fluid manipulation without pumps or valves, simplifying operation and reducing reagent use. High-viscosity silicone oils (e.g., 5,000–10,000 cSt) improve sealing but frequently block microfluidic channels, reducing usability. In contrast, low-viscosity oils (50–100 cSt) reduce blockages but may compromise sealing. This study addresses these challenges by optimizing the viscosity of silicone oil and the curing conditions of PDMS. Low-viscosity silicone oil (50 cSt) was identified as optimal, ensuring smooth slipping and reliable sealing without blockages. Curing conditions were also adjusted to balance adhesion and stiffness: lower temperatures (50–60°C) enhanced van der Waals adhesion, while higher temperatures (80°C) increased stiffness. A mixed curing approach (80°C for the top layer, 60°C for the bottom layer) further improved performance. Biocompatibility testing using human osteosarcoma cells demonstrated minimal cytotoxicity with 50 cSt oil, supporting cell viability (95%) comparable to traditional multiwell plates. These findings provide practical guidelines for fabricating reliable and biocompatible SlipChips.

Investigating the intricacies of chemistry and biology often requires careful surveys using minimal reagents [50–52]. Conventional microfluidic devices that require pumps and valves for biological and chemical assays [53–55]. Centrifugal microdevices [19,56] or paper-based microfluidic devices [57] are used to remove the external components. The SlipChip is a simple microfluidic device consisting of two aligned layers with flow channels and microwells, enabling researchers to perform operations efficiently [58–61]. The SlipChip operates solely based on a 'slip action' for fluid manipulation. This platform creates isolated reaction chambers with minimal sample consumption while maintaining high throughput through its ability to initiate, reroute, and isolate fluid flow by engaging or disengaging microfluidic channels. Glass SlipChips are commonly used due to their chemical resistance and precise fabrication [61]. However, their complex manufacturing process of etching with the use of hazardous chemicals

and lack of gas permeability make them unsuitable for applications such as cell culture, where gas exchange is critical [62].

Polydimethylsiloxane (PDMS) SlipChips are a cost-effective and easily fabricated alternative [63]. Unlike glass SlipChips requiring harsh etching, PDMS versions are easily fabricated simply by molding. Precursors are mixed, cast onto a mold, and baked, precisely replicating features. This mild process enables rapid prototyping. Additionally, PDMS's gas permeability and bio-inertness make it ideal for cell-based assays [64,65]. Despite these advantages, PDMS introduces challenges such as increased friction between layers. Silicone oil lubricants can reduce this friction and facilitate slipping, but excessive lubrication weakens adhesion, complicating controlled slip motion. High-viscosity silicone oils (5,000 cSt [66] and 10,000 cSt [26,63,67]) have been used in previous studies to address slipping challenges by enhancing sealing performance. However, high-viscosity oils risk blocking microchannels, which impedes fluid flow. Furthermore, their potential cytotoxicity can make the device unusable, especially for cell-based work. On the other hand, low-viscosity oils are less likely to cause blockages but may reduce sealing performance. Therefore, it is crucial to explore strategies to balance these competing factors effectively.

A key factor influencing the performance of PDMS SlipChips is the cross-linking density of the PDMS material, which is determined by the curing temperature[68]. Lower curing temperatures enhance adhesion and reduce stiffness, while higher curing temperatures increase stiffness but diminish adhesion [69,70]. This behavior arises from tethered or free polymer chains on cured PDMS surfaces that interact via van der Waals forces during contact [71,72]. However, the effects of curing conditions on interlayer adhesion and their interplay with lubricant properties remain unclear. Further investigation is needed to clarify how curing conditions influence these interactions and optimize Slip-Chip performance.

Also Leak-free flow in a PDMS SlipChip requires maintaining moderate pressure between the top and bottom layers. The bonding strength between these layers is critical - too strong bonding leads to high friction that impedes the slip action. This study explores a simple approach to balance the slip action and prevent leakage by optimizing the cross-linking density via controlled curing temperatures of each PDMS layer, with silicone oil used as a lubricant between layers. Curing temperature affected the surface energy of PDMS and modulated the adhesion

forces of a silicone oil responsible for the interlayer bonding. Organic and inorganic fluids were injected into a SlipChip, and qualitative testing examined the maximum fluid volume that the SlipChip could withstand without leaking. Quantitative pneumatic testing evaluated the achievable sealing pressures. Our findings reveal an effective way to tune the PDMS cross-linking and interlayer adhesion to enable leak-free operation and smooth slipping motion.

The design of SlipChip enables the high-throughput generation of multiple drug concentrations and has been applied to biological assessments such as PCR tests, bacterial detection, and drug development [21,25,73,74]. SlipChips show promise for drug uptake studies and disease biomarker measurements. While both glass and PDMS SlipChips have been used for antimicrobial testing, bacterial growth analysis, and antibiotic testing [25,59–61,73,75,76], research on mammalian cell growth in PDMS SlipChips remains limited [77].Although PDMS is an inert, non-toxic, and biocompatible material, some lubricants may exhibit cytotoxicity to mammalian cells, necessitating thorough biocompatibility testing.

This study investigates the use of low-viscosity silicone oils (50–100 cSt) as an alternative to high-viscosity oils, seeking to mitigate issues like channel blockages while maintaining effective sealing and slipping performance in PDMS SlipChip. The effects of PDMS curing temperatures on interlayer adhesion and stiffness were examined, identifying an optimal combination of 80°C for the top layer and 60°C for the bottom layer. Biocompatibility testing using human osteosarcoma cells demonstrated that 50 cSt silicone oil supports cell viability comparable to traditional multiwell plates while exhibiting minimal cytotoxicity. These findings offer practical guidelines for fabricating reliable and biocompatible SlipChips, demonstrating that low-viscosity lubricants effectively address performance trade-offs.

The optimized 50 cSt silicone oil and dual-temperature curing protocol (60°C bottom, 80°C top) ensure consistent device performance across the complete molecular weight spectrum required for osteosarcoma therapy—from small molecule chemotherapeutics like doxorubicin (~580 Da) to emerging monoclonal antibody therapies (~150 kDa). This broad compatibility addresses the critical need for versatile drug screening platforms in precision oncology.

3.2 Material and Methods

This section describes the design and fabrication of SlipChip molds and PDMS-based devices.

3.2.1 Design of PDMS SlipChip

The SlipChip platform features two primary design configurations, each serving distinct functional purposes within microfluidic experimentation. As shown in Figure 13(a), the first configuration is specifically engineered to evaluate the sealing performance of the PDMS interlayer. In this design, a network of microwells—each with a diameter of 2 mm—is interconnected by microchannels embedded in both the top and bottom layers. To simulate a range of sealing conditions, structural obstructions were deliberately introduced into the fluid paths. The bottom layer incorporates uniform obstructions of 0.9 mm, while the top layer includes a gradient of obstruction sizes, decreasing progressively from 0.9 mm to as small as 0.12 mm. This deliberate variation in microchannel constriction enables precise assessment of where and how leakage may occur under suboptimal sealing, making it a useful diagnostic tool for evaluating PDMS layer bonding and interface integrity.

Figure 13(b) illustrates the second configuration, which is designed for the generation of concentration gradients—a common requirement in cell culture and biochemical assays. In this setup, the top PDMS layer includes six microwells arranged in a series, with diameters tapering from 3.0 mm to 1.4 mm in defined steps (3.0 mm, 2.6 mm, 2.2 mm, 2.0 mm, 1.8 mm, and 1.4 mm). The depth of each microwell is uniformly set at 0.35 mm. This structure promotes controlled fluid loading and facilitates diffusive mixing across the wells when overlaid with a corresponding bottom layer. The sequential layout and varying volumes of the wells allow for passive gradient formation as two fluids intermix across the interface, supporting applications such as drug testing or molecular diffusion studies.

Operational challenges are depicted in Figures 13(c) and 13(d). These highlight critical issues such as air bubble entrapment between PDMS layers, which can obstruct fluid pathways, and insufficient interlayer sealing, which can cause fluids to leak into unintended regions. These problems emphasize the importance of careful alignment, air removal, and adequate sealing during SlipChip assembly to ensure reliable performance in both testing and practical applications.

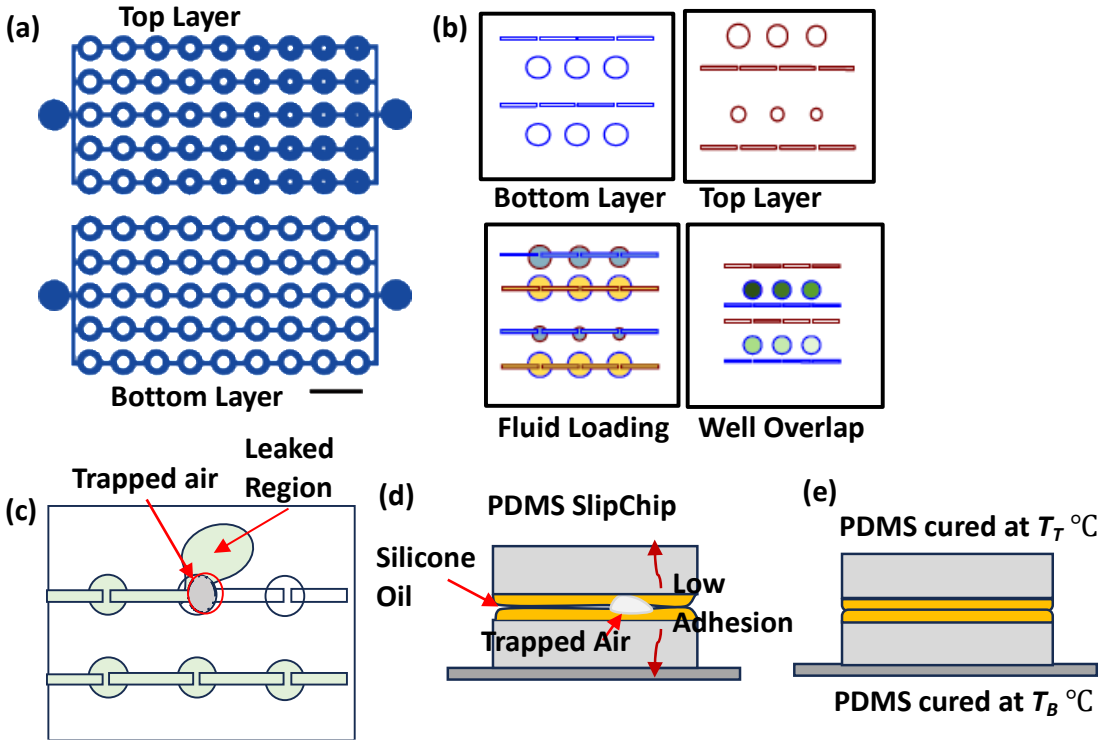

Figure 13 Design and characterization of PDMS SlipChip. (a)Test chip-like SlipChip with connected channels and obstructions for burst pressure measurement. Scale Bar: 4mm. (b) SlipChip to develop gradient concentration. (c) Top view and (d) Side view showing air.

3.2.2 Fabrication of PDMS SlipChip

A SU-8 mold was fabricated on a silicon wafer using standard photolithography with SU-8 3050 negative photoresist [78]. The PDMS base and curing agent (Silpot 184 W/C by Toray Dow Corning) were mixed at a ratio of 10:1 and poured onto the mold.

In all protocols, one layer was polymerized at 80°C for one hour and fixed as a baseline. The other PDMS layers were subjected to five distinct temperature protocols to optimize their mechanical properties. Variations in the process involved steps applied to the other layer only: (i), (ii), (iii): The other layer was baked at 50°C for two hours, 60°C for two hours, or 80°C for one hour, respectively. (iv), (v): The other layer underwent 80°C for 1 hour and an additional thermal treatment at 100°C or 120°C for another hour, respectively. These protocols were designed to achieve specific mechanical properties, ensuring that the layer with additional treatment became slightly stiffer to facilitate handling during slipping. SlipChip performance was evaluated through leakage testing, pneumatic testing, and tensile testing across a range of curing temperatures: 50 °C, 60 °C, 80 °C, 100 °C, and 120 °C. These temperatures were selected to balance efficiency and

safety—lower temperatures were chosen to accelerate the curing process compared to room temperature, while higher temperatures were kept within a safe limit to ensure suitability for lab-scale fabrication and minimize the risk of accidents during student-led experiments.

Molds for gradient concentration SlipChips were fabricated using LCD VAT 3D printing (Sonic Mini 8K, Phrozen). Poly(lactic acid) (PLA) frames were fabricated using an FDM 3D printer (Adventurer 4, FlashForge) and mounted onto the top PDMS layer to enhance structural stability during slipping. The SlipChip itself was fabricated by soft lithography using a 10:1 ratio of the PDMS prepolymer.

3.2.3 Contact Angle of Silicone Oil on PDMS with Different Degrees of Cross-linking

Curing PDMS at various temperatures i-e 50°C, 60°C, 80°C, 100°C and 120°C gave different degrees of cross-linking densities which affect its surface properties (Figure 15). To have an estimate of those surface properties contact angle of silicone oil on those PDMS materials was measured. A drop of silicone oil was placed on each PDMS and its contact angle was directly measured using a USB digital microscope (SANWA Supply, Taiwan) at 13.6X magnification.

3.2.4 Pneumatic Test for Separating Two Layers

A thin layer of silicone oil (120 mPa·s, 0.967 g/mL at 20 °C, #85409, Sigma Aldrich) was spin-coated onto the bottom layer at 1500 rpm to ensure uniform coverage. After alignment, the assembled SlipChip was placed under vacuum (gauge pressure: –0.07 MPa) for 20 minutes to remove trapped air and enhance sealing between layers.

A pneumatic test was conducted to measure adhesion between SlipChip layers and PDMS ageing by determining the maximum pressure difference the SlipChip could withstand (Figure 14(a)). A 5 µM aqueous solution of Rhodamine 6G (R0039, Tokyo Chemical Industry Co., Ltd.) [40] was prepared by dissolving the powder in water. A 0.01 M aqueous iodine solution was prepared by diluting a 0.5 M iodine solution (15-0610, Sigma-Aldrich) [79] with water. One of these solutions was selected and flowed through a test device that mimicked the actual SlipChip design. The device was then held in hand while pneumatic pressure was applied at both the inlet and outlet using a pneumatic pump. The gauge pressure was gradually increased from 0 kPa until the test device ruptured (Figure 14(b)), and the corresponding pressure readings were recorded as the rupture (burst) pressure. The SlipChip was then heated at 60°C, and experiments were repeated

after 2 hours each to determine ageing and adhesion strength of PDMS cured at different temperatures. Heating of PDMS at 60°C was chosen to accelerate PDMS ageing and speed up the experimental process.

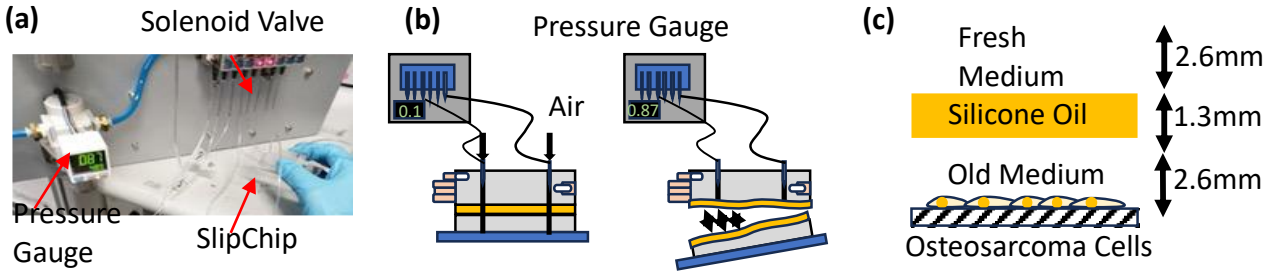

Figure 14 Pneumatic test on SlipChip mimicking device. (a) Apparatus used for the pneumatic test, showing the setup for applying air pressure to the SlipChip mimicking device. (b) Schematic representation of the rupture mechanism caused by increasing air pressure. (c) Biocompatibility testing of silicone oil.

3.2.5 Tensile Testing of PDMS Cured at Different Temperatures

To further validate the pneumatic testing results, tensile tests were performed on PDMS samples cured at different temperatures. A mold for the tensile specimens was de-signed using AutoCAD and fabricated via an LCD VAT 3D printer (Saturn3 Ultra, ELE-GOO). Standard dumbbell-shaped test specimens were then prepared by casting PDMS in the mold and curing at 50°C, 60°C, 80°C, 100°C, and 120°C.

The specimens measured 130 mm in overall length, with a 90 mm shoulder-to-shoulder distance, a 33 mm gauge length, and a 12.5 mm gauge width. The grip sections were 30 mm wide, and the overall thickness was 2 mm.

Using a tensile testing machine (MCT-2150, A&D Co., Ltd.), the prepared specimens were clamped in the grips and stretched until failure (breaking point). The modulus of elasticity (Young's modulus) was determined from the initial linear region of the resulting stress-strain curve.

3.2.6 Characterization of Silicone Oil Properties: Leakage Testing and Layer Thickness Analysis

To analyze silicone oil viscosity effects on SlipChip adhesion, we used devices fabricated with optimized curing conditions (top layer at 80°C, bottom layer at 60°C). Two ShinEtsu silicone oils with different viscosities were tested: KF-96-50CS (50 cSt) and KF-96-100CS (100 cSt). The oils were spin-coated onto the PDMS layers at four different speeds: 1000, 1500, 1800, and 2000

rpm. To evaluate sealing performance, we conducted leakage tests by connecting a micropipette to the SlipChip inlet and gradually increasing the iodine solution volume from 0 to 200 µL, with each loading step performed within 10 s.

To characterize the oil layer formation, deposition height measurements were per-formed using Z-stack imaging with an inverted fluorescence microscope (Nikon Eclipse Ti-E, Tokyo Japan) and software NIS-Element AR. 200 µL of each oil was placed at five different locations of the four different chips (center, top right, bottom right, top left, and bottom left) and spin-coated at 1000, 1500, 1800, and 2000 rpm. Each of the spin-coated chips was placed under the microscope, and elevation levels were obtained by Z-stack imaging. The surface adjacent to the channel was focused and considered the top surface. The bottom surface was the reference plane (Z = 0) for channel depth. The elevation difference between the top and bottom surfaces determined the silicone oil deposition height.

3.2.7 Bio-compatibility Test with Silicone Oil

We evaluated the biocompatibility of silicone oils using human osteosarcoma cells (SAOS-2, Tohoku University, Sendai, Japan) and their metastatic variant (LM-7, MD Anderson Cancer Center). Cells were seeded at a density of 100 cells/µL in Dulbecco's Modified Eagle Medium (DMEM, High Glucose, Fuji Films Wako Co. Ltd) in a flat-bottom 96-well plate (1-1601-06, Violamo, AS ONE Corporation Japan), with a total volume of 100 µL per well. The biocompatibility assessment focused on the diffusion of fresh culture medium and oxygen to the cells through the silicone oil layer, as well as the effects of direct contact and oil molecular weight. Cell viability was analyzed using a Calcein-AM and propidium iodide (PI) staining assay (companies). Calcein-AM and PI solutions were diluted 1:10 in PBS before application. Images were captured using an inverted microscope (NIKON ECLIPSE Ti-E, Tokyo, Japan).

A layer of silicone oil was placed between the cancer cells and the cell culture medium to examine its effect on nutrient diffusion. Specifically, 50 µL of silicone oil (50 cSt or 100 cSt) was added above the culture medium 24 hours after cell adhesion (Fig. 22(c)). The silicone oil layer depth was maintained at 1.3 mm. Fresh medium was introduced from the top, followed by a 48-hour incubation period. Live/dead cell assays were performed to assess cell viability, focusing on

the diffusion of nutrients through the silicone oil layer. Additionally, the experimental setup allowed for examining the impact of oil viscosity on nutrient diffusion.

3.2.8 Demonstration of Diffusion Mechanism in SlipChip

The mixing process in the SlipChip generates concentration gradients through a volume-based dilution system. The bottom layer contains uniform microwells (3.0 mm diameter,2.5 mm^3 volume), while the top layer features wells with decreasing diameters (3.0mm to 1.4mm), corresponding to volumes from 2.5mm^3 to 0.5mm^3. Both layers have a uniform depth of 0.35 mm.

The SlipChip design pairs microwells from the top and bottom layers to create controlled mixing chambers without introducing physical obstructions, minimizing the risk of bubble formation during fluid manipulation. As microwell sizes in the top layer decrease, the total volume in each well pair progressively reduces, allowing the formation of an intrinsic concentration gradient during mixing.

Using a SlipChip fabricated under optimized curing conditions (bottom layer at 60°C, top layer at 80°C), we generated concentration gradients with a 4 mM ethanol-based Rhodamine 6G solution. Fluorescence measurements were performed using an inverted microscope (Ti-E, Nikon, Japan) at 2× magnification. The concentration in each well was determined by the total mixing volume, with the initial well pair (5.0 mm^3 total volume) yielding a concentration of 2.0 mM.

3.2.9 Demonstration of Cell Culture in SlipChip

A PDMS SlipChip was fabricated using a two-layer design: the top layer was cured at 80°C and the bottom layer at 60°C, with a 50 cSt silicone oil layer applied between them to enable controlled slipping. SAOS-2 cells (Tohoku University, Sendai, Japan) were seeded at a density of 100 cells/μL in culture medium composed of Dulbecco's Modified Eagle Medium (DMEM) supplemented with 10% fetal bovine serum (FBS, COSMO BIO), 100 U/mL penicillin, and 100 μg/mL streptomycin (15070063, Gibco, Thermo Fisher Scientific). The cells were maintained at 37°C in a humidified atmosphere with 5% CO2.

After 24 hours of incubation, cell viability was assessed using live/dead cell assays. Adhered cells were stained with Calcein-AM to label live cells and PI to label dead cells, followed by a 50-minute incubation at 37°C [80,81]. Calcein-AM is converted by intracellular esterase into green-fluorescent compounds in live cells, while PI binds to DNA in dead cells with damaged

membranes, emitting red fluorescence. Fluorescence imaging was performed using an inverted microscope (NIKON ECLIPSE Ti-E, Tokyo, Japan). Comparison with SAOS-2 cells cultured in 96-well plates under the same conditions (with 50 cSt silicone oil) showed comparable cell viability and morphology between the two systems.

3.3 Results and Discussion

3.3.1 Contact Angle of Silicone Oil on PDMS with Different Degrees of Cross-linking

Different cross-linking densities controlled by curing temperatures affect the surface properties of PDMS. An estimation of the change in surface properties for the PDMS cured at 50°C, 60°C, 80°C, 100°C and 120°C was made by measuring the contact angle of a drop of silicone oil placed on the respective PDMS surfaces. As shown in Figure 15(a), it was found that PDMS cured at 50°C had the lowest contact angle of 9.2°. PDMS cured at 60° C and 80°C had a contact angle of 10° and 13.4° (Figure 15(b), (c)). PDMS cured at higher temperatures, i-e 100°C and 120°C had a contact angle of 19.7° and 18.6° (Figure 15(d), (e)). These results suggest that PDMS

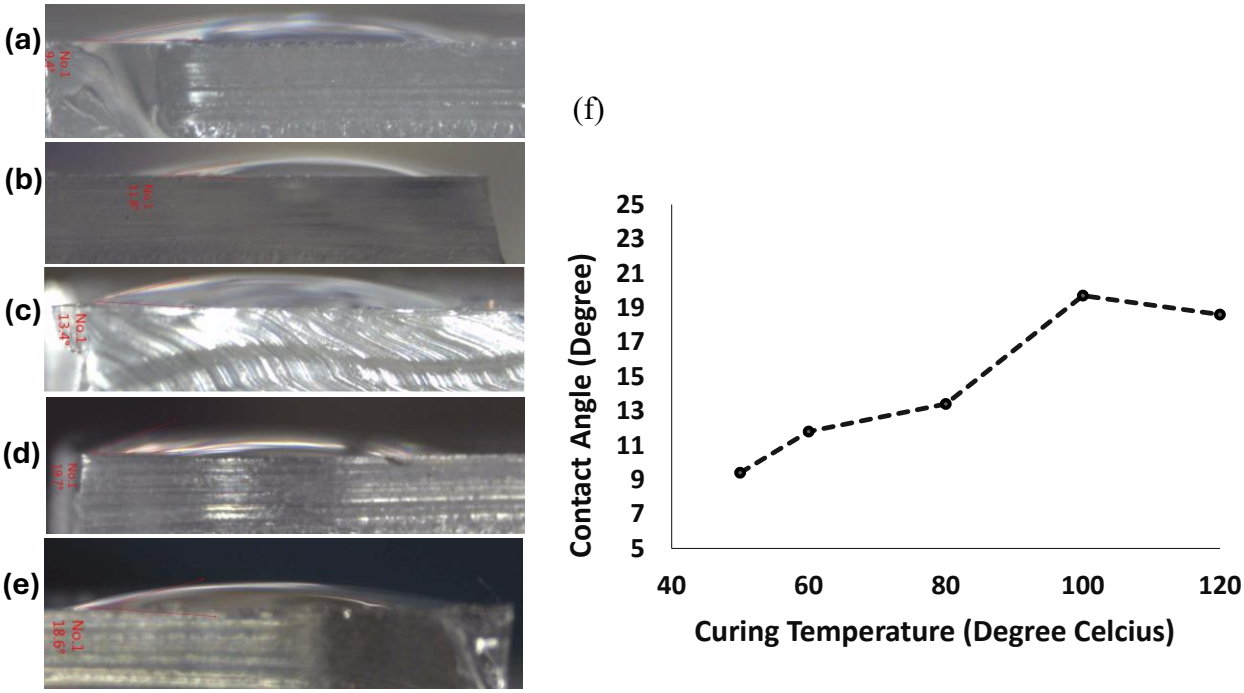

Figure 15 Contact angles with (a) 50°C cured PDMS, (b) 60°C cured PDMS, (c) 80 °C cured PDMS (d) 100°C PDMS (e) 120°C cured PDMS (f) Variation in contact angle of silicone oil and PDMS with changing temperature.

surfaces with lower cross-linking densities had maintained lower contact angles with silicone oil droplets, thus depicting higher surface energies [82,83].

3.3.2 Pneumatic Test

Figure 16(a) shows the maximum pressures (rupture pressures) that a SlipChip, constructed with 120 mPa·s silicone oil applied by spin-coating at 1500 rpm, can withstand under various curing conditions. The sample cured at 50°C for two hours on one side exhibited the highest rupture strength, requiring 61±10 kPa for the rhodamine solution and 47±10 kPa for the iodine solution. This superior performance is attributed to the reduced cross-linking density at lower curing temperatures, which increases the number of tethered or free polymer chains on the PDMS surfaces. These additional chains enhance van der Waals forces between layers, resulting in stronger adhesion and higher rupture resistance [70-73]. Similarly, the sample cured at 60°C for two hours exhibited relatively high rupture pressures (40±8 kPa and 37±10 kPa for rhodamine and iodine solutions, respectively). Although lower curing temperatures (e.g., 50°C and 60°C) enhance adhesion via increased van der Waals forces from a higher density of free polymer chains, they also produce softer PDMS layers with reduced structural integrity. Combining curing the bottom layer at 60°C and the top layer at 80°C, a balance between adhesion and stiffness is achieved.

In contrast, the sample with both sides cured at 80°C for one hour (the standard curing condition) showed lower rupture pressures of 38±10 kPa for rhodamine and 34±9 kPa for iodine solutions, indicating that a higher cross-linking density reduces interlayer adhesion. Furthermore, samples subjected to additional curing at higher temperatures (100°C and 120°C) required the lowest pneumatic pressures to separate the layers—2±1 kPa and 2±1 kPa for rhodamine and iodine solutions at 100°C, and 5±1 kPa and 4±1kPa for rhodamine and iodine solutions at 120°C—demonstrating that excessive cross-linking weakens adhesion.

Notably, no significant difference in rupture pressure was observed between the rhodamine and iodine solutions under any curing condition, as indicated by overlapping error ranges. While both solutions exhibited varying rupture pressures under different curing temperatures, the differences between the two solutions at each temperature point fell within the experimental

uncertainty. This suggests that the adhesion strength is primarily governed by the PDMS cross-linking density rather than by the chemical nature of the test solutions.

Figure 16(d) presents the results of an aging study, evaluating the pneumatic sealing pressure of PDMS SlipChips over a 4-hour period. Samples were cured at five different temperatures (50°C, 60°C, 80°C, 100°C, and 120°C), and measurements were taken at 0, 2, and 4 hours. The data reveal a clear inverse relationship between the initial sealing pressure (at time = 0 hours) and the curing temperature; samples cured at lower temperatures exhibited significantly higher initial pressures than those cured at higher temperatures. Specifically, the initial pressure was highest for the 50°C sample (approximately 49 kPa) and lowest for the 120°C sample (approximately 3 kPa).

The aging behavior over the 4-hour test period varied significantly with the curing temperature. Samples cured at 50°C and 60°C showed relatively slow degradation, maintaining a substantial portion of their initial pressure (declining to approx. 40 kPa and 35 kPa, respectively). In contrast, the sample cured at 80°C, which started at a moderate pressure (approx. 31 kPa), exhibited a pronounced and relatively linear decrease, dropping to approximately 6 kPa after 4 hours. Samples cured at 100°C and 120°C displayed poor initial sealing performance (approx. 6 kPa and 3 kPa, respectively). While the 100°C sample showed minimal further pressure loss, the 120°C sample's sealing capability rapidly diminished to essentially zero within the 4-hour timeframe. These results suggest that while lower curing temperatures yield higher initial sealing pressures, the stability over time can vary, with 80°C showing significant degradation. Conversely, curing at 100°C or 120°C results in intrinsically weak initial sealing.

Overall, this study highlights the critical role of PDMS curing conditions when using low-viscosity oils. Unlike previous studies [26,63,66,67]that primarily relied on high-viscosity silicone oils (e.g., 5,000–10,000 cSt), where the effects of curing conditions were less significant, our results demonstrate that with low-viscosity oils (e.g., 120 cSt), the curing temperature of PDMS significantly influences interlayer adhesion. Lower curing temperatures enhance adhesion by increasing the number of tethered or free polymer chains on PDMS surfaces, which amplify van der Waals forces. This interplay between curing conditions and lubricant properties provides a simpler and more effective approach for achieving reliable sealing and controlled slipping performance in PDMS SlipChips.

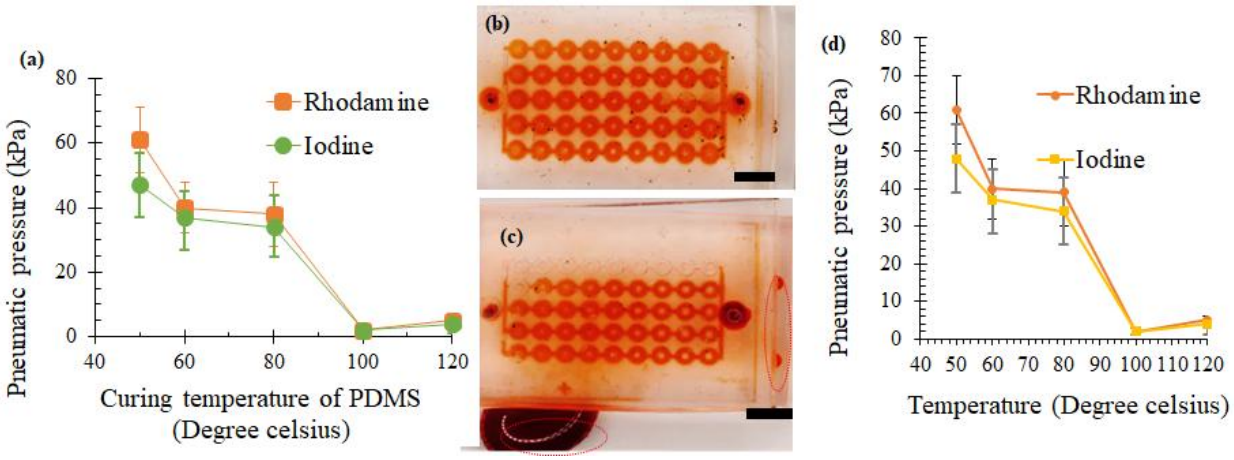

Figure 16 Adhesion measurements of PDMS SlipChip. (a) Pneumatic pressure measurements across different curing temperatures. (b) Leakage test with 50 cSt silicone oil at 1000 rpm. (c) Leakage test with 100 cSt silicone oil at 1000 rpm. Iodine solution flow in SlipChip (d) Effect of aging at 60 °C on the pneumatic pressure of PDMS samples initially cured for 2 h at different temperatures (50 °C, 60 °C, 80 °C, 100 °C, and 120 °C). Pressure was measured after 0, 2, and 4 h of aging at 60 °C. Results are presented as the mean ± standard deviation (N = 3).

3.3.3 Tensile Testing of PDMS Specimen Cured at Different Temperatures

Figure 17(a) presents the results of tensile testing. PDMS specimens cured at higher temperatures were more difficult to stretch and break, indicating increased rigidity.

This rigidity correlates directly with higher cross-linking density. Conversely, specimens cured at lower temperatures (50–60°C) exhibited greater elongation before failure, reflecting reduced cross-linking. This observation aligns with the higher burst pressures seen in Figure 16(a). It suggests that the increased availability of free polymer chains on surfaces cured at lower temperatures enhances interlayer van der Waals adhesion

Maximum elongation (99 mm) was observed at 60°C. This represents an optimal balance between cross-linking density and chain mobility, yielding both strength and flexibility. Interestingly, specimens cured at 50°C showed slightly less elongation (75 mm) compared to those at 60°C. This suggests that very low curing temperatures might result in insufficient cross-linking, creating a more fragile network structure. Notably, these same 50°C samples exhibited the highest burst pressure in pneumatic testing (Figure 16a).

Figure 17(b) quantifies the increase in stiffness using the modulus of elasticity, measured at 40% strain, which reflects the degree of cross-linking. The modulus remained low for specimens cured at 50°C (0.51 MPa) and 60°C (0.53 MPa). However, it increased sharply to 2.25 MPa at 80°C, and further rose to 4.31 MPa at 100°C and 5.45 MPa at 120°C. This progressive rise in modulus with curing temperature is consistent with previous findings by Konku-Asase et al. [84]. Although our values at 100°C and 120°C were slightly higher than their reported 3.7 MPa, the overall trend confirms that higher curing temperatures yield stiffer PDMS due to increased cross-linking density.

This observed increase in stiffness inversely correlates with the burst pressure results shown in Figure 16(a). Together, these findings reveal a critical trade-off in SlipChip design. Lower-temperature curing enhances sealing properties (higher burst pressure) by producing softer PDMS with more free polymer chains available for adhesion. In contrast, higher-temperature curing improves structural integrity by creating stiffer materials but compromises interlayer adhesion because fewer free chains are available. Consequently, optimizing the curing temperature is essential for balancing mechanical strength and sealing performance in PDMS SlipChips.

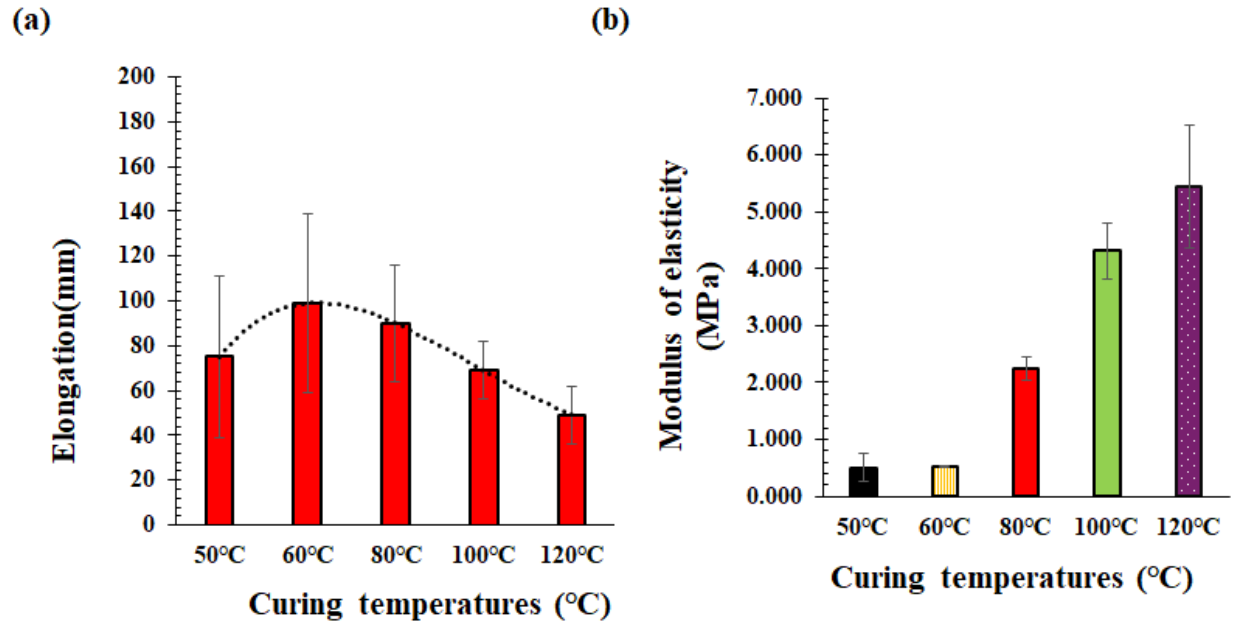

Figure 17 Effect of curing temperature on the mechanical properties of PDMS. (a) Elongation at break of PDMS samples cured at 50, 60, 80, 100, and 120°C. (b) Modulus of elasticity of PDMS samples cured at 50, 60, 80, 100, and 120°C.

3.3.4 Effects of Viscosity of Silicone Oils on Adhesion Between SlipChip Layers

Using the optimized PDMS curing protocol (top layer at 80°C and bottom layer at 60°C), we evaluated leakage performance using two different viscosity silicone oils. Figure 16(b,c) illustrates the leakage test results using an iodine solution. For devices coated with 50 cSt silicone oil, no leakage was observed when 200 µL of solution was injected over 10 seconds (equivalent to 20 µL/s flow rate), regardless of the spin coating speed (1000–2000 rpm). In contrast, devices coated with 100 cSt silicone oil showed different behavior depending on the spin coating speed. At lower speeds (1000 rpm and 1500 rpm), leakage occurred before reaching the target flow rate of 20 µL/s. However, at higher spin speeds (1800 rpm and 2000 rpm), the devices maintained proper sealing even at this flow rate.

This difference in sealing performance can be attributed to the nonuniform deposition of the higher viscosity 100 cSt silicone oil at lower spin speeds. Its higher viscosity causes the oil to form smaller droplets during spin coating, which later coalesce into larger bubbles [85]. These bubbles accumulate unevenly on the bottom PDMS layer, trapping air and increasing the separation between PDMS layers. This greater separation reduces van der Waals forces between the layers, weakening adhesion and leading to leakage under high flow rates.

Furthermore, as shown in Figure 18, the average deposition height of the oil gradually decreases with increasing spin-coating speed. Average deposition heights for 50 cSt and 100 cSt silicone oils were measured at 1000 rpm, 1500 rpm, 1800 rpm, and 2000 rpm. At 1000 rpm and 1500 rpm, the average deposition height for 100 cSt silicone oil exceeded 60 µm in thickness, in contrast to the thinner coat for 50 cSt oil. Although these measurements were taken before assembling the SlipChip layers, they provide insights into the initial oil distribution patterns. The significant difference in deposition heights between 50 cSt and 100 cSt oils, particularly at lower spin speeds, helps explain the observed variations in sealing performance. The thicker oil layer formed by 100 cSt oil at low rpm likely contributes to the formation of larger bubbles and subsequent leakage issues when the layers are assembled.

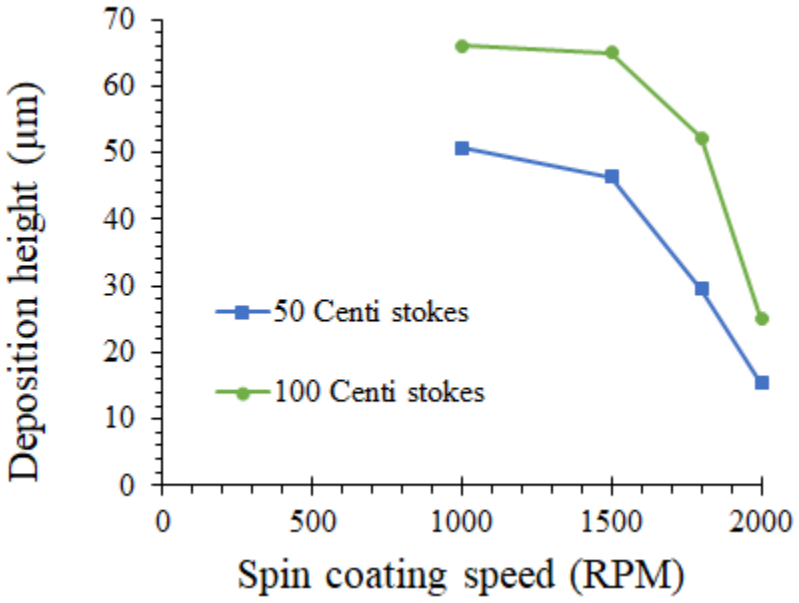

Figure 18 Deposition height of silicone oil on a bottom PDMS layer (cured at 60° C) at different spin coating speeds.

These results are noteworthy because they demonstrate that even low-viscosity silicone oil (50 cSt) can maintain high cell viability, a finding that is significant given previous studies showing that higher-viscosity silicone oils (e.g., 5,000 cSt) are more cytotoxic and suppressive to cell growth [116-117]. This highlights the potential utility of 50 cSt silicone oil as a safer and less cytotoxic option for applications requiring prolonged cell culture.

3.3.5 Biocompatibility Test of Silicone Oils

Figure 19 presents the results of a live/dead cell analysis conducted after 48 hours of cellular incubation in a 96-well plate. The fluorescence microscopy images show live cells stained with Calcein-AM (green fluorescence; Figure 19a, c, e, g) and dead cells stained with PI (red fluorescence; Figure 19b, d, f, h) for both SAOS-2 and LM-7 cells exposed to 50 cSt and 100 cSt silicone oils. The predominance of green fluorescence and minimal red fluorescence indicates high cell viability across all conditions. SAOS-2 cells (Figure 19 a-d) particularly demonstrated uniform cell distribution and high viability under both oil viscosities.

Quantitative analysis (Figure 19i) revealed that SAOS-2 cells maintained approximately 86% viability in both 50 cSt and 100 cSt oils, while LM-7 cells showed slightly lower viability at approximately 80% and 79% in 50 cSt and 100 cSt oils, respectively. While a slight decrease in viability was noted with 100 cSt oil compared to 50 cSt oil, this difference was minimal and not statistically significant. Higher-viscosity oils may slightly limit oxygen and nutrient diffusion due to their denser structure [88,89].

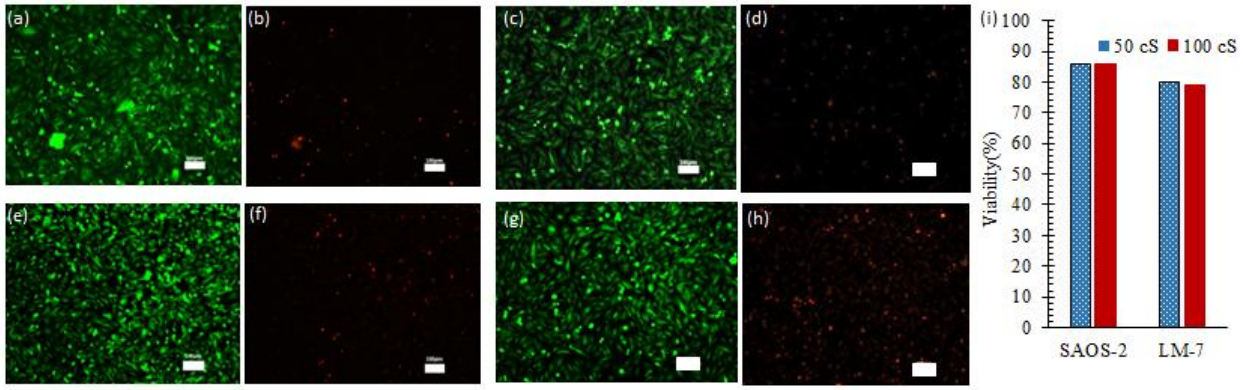

Figure 19 Live/Dead cell assay for SAOS-2 and LM-7 cells with silicone oils in a 96-well plate. (a,b) SAOS-2 cells for 50 cSt oil, (c,d) SAOS-2 cells for 100 cSt oil. (e,f) LM-7 cells 50 cSt oil. (g,h) LM-7 cells 100 cSt oil. Scale bars: 100µm. (i) Cell viability

3.3.6 Diffusion Mixing in SlipChip

Figure 20 illustrates the creation of a Rhodamine 6G concentration gradient in a SlipChip using ethanol as the solvent. Starting from a 4 mM stock solution, a single dilution was performed across six microwells with varying volumes, resulting in a concentration of 2.0 mM in the first well and 3.3 mM in the sixth well. Subsequent mixing in progressively smaller wells naturally created the gradient (Figure 20(a)).

To quantify the gradient, fluorescence intensities were measured for each microwell and normalized to facilitate comparison. The normalized intensity, denoted as $\bar{I}$, was calculated using the formula:

$$\bar{I} = \frac{I - I_{min}}{I_{max} - I_{min}} \quad \text{.....(3.1)}$$

where I is the measured intensity, I_{min} is the intensity of the lowest concentration (well 1), and I_{max} is the intensity of the highest concentration (well 6). This normalization ensured

that fluorescence intensity values ranged from 0 (well 1) to 1 (well 6), facilitating direct comparison between experimental and theoretical values.

This normalization ensured that the intensity in well 1 was set to 0 ($\bar{I}$=0) and in well 6 to 1 ($\bar{I}$=1), providing a standardized scale for comparing experimental and theoretical values. The relationship between fluorescence intensity (I) and Rhodamine 6G concentration (C) was found to be linear and is expressed as: $I = 4.4 \times 10^5 C - 7.8 \times 10^5$. Here, C represents the Rhodamine 6G concentration in mM. The coefficient of determination ($R^2 = 0.98$) indicates a strong correlation between fluorescence intensity and concentration.

The normalized fluorescence intensities, plotted in Figure 20(b), showed a gradual increase from well 1 to well 6, consistent with theoretical calculations. Statistical analysis (Figure 20(c)) confirmed a strong linear correlation between fluorescence intensity and theoretical concentration. These results validate that the SlipChip can generate reproducible concentration gradients, making it a reliable tool for biochemical assays requiring controlled diffusion and mixing.

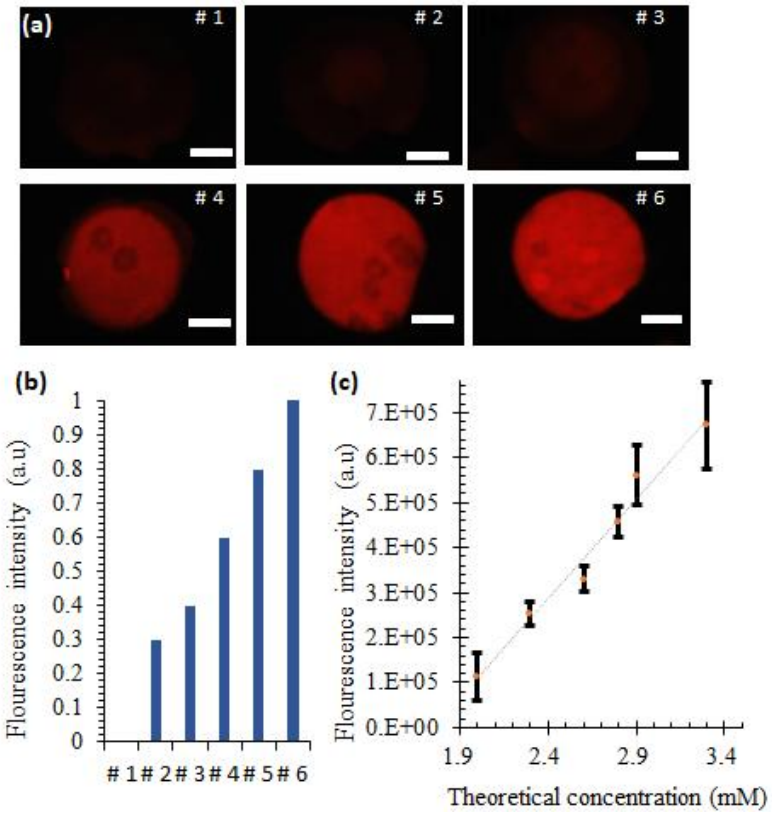

Figure 20 Fluorescence-based concentration gradient in SlipChip with 3.0 mm diameter microwells. Scale bars: 1mm. (a) Fluorescence images of microwells with various concentrations of Rhodamine 6 G. (b) Normalized fluorescence intensity against each well number. (c)Average fluorescence intensity against theoretical concentration.

3.3.7 SAOS-2 Cell culture in PDMS SlipChip

SAOS-2 cells were cultured in a PDMS SlipChip and a standard 96-well plate for a comparative study of cell health, morphology, and proliferation. Figure 21 illustrates the results of cell culture in both systems. Bright-field images (Figures 21(a) and 21(d)) show that SAOS-2 cells exhibited typical epithelial-like morphology in both systems, indicating good cell health. Calcein-AM staining (Figures 21(b) and 21(e)) confirms that cells were well-elongated and spread, supporting their viability. The percentage of live cells after 24 hours was 93.2%±1.3% (N=3) in the SlipChip and 94.6%±0.5% (N=2) in the 96-well plate (Figure 21(h)), demonstrating that the SlipChip provides a comparable environment for maintaining cell health.

Cell length was analyzed as an indicator of cell culture quality. Shorter cell lengths and rounded shapes typically signify a stressed state, whereas elongated cells indicate a relaxed state and healthy proliferation. As shown in Figure 21(g), the average cell length of SAOS-2 cells was 86.9 µm (N=62) in the SlipChip and 82.1 µm (N=17) in the 96-well plate, consistent with previous findings of 78 µm, further supporting the suitability of the Slip-Chip for cell culture [90].

Cell proliferation was evaluated based on cell density after 24 hours. Cells were seeded at an initial density of 100 cells/µL in both systems. After 24 hours, the cell density reached 550 cells/µL (N=3) in the SlipChip and 898 cells/µL (N=2) in the 96-well plate. The slightly lower density observed in the SlipChip is likely due to medium evaporation caused by the porous nature of PDMS. Overall, these results demonstrate that PDMS is a biocompatible substrate for cell culture and that the three-dimensional encapsulated environment provided by the SlipChip is suitable for high-throughput biochemical analysis.

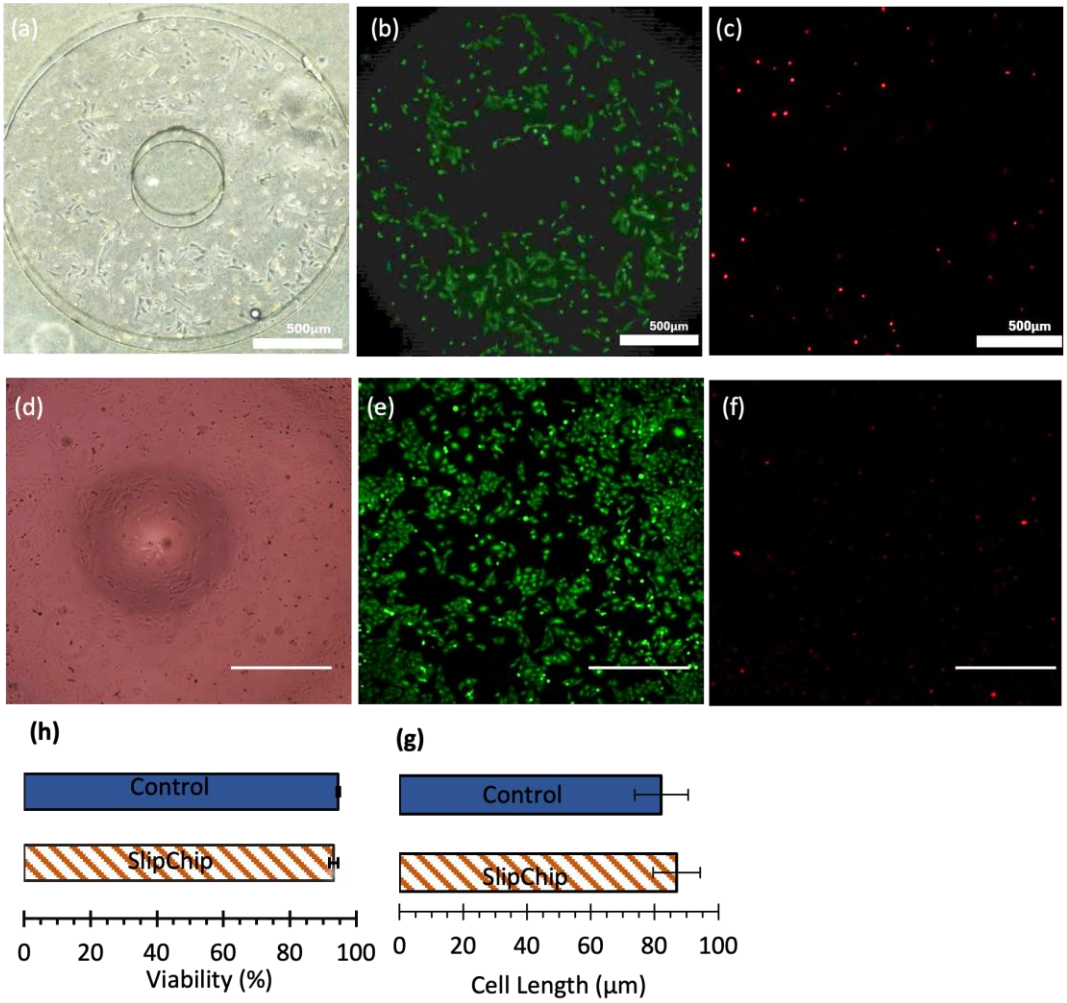

Figure 21 Comparison of cell culture in SlipChip and 96-well plate. (a)-(c) Bright-field, live (Cal-cein-AM-stained), and dead (PI-stained) cell images of SAOS-2 cells cultured in the SlipChip. Scale bar: 500 μm. (d)-(f) Bright-field, live (Calcein-AM-stained), (g) Average SAOS-2 cell length in the SlipChip (mean ± STD: 86.9 ± 7.3 μm) and 96-well plate (mean ± STD: 82.1 ± 8.4 μm). (h) Live and dead cell assay results showing comparable cell viability in both systems.

3.3.8 Comparative Analysis of SlipChip Performance

Table 3 provides a comprehensive comparison of different SlipChip systems across critical parameters, including materials, lubricants, sealing methods, and biological applications. Our PDMS SlipChips with low-viscosity silicone oil (50 cSt) achieve performance comparable to high-viscosity alternatives while offering significant fabrication advantages. Chang et al.'s configuration using 10,000 cSt silicone fluid showed marginally higher cell viability (>99% vs. 95%) [63], but our direct spin-coating approach substantially simplifies manufacturing compared to their multi-step procedure, while maintaining similar culture durations and sealing performance.

The high cell viability in Chang et al.'s system[76] using high-viscosity silicone fluid may be attributed to their multi-step coating process, which likely creates an exceptionally thin lubricant layer that minimizes direct cell exposure while maintaining effective sealing. Direct application of high-viscosity oils would typically increase microchannel blockage rates. The comparable cell viability between mammalian systems confirms that low-viscosity oils effectively support cell culture without the blockage issues of higher-viscosity lubricants, providing a more accessible approach for general laboratory use.

While mammalian cell culture applications span multiple days, where material properties and gas permeability become critical factors, bacterial assays require significantly shorter timeframes, making the choice between glass and PDMS less consequential for these applications. This material flexibility is evidenced by successful bacterial studies using both PDMS with silicone oil (Li et al.) and glass with fluorinated oil (Shen et al.)[74,77]. The comparable performance across these different material configurations for short-term bacterial applications further validates SlipChip as a versatile platform adaptable to various biomedical applications with different temporal requirements.

Table 3. Effects of the viscosity of silicone oil on sealing performances and biocompatibility

Material	Lubricant	Sealing procedure	Cell type	Culture/Assay period	Cell Viability / cytotoxicity	Reference
PDMS	50 cSt silicone oil	Direct spin-coat	Mammalian (SAOS-2)	4 days	95% (Live/Dead assay)	This study
PDMS	10,000 cSt silicone fluid	Spin-coat, transfer, assemble	Mammalian (A549, MRC-5, ES-D3)	4–10 days	>99% (Live/Dead assay)	Chang et al., 2015 [91]
PDMS	Silicone oil	Spin-coat, transfer, assemble	Bacteria (*E. coli* O157:H7, *S. aureus*, *S. typhimurium*, *L. monocytogenes*)	30–60 min	Not specified (biosensing only)	Li et al., 2024 [92]
Glass	Fluorinated oil (FC-40)	Direct capillary fill	Bacteria (*E. coli* RP437, RP1616)	30–60 min	Not specified (Recovered cells were culturable)	Shen et al., 2014 [24]

3.4 Conclusions

This study investigated and addressed critical limitations associated with the use of high-viscosity silicone oils in PDMS-based SlipChip microfluidic devices. SlipChips are increasingly employed in biomedical applications for their unique ability to control fluid flow through sliding interfaces. However, the choice of lubricant and fabrication parameters significantly affects device performance. High-viscosity silicone oils, while commonly used to prevent leakage, often introduce problems such as microchannel blockages, increased resistance to motion, and inconsistent fluid delivery. These issues hinder the functionality and reproducibility of SlipChip systems, especially in sensitive biological applications.

To overcome these challenges, we explored the use of low-viscosity silicone oils as an alternative to their higher-viscosity counterparts. We also optimized the thermal curing conditions of the PDMS layers, recognizing that curing temperature affects surface properties such as adhesion, stiffness, and interaction with lubricants. Our experimental findings showed that a dual-layer curing protocol—curing the bottom PDMS layer at 60°C and the top layer at 80°C—provided the most effective balance. This configuration enhanced adhesion at the contact interface to ensure reliable sealing, while the increased stiffness of the top layer facilitated smooth and consistent slipping during device operation.

Among the lubricants tested, a low-viscosity silicone oil with a viscosity of 50 centistokes (cSt) was identified as the most effective. This oil minimized the risk of channel blockage while maintaining the essential characteristics required for SlipChip functionality, including effective sealing and smooth sliding behavior. Importantly, the use of 50 cSt silicone oil also demonstrated low cytotoxicity, making it suitable for applications involving live cells.

To validate biocompatibility, in vitro testing was performed using SAOS-2 osteosarcoma cells. The results confirmed that the 50 cSt silicone oil did not adversely affect cell viability. Cell proliferation and morphology were comparable to those observed in standard multiwell tissue culture plates, confirming the lubricant's compatibility with biological assays and cell culture environments.

Overall, this study highlights the critical role of lubricant viscosity and PDMS curing conditions in determining the performance of SlipChips. The combination of low-viscosity lubricant and optimized curing not only resolved key issues such as channel blockages and impaired slipping but also enhanced biocompatibility. These improvements offer significant practical value for researchers developing microfluidic platforms for biological applications.

The demonstrated reliability and biocompatibility of the modified SlipChip system position it as a promising tool for a variety of downstream applications, including high-throughput drug screening, protein detection assays, and mammalian cell culture studies. By offering a scalable, reproducible solution to existing limitations, this work paves the way for the broader use of SlipChips in both research and clinical diagnostics.

Chapter 4 Micrometer-Controlled Alignment and Optimized Width Ratio with Magnetic Sealing for Leak and bubble-Free Gradient Formation in PDMS SlipChip

4.1 Introduction

The SlipChip is widely used in precision medicine, drug studies, and bacterial detection for its ability to run multiple microscale tests via simple slip motion. However, its performance depends on preventing leakage and bubble formation, requiring precise alignment and effective sealing. To address this, we developed an optimized SlipChip with a magnetic aligner for accurate x-y movement and an oil absorption method to prevent leakage. We optimized a dimensionless factor known as the width ratio between the microchannel and microwell to minimize bubbles. Fluid tracing with dye confirmed smooth operation and reliable gradient generation.

SlipChips are a novel type of microfluidic devices known for multiple and cost-effective assessments at the lab and industrial scale. The device's capability of minimal sample consumption (biological or chemical) makes it a cost-friendly choice. The precision of the system is marked by controlled fluid flow through simply designed microchannels. By combining these elements, SlipChip is able to deliver high through put assessments. These are easily controlled gadgets with a series of discrete channels and microwells in the top and bottom layers. Just sliding the top layer over the bottom layer provides fluidic control and transport from one microwell to another. Smooth sliding for its operation is important; this is why the lubricant is positioned between the top and bottom layers [21,25,93,94]. The SlipChip's unique design allows for diffusive mixing of fluids when microwells overlap during the slipping motion [93]. This clever mechanism enables the device to perform multiple isolated biochemical fluid analyses within individual microwells. By leveraging this overlap-induced mixing, the SlipChip can efficiently conduct a variety of complex fluidic tests in a compact and controlled environment [93]. Using the SlipChip, Yu. M has performed the Digital Loop-Mediated Isothermal Amplification of Hepatitis B virus. A similar work on human papillomavirus is demonstrated by Yu. Z [95]. Shen. F did a digital PCR on SlipChip [25]. Cai. G *et al.* has done bacterial detection in an enzymatic assay using SlipChip [26]. Shen c., et al has done a similar study of bacterial chemotaxis of E.coli strain using SlipChip [74]. However, the slip action

of the device also comes with an operational constraint. To have a good slipping motion, we cannot permanently seal the PDMS layers. This lack of sealing makes excessive air traps within the device, causing leakage [93]. This liquid loss leads to less sensitivity and unstable analysis. To avoid air trapping and improve the sealing between PDMS layers researchers have been trying to hold the device in clamps or clips [96,97]to improve the sealing pressures so that the fluid can flow in tightly enclosed channels. However, these setups allow 1-D movement only. Our research aims to address these challenges by implementing magnetic sealing and a novel lubrication protocol of oil absorption. We leveraged the porous nature of PDMS [98] by saturating the SlipChip layers with silicone oil, effectively preventing fluid escape [99–101].

The inherent hydrophobicity of PDMS makes microfluidic devices, particularly SlipChips, susceptible to bubble formation—an issue that poses significant challenges for maintaining reliable sealing. Bubbles can severely compromise device performance by displacing fluid within microwells, altering intended volumes. Studies have shown that microchannel geometry can influence bubble dynamics [102]. According to Young's Laplace equation, narrower channels induce higher pressure differences, which enhance fluid velocity [103]. We hypothesized that transitioning from narrow microchannels to wider microwells would result in a sudden velocity drop, thereby reducing shear stress and promoting bubble detachment rather than entrapment [102,104]. To address this, we introduced the concept of a dimensionless "width ratio" (WR)—defined as the ratio of microwell to microchannel width—and postulated that a higher WR would decrease the likelihood of bubble formation. To test this, we fabricated SlipChips with WRs of 3, 4, and 5. To our knowledge, no prior study has systematically optimized WR for bubble minimization in PDMS-based SlipChips.

Conventional designs often suffer from bubble formation, poor sealing, and misalignment due to clamping-based assembly, limiting their applicability in sensitive fields like protein detection and drug delivery. To overcome these limitations, we developed SlipChips incorporating WR optimization, an oil absorption lubrication strategy, and a novel 3D-printed magnetic aligner enabling precise two-dimensional movement. The aligner leverages magnet–spring force interactions to facilitate smooth and accurate alignment, while the oil absorption protocol ensures reliable sealing without leakage. This integrated approach represents a significant advancement in SlipChip design, addressing critical gaps in microwell optimization, lubrication, and alignment precision for improved device performance and operational reliability.

4.2 Materials and Methods

4.2.1 Design of SlipChip

SlipChips were designed with width ratios of 3, 4, and 5, and varying top-layer depths to generate gradient concentrations. Each layer contains microwells connected by uniform 0.18 mm-wide channels. During operation, aligned channels enable fluid loading, and overlapping microwells facilitate diffusive mixing. Pitcher-like channel openings ensure complete microwell filling when layers are aligned. While bottom-layer microwells have fixed dimensions (0.15 mm depth), top-layer depths vary to create gradients. Detailed top layer dimension for width ratio 3,4 and 5 are listed in Table 1.

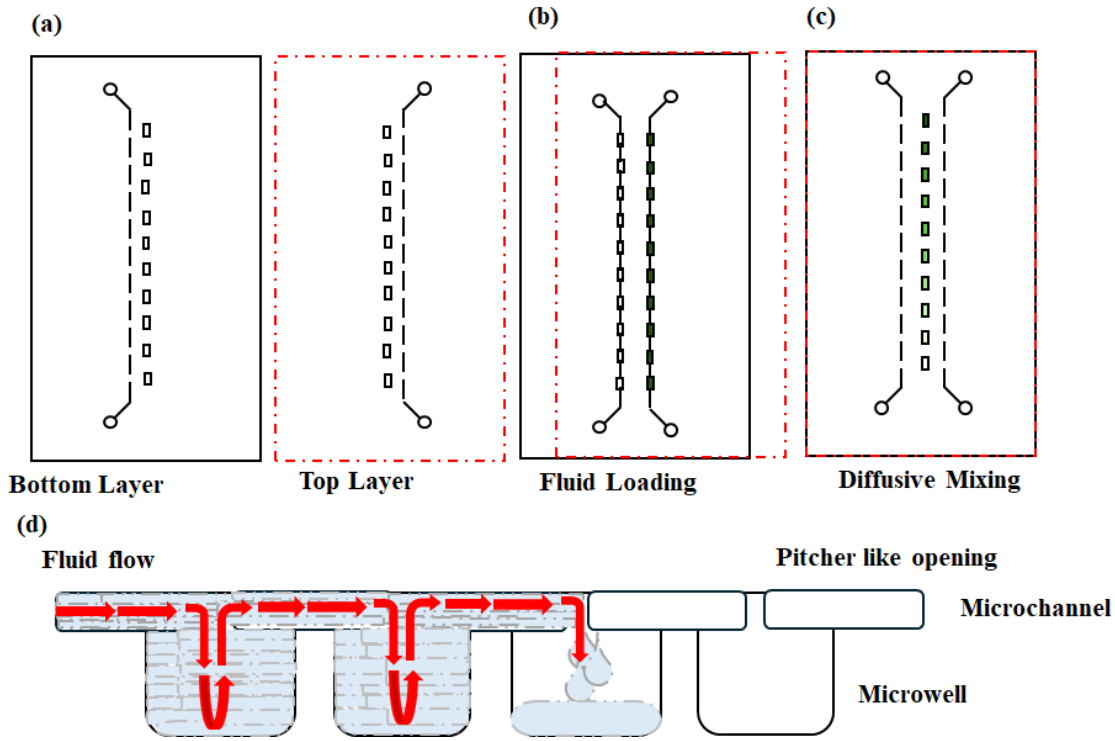

Figure 22 The operation and working mechanism of SlipChip. (a) Top and bottom layer of SlipChip. (b) Fluid loading phase after microchannel and microwell overlapping (c) Diffusive mixing phase by microwell overlapping in both layers. (d) Fluid flowing through microchannels and filling microwells.

4.2.2 Design and Fabrication of the Magnetic Aligner

The magnetic aligner (Figure 23) was designed for precise and reversible translation of SlipChip layers along the x–y axes. It ensures consistent sealing during operation through a combination of magnetic and mechanical components. The system includes upper and lower

supports with alignment windows and magnet seats. These supports are housed in a custom 3D-printed base (FDM, Adventurer 4, FlashForge). Neodymium magnets (20 mm × 12 mm × 5 mm, MonotaRO Co., Ltd.) provide vertical sealing force and lateral alignment. Two orthogonally mounted micro gauges enable controlled movement in both directions. Mechanical springs opposite the gauges store elastic energy for auto-return functionality. This spring–magnet design supports smooth slipping and precise microwell overlap. Embedded PLA frames in the PDMS structure ensure alignment and mechanical stability. Together, these features enable leak-free operation and reliable device performance.

Table 4. Dimensions and Volumes of SlipChip Top Layer

Width Ratio	Measurement	1	2	3	4	5	6	7	8	9	10
WR3	Depth (mm)	0.15	0.30	0.45	0.60	0.75	0.90	1.05	1.20	1.35	1.50
	Volume (mm^3)	0.072	0.144	0.216	0.288	0.360	0.432	0.504	0.576	0.648	0.720
WR4	Depth (mm)	0.15	0.30	0.45	0.60	0.75	0.90	1.05	1.20	1.35	1.50
	Volume (mm^3)	0.135	0.270	0.405	0.540	0.675	0.810	0.945	1.080	1.215	1.350
WR5	Depth (mm)	0.15	0.30	0.45	0.60	0.75	0.90	1.05	1.20	1.35	1.50
	Volume (mm^3)	0.18	0.365	0.548	0.769	0.914	1.096	1.279	1.462	1.645	1.828

4.2.3 Fabrication of the SlipChip

SlipChips were fabricated using polydimethylsiloxane (PDMS, Silpot 184 W/C, Dow) through a two-layer casting technique designed to enhance mechanical integrity and preserve microscale structural fidelity. To improve the overall stability and handling of the devices, polylactic acid (PLA) support frames were incorporated. These frames were produced using a fused deposition modeling (FDM) 3D printer (Adventurer 4, FlashForge), offering precise dimensional control and ease of customization for different experimental designs.

High-resolution molds were created using LCD VAT stereolithography with the Sonic Mini 8K printer (Phrozen), which offers exceptional accuracy suitable for microfluidic applications. Following initial printing, the molds underwent a thorough ultraviolet (UV) curing process for 24 hours to ensure complete polymerization and structural strength. Subsequently, they were post-cured in an oven at 80 °C for an additional 4 hours to further harden the features and enhance their durability during PDMS casting.

To facilitate easy demolding and maintain fine feature details, the mold surfaces were treated with PFOTS (perfluorooctyltrichlorosilane)—a fluorinated silane compound known to impart hydrophobicity and reduce adhesion between the mold and PDMS. This step was critical in ensuring that the final PDMS structures retained sharp, accurate geometries without tearing or distortion during the release process.

PDMS base and curing agent were mixed in a 10:1 ratio by weight and degassed to remove trapped air bubbles. The mixture was then poured into the silanized mold to create the first layer, which was partially cured at 60 °C for 40 minutes. At this semisolid stage, the pre-fabricated PLA frames were carefully positioned onto the PDMS layer. After an additional 30 minutes of heating, a second layer of PDMS was poured over the frames to encapsulate them fully. The entire assembly was then cured completely, removed from the mold, and cleaned with isopropanol and ethanol. Final inspection ensured there were no surface defects or deformities.

.

4.2.4 Effects of Oil Viscosities on their Absorption in PDMS

To ensure smooth slipping of SlipChip layers without clogging micropatterns, a novel oil absorption technique was employed using the inherent porosity of PDMS. Silicone oils of four viscosities (50 cSt, 100 cSt, 500 cSt, and 1000 cSt), each dyed with Oil Red O (Sigma Aldrich, St. Louis, MO, USA), were tested [93]. Four pieces of PDMS were placed in each of the dyed oil and its absorption was observed after 24 hours.

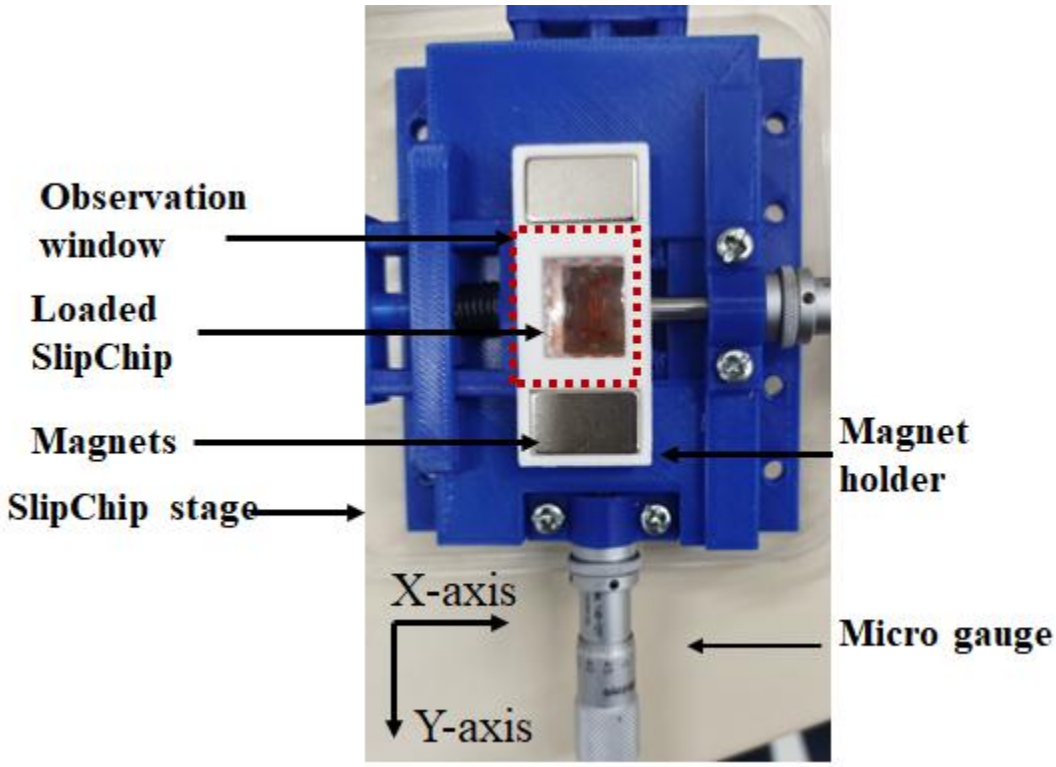

Figure 23 Magnetic aligner holding layers of SlipChip in frames containing magnets.

4.2.5 Pneumatic Testing as a Measure of Adhesion between PDMS Surfaces

To prevent clogging of micropatterns, residual oil was removed from PDMS surfaces after full absorption. Adhesion between PDMS layers was then quantified based on the pneumatic pressure required to separate them. Pairs of PDMS layers, each pre-soaked in a specific oil and subsequently cleaned, were aligned and stacked. Pneumatic pressure was gradually applied through the inlet and outlet ports until the layers detached [93]. The pressure at the point of separation was recorded as a measure of interfacial adhesion strength.

4.2.6 Effects of temperature on Oil Absorption

Small PDMS cubes were immersed in each oil within Petri dishes at two temperature conditions: room temperature and 55 °C (Figure 24). Initial absorption tests were conducted over 24 hours, followed by a focused study on time and temperature dependence using freshly cut PDMS cubes in 1000 cSt oil. Oil penetration depth was measured with a digital microscope (KEYNEX, VHX-7000) at 20× magnification.

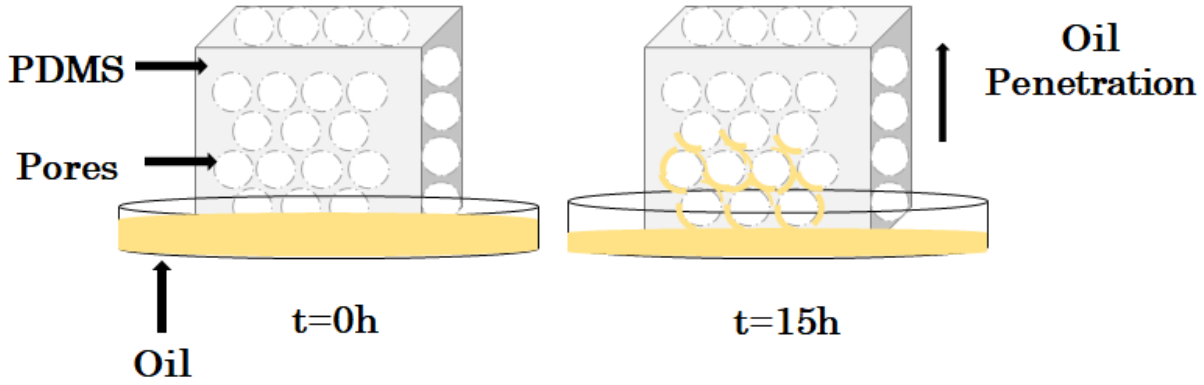

Figure 24 Schematic of oil penetration into porous PDMS.

4.2.7 Demonstration of Diffusive Mixing

After fabrication, the bottom SlipChip layers were lubricated by stamping with silicone oil and assembled onto the top layers. The assembled device was then incubated at 55 °C for 2 hours to facilitate oil absorption and ensure smooth interlayer movement. Device performance was assessed by generating six gradient concentrations of a green food dye (2% w/v in isopropanol; MonotaRO, Japan) through diffusive mixing. As illustrated in Figure 22 (c), equal-volume microwells in the bottom layer were filled with the dye solution, while the top layer was loaded with pure isopropanol. The magnetic aligner was used to precisely align the microwells, initiating lateral diffusion between the layers. Once mixing was complete, the layers were returned to their original positions to isolate discrete concentration zones. Microscopic images were captured at 20× magnification using a digital microscope (KEYNEX, VHX-7000), and intensity values from each microwell were compared with theoretical concentrations. Additionally, bubble formation was quantified across different SlipChip designs by calculating the percentage of each microwell's cross-sectional area occupied by bubbles.

4.3 Results and Discussions

4.3.1 Effects of Oil Viscosities on its Absorption

Sacrificial testing was performed to evaluate oil absorption. As shown in Figure 25, PDMS samples submerged in each oil for 24 hours were examined under a digital microscope to measure the depth of oil penetration. Results showed that all oils, regardless of viscosity, fully permeated the porous PDMS within 24 hours, confirming effective oil absorption across all conditions.

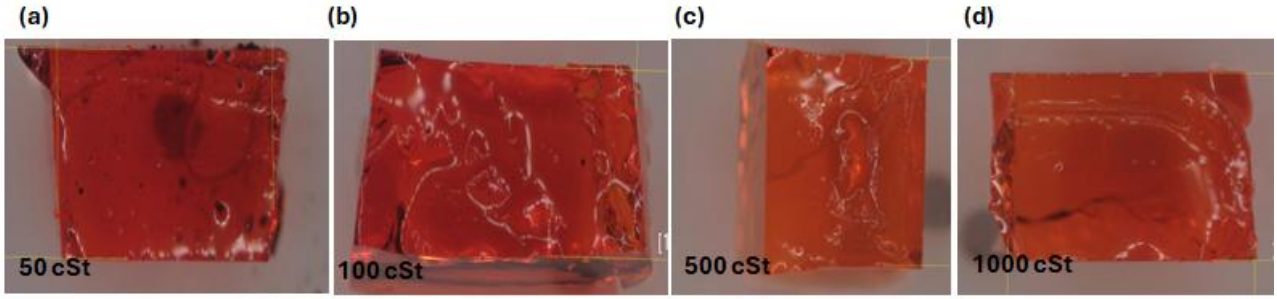

Figure 25 PDMS blocked soaked in silicon oil for 24 hours. (a) 50cSt silicone oil, (b) 100cSt silicone oil, (c) 500 cSt silicone oil, and (d) 1000 cSt silicone oil.

4.3.2 Adhesive Measurement with Pneumatic Testing

To prevent practical issues such as micropattern clogging, PDMS layers soaked in various silicone oils were thoroughly cleaned to remove surface residues. Layers treated with the same type of oil were then paired and subjected to pneumatic testing to evaluate interfacial adhesion after oil absorption, under conditions where no visible oil remained on the surfaces. The test involved gradually increasing pneumatic pressure until the layers separated. As shown in Figure 26, among all samples, the PDMS layers treated with 1000 cSt silicone oil exhibited the highest separation pressure of 260 kPa, indicating strong post-absorption adhesion.

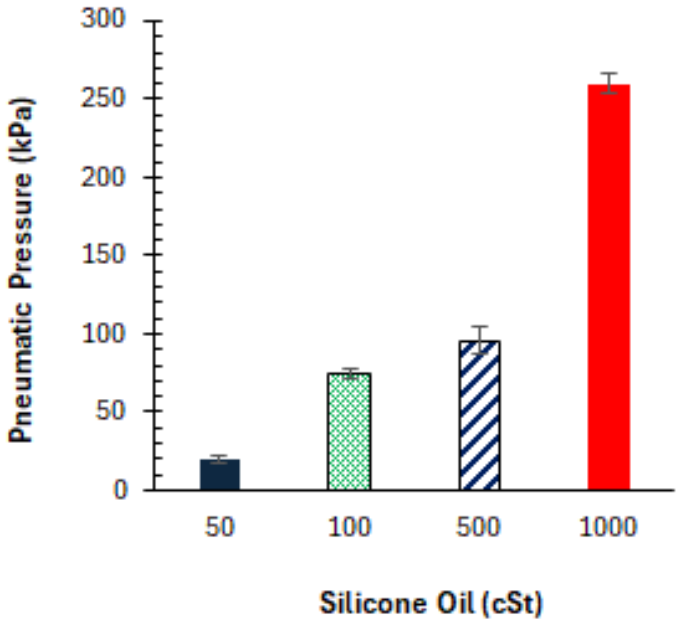

Figure 26 Pneumatic testing on PDMS surfaces soaked in 50cSt, 100 cSt, 500 cSt, and 1000cSt silicone oil.

4.3.3 Effects of Temperature on Oil Absorption

Based on the results of pneumatic adhesion testing, 1000 cSt silicone oil was identified as the most effective lubricant for use between SlipChip layers. To optimize the lubrication process, the time-dependent behavior of oil absorption into PDMS was further investigated using 1000 cSt oil. As shown in Figure 27(i), PDMS samples incubated at 55 °C exhibited significantly faster oil penetration, reaching a depth of approximately 6600 µm, compared to 3677 µm for samples maintained at room temperature. These results demonstrate that elevated temperatures substantially enhance the rate and extent of oil absorption. Notably, at all measured time points (excluding the initial 0 h), oil penetration at 55 °C exceeded that observed at room temperature, confirming the thermal acceleration of the lubrication process. Consequently, pre-heating PDMS layers in silicone oil was established as a practical method to expedite soaking and improve lubrication efficiency. The final validation involved testing SlipChip layers soaked in 1000 cSt silicone oil for 6 hours at 55 °C, confirming consistent and effective lubrication under these conditions.

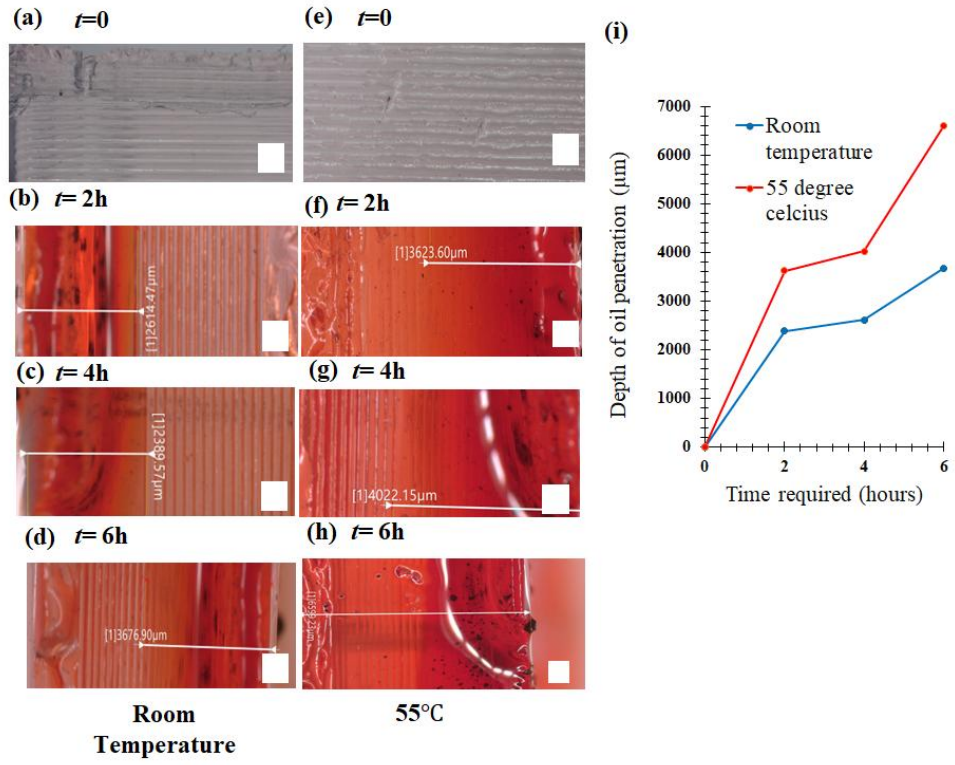

Figure 27 Temperature and temporal assessment of 1000 cSt silicone oil absorption in PDMS. (a),(b),(c),(d) Oil absorption at room temperature for 0h, 2h, 4h, and 6h. (e), (f),

(g), (h) oil absorption at 55°C for 0h, 2h, 4h, and 6h. (i) Comparison of 1000 cSt silicone oil penetration in PDMS at room temperature and 55°C.

4.3.4 Development of Gradient Concentrations in SlipChip with Different Width Ratios

SlipChips, fabricated via soft lithography and assembled within a custom 3D-printed magnetic aligner, were lubricated using an oil absorption technique involving 1000 cSt silicone oil at 55 °C. As shown in figure 28(a), (b) and (c), devices with width ratios (WR) of 3, 4, and 5 were tested using a green food dye–isopropanol (IPA) system to evaluate performance. Each test was conducted in triplicate to ensure reproducibility. Throughout all trials, no leakage was observed in any of the SlipChip configurations. These results confirm that the oil absorption method, combined with magnetic sealing, effectively facilitates smooth interlayer slipping while maintaining robust sealing between the PDMS layers. This approach proved reliable across all width ratios and ensured consistent fluid containment during operation. Figure 28(d) illustrates the gradient concentration profiles achieved in each SlipChip design. The SlipChip with a width ratio (WR) of 3 failed to produce a consistent gradient, exhibiting a highly irregular pattern with sharp drops—likely due to bubble entrapment disrupting fluid volumes. The WR 4 design showed an overall increasing trend, but with noticeable fluctuations at microwells 3 and 5, again suggesting interference from bubble presence. In contrast, the SlipChip with WR 5 demonstrated a smooth and gradual formation of concentration gradients. This consistent behavior is attributed to minimal or no bubble formation, resulting in more uniform fluid distribution and reliable diffusive mixing.

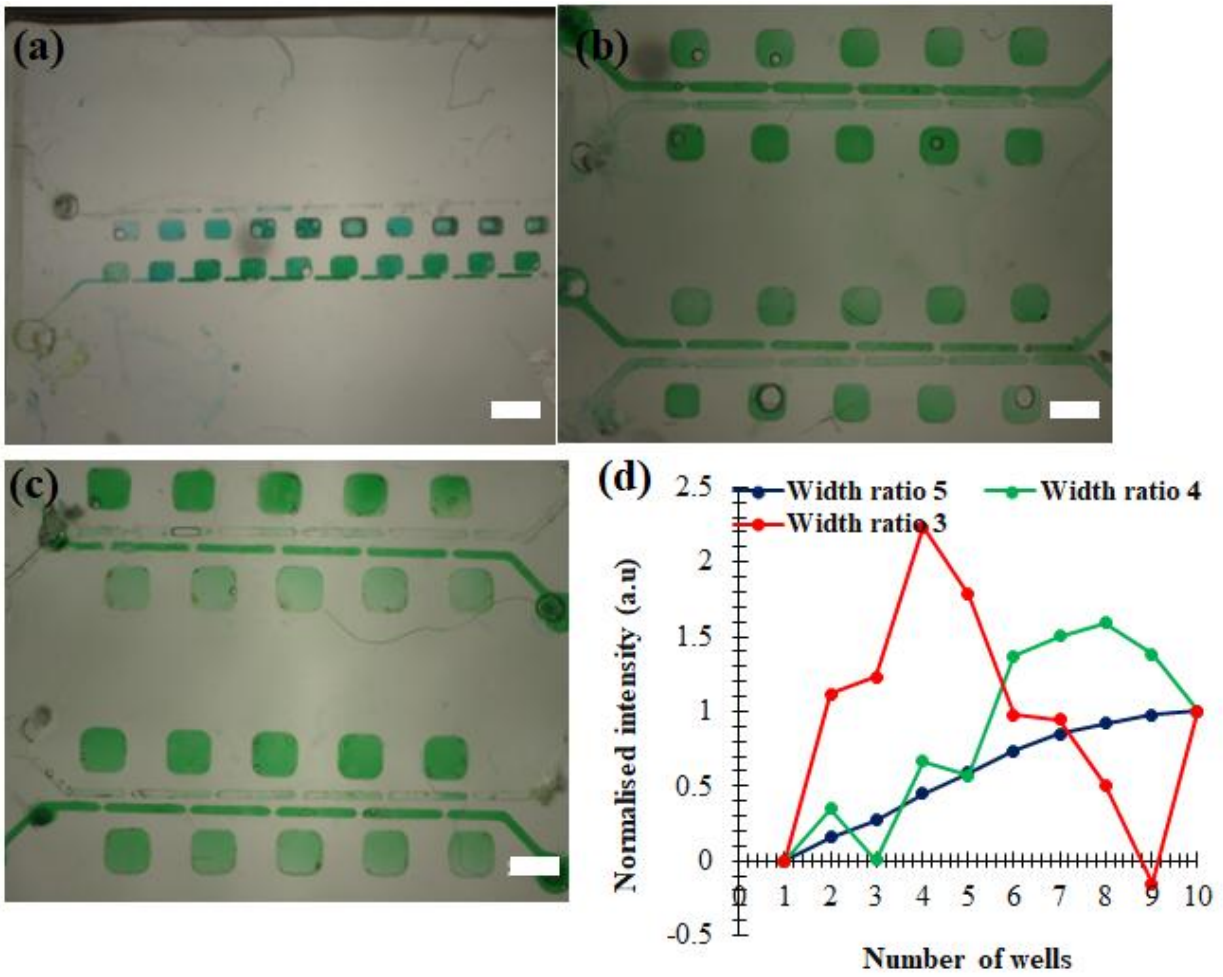

Figure 28 Results of diffusive mixing (N=3) (a) Width ratio 3, (b) Width ratio 4, (c) Width ratio 5. The scale bars are 1000μm. (d) Development of gradient concentrations in SlipChips with width ratios of 3, 4, and 5 (N=3).

4.3.5 Effects of Width Ratio on Bubble Prevention

As shown in Figure 29(a), the average number of bubbles observed in the device decreased with increasing width ratio (WR). The SlipChip with WR 3 exhibited the highest bubble count (13), while the WR 5 design had the fewest (5). This trend can be attributed to the effect of microwell geometry on fluid dynamics—wider microwells slow the fluid velocity, reducing the energy available to sustain shear stresses [102,104]. This lower energy state facilitates bubble detachment, as the fluid more easily displaces bubbles from the microwells. Figure 29(b) further confirms that bubble coverage is significantly higher in narrower microwells. In these confined geometries, microbubbles are more prone to coalescing into larger bubbles [105,106]. Additionally, the higher pressure gradients in narrower channels demand greater energy to drive fluid movement. When insufficient energy is available, larger bubbles remain trapped, obstructing fluid entry and

flow, thereby contributing to clogging in SlipChips with lower WRs. In contrast, in devices with wider microwells, the transition from narrow channels to broader wells results in a substantial drop in fluid velocity relative to pressure, increasing shear stress at the interface. This condition favors bubble detachment and reduces the likelihood of air entrapment [107].

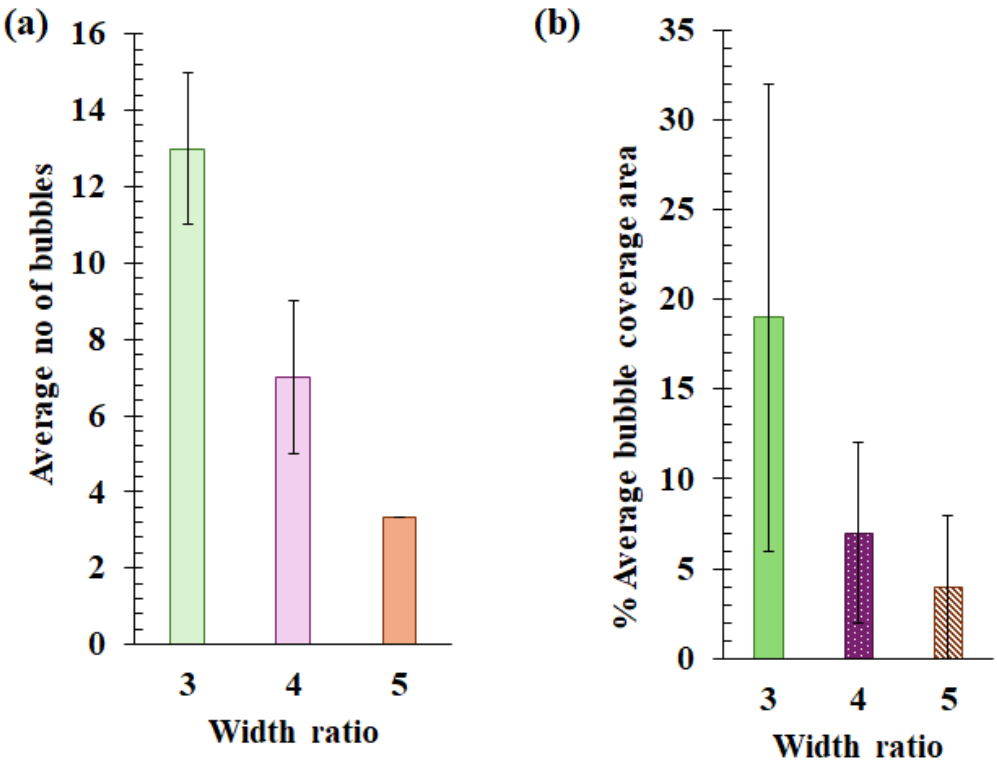

Figure 29 Bubbles remained in SlipChip with width ratios 3,4 and 5. (a) Average number. (b) Average bubble coverage area.

4.4 Conclusions

This study presents the development and validation of a polydimethylsiloxane (PDMS)-based SlipChip system that integrates magnetic sealing with a novel oil absorption lubrication strategy to achieve smooth, reliable, and leak-free microfluidic operation. Traditional SlipChip designs often face challenges related to air bubble formation, fluid leakage, and lubricant contamination, all of which can compromise the precision and reproducibility of bioanalytical assays. In response, this work introduces geometric optimization and innovative lubrication techniques to overcome these obstacles and improve overall device performance.

A key focus of the study was the geometric modification of the SlipChip's microstructure, specifically the width ratio (WR) between microchannels and microwells. Three different WR

configurations—WR 3, WR 4, and WR 5—were systematically investigated to assess their effect on air bubble formation and fluid dynamics. It was found that increasing the WR led to a marked reduction in both the number and surface coverage of air bubbles. This is significant because the presence of bubbles in microfluidic systems can disrupt the uniform flow of fluids, distort concentration gradients, and interfere with cell behavior in biological applications. Among the three designs, the SlipChip with WR 5 demonstrated the most effective and consistent generation of concentration gradients across ten microwells, indicating its superior performance for analytical precision and controlled reagent delivery.

The lubrication strategy also played a crucial role in the system's success. Unlike traditional approaches that leave a thin film of silicone oil between PDMS layers, our method involved the application of 1000 cSt silicone oil followed by surface cleaning to remove excess lubricant. This oil absorption technique maintained a dry yet mobile interface, preserving sealing integrity while allowing the top PDMS layer to slip freely over the bottom layer. Achieving leak-free performance without residual surface oil is especially valuable for bioassays and diagnostic platforms where contamination must be minimized.

Furthermore, the ability to operate the SlipChip without bubble interference ensures more accurate fluid loading and improves the reliability of experiments involving sensitive biological samples. This is particularly beneficial in cell-based assays, where bubble-induced shear stress or misdistribution of media can negatively impact cell viability. In this context, the device demonstrated strong potential for applications involving osteosarcoma cell research, enabling consistent gradient formation and safe fluid manipulation.

In conclusion, the integration of geometric optimization with an innovative lubrication strategy has resulted in a highly functional PDMS-based SlipChip platform. The combination of WR 5 design and post-lubrication cleaning allows for reliable operation, minimized bubble interference, and precise fluid control—all critical parameters for the success of biomedical applications. This work lays a strong foundation for extending SlipChip use in protein detection, targeted drug delivery, and broader microfluidic diagnostics, particularly in research involving mammalian cell cultures.

The magnetic aligner system and WR=5 optimization eliminate the three primary technical barriers that have previously prevented reliable biological gradient formation: leakage (solved by

oil absorption method), bubble formation (solved by width ratio optimization), and misalignment (solved by magnetic aligner). This technical foundation enables the transition from proof-of-concept demonstrations to practical MEC determination for clinical translation.

Chapter 5 SlipChip-based 3D Cell Culture for the Study of Osteosarcoma Cell Growth

5.1 Introduction

Osteosarcoma (OS) is a highly aggressive primary malignant bone tumor that commonly affects both adolescents and adults [108]. One of the most challenging aspects of OS is its high metastatic potential and strong resistance to chemotherapy and radiotherapy, often resulting in tumor recurrence even after intensive therapeutic regimens [109]. Understanding the biological mechanisms that drive cell proliferation and resistance is essential for developing more effective treatments. In this context, abnormal cell growth is not only a hallmark of cancer progression but also a key factor that underlies metastasis and chemoresistance. This research addresses the critical absence of integrated systems that can both reproduce complex osteosarcoma tumor microenvironments and systematically evaluate drug efficacy—a fundamental gap that limits the development of personalized treatment protocols. The platform's versatility supports therapeutic evaluation across molecular weights ranging from 500 Da to greater than150 kDa, addressing the diverse drug classes relevant to modern osteosarcoma treatment.

In the present study, we investigated the effect of ascorbic acid (AsA)—the active form of vitamin C—on osteosarcoma cell proliferation using a PDMS-based SlipChip microfluidic platform. Vitamin C has recently gained renewed interest in cancer research due to its diverse physiological roles, including collagen synthesis, immune modulation, and induction of apoptosis in malignant cells [109], [110]. It enhances immune cell activity, particularly increasing the number and function of white blood cells, which contribute to the body's defense against cancer [111]. Moreover, high concentrations of AsA have been reported to exhibit selective cytotoxicity toward tumor cells, while promoting apoptosis and reducing the viability of cancerous tissues. Notably, as osteosarcoma is believed to originate from mesenchymal stem cells, vitamin C may influence differentiation pathways, with some studies suggesting that AsA supports the redirection of osteosarcoma cells back toward an osteoblast lineage [112,113].

Using the SlipChip-based 3D culture environment, we evaluated osteosarcoma cell growth under AsA stimulation, leveraging time-lapse microscopy to analyze cellular changes in real time. The PDMS SlipChip offered precise control over the cellular microenvironment, enabling us to monitor AsA-induced effects such as morphological alterations, reductions in cell density, and loss

of viability. These findings were further validated using live/dead cell assays and compared to two-dimensional (2D) tissue culture dishes, where one served as the control and the other was exposed to AsA.

The results clearly indicated that AsA treatment induced cytotoxic effects, reduced cell proliferation, and triggered apoptotic responses in the osteosarcoma cells. Compared to the control, AsA-treated cultures displayed significant changes in cell morphology and viability, supporting the notion that vitamin C may be an effective agent in attenuating the aggressive characteristics of osteosarcoma cells. The SlipChip platform, by mimicking in vivo-like 3D conditions, provided more realistic insights into tumor behavior than traditional 2D models.

In conclusion, this study presents a novel application of microfluidic SlipChip technology for analyzing the effects of vitamin C on osteosarcoma cells. The findings highlight the potential of AsA to suppress abnormal cell growth and promote apoptosis, offering a promising direction for future therapeutic strategies. Further research incorporating variable drug concentrations, co-culture systems, and metastatic models will provide deeper insights into combating the recurrence and resistance often associated with osteosarcoma [30], [113].

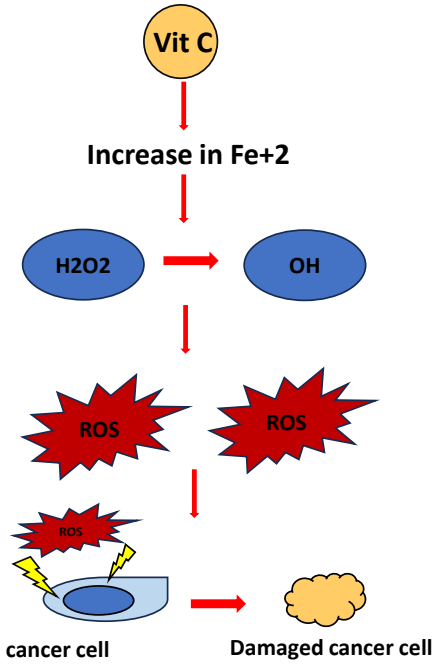

Figure 30 Schematic of death induced by vitamin C in cancer cells.

5.2 Materials and Experimental Methods

5.2.1 Methodology

As shown in Figure 31(a), a comparative evaluation was conducted between a conventional two-dimensional (2D) cell culture method using a standard polystyrene tissue culture dish and a three-dimensional (3D) culture method developed using a custom-designed SlipChip. The 3D configuration aimed to more accurately mimic the in vivo tumor microenvironment by enabling spatially relevant cell-cell and cell-matrix interactions. The design and structure of the SlipChip, illustrated in Figure 31(b), consisted of two aligned polydimethylsiloxane (PDMS) layers—top and bottom—each containing wells. When assembled, the wells from both layers were aligned to form enclosed 3D micro-compartments capable of supporting cell growth in three dimensions.

To ensure a tight seal and prevent medium leakage, the edges of the SlipChip were coated with a high-viscosity PDMS elastomer base (4000 centi-stokes) following assembly. This sealing method provided structural stability and maintained the sterility and integrity of the cell culture environment throughout the experimental period. The assembled SlipChip offered a confined and gas-permeable microenvironment suitable for observing cell behavior under different treatment conditions.

Cell culture experiments were carried out in the SlipChip compartments under two distinct conditions—with and without the addition of ascorbic acid (AsA). This allowed for the direct assessment of the effects of both the 3D culture environment and ascorbic acid treatment on osteosarcoma cell proliferation. Ascorbic acid was selected due to its reported cytotoxic and anti-proliferative effects on malignant cells, particularly in the context of bone-related cancers.

The resulting observations provided insight into how the spatial environment and biochemical stimuli interact to influence osteosarcoma cell behavior. Differences in cell morphology, proliferation rate, and viability between the standard 2D culture and SlipChip-based 3D culture systems were used to evaluate the effectiveness of this platform for studying cancer cell dynamics in vitro.

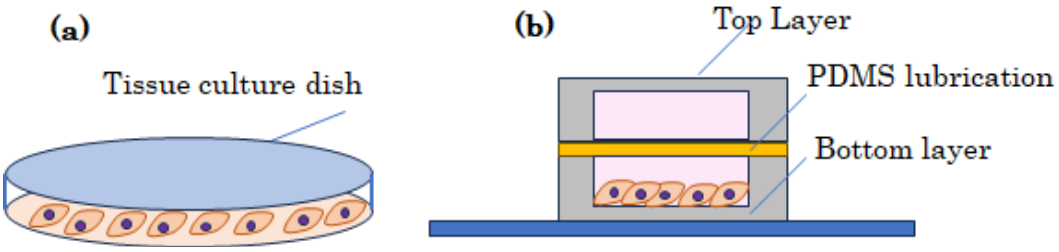

Figure 31 Cell culture in two different conditions. (a) A tissue culture dish. (b) A PDMS SlipChip.

5.2.2 Fabrication of SlipChip

The SlipChip platform was designed with identical chamber geometries in both the top and bottom PDMS layers. Each chamber measured 10 mm in length and width, with a depth of 0.2 mm. The top layer was equipped with microchannels functioning as fluid inlets and outlets. When the two layers were properly aligned, with one chamber oriented directly over the other, a sealed three-dimensional (3D) compartment was formed. This 3D configuration is particularly advantageous for creating controlled microenvironments suitable for various biological and chemical applications, including cell culture.

The fabrication process began with the creation of a master mold using 3D printing technology. This method allowed for rapid prototyping and precise structural definition of the SlipChip features. After printing, the mold was treated with a salinization process to reduce surface adhesion and facilitate easy demolding. PDMS (polydimethylsiloxane) was then poured over the mold and cured using standard soft lithography techniques, yielding highly accurate PDMS replicas of the designed microstructures.

PDMS was selected as the material of choice due to its favorable properties, particularly for biological applications. It is biocompatible, optically transparent, and porous, allowing gases such as oxygen and carbon dioxide to diffuse freely through its matrix. This gas permeability is crucial for maintaining healthy cell cultures, as it supports cellular respiration and prevents hypoxic conditions in confined microenvironments. Additionally, PDMS provides a surface suitable for cell adhesion, contributing to better cell proliferation and viability during culture processes [114].

In summary, the PDMS-based SlipChip with aligned 3D compartments offers a robust and biologically supportive platform for in vitro studies. Its design and material properties make it

well-suited for advanced microfluidic applications, including drug testing, tissue modeling, and cancer research.

5.2.3 Cell Culture Experiment

The human osteosarcoma cell line, SAOS-2, was obtained from Tohoku University in Sendai, Japan, for use in this study. These cells are commonly used as an in vitro model for bone cancer research due to their stable growth characteristics and relevance to human osteogenic tumors. The cells were cultured in Dulbecco's Modified Eagle Medium (DMEM), which was supplemented with 100 U/mL penicillin and 100 μg/mL streptomycin (Gibco, Thermo Fisher Scientific Co. Ltd.) to prevent bacterial contamination, along with 10% fetal bovine serum (FBS; COSMO BIO) to provide essential nutrients and growth factors. Cultures were maintained in a humidified incubator at 37°C with 5% CO_2 to replicate physiological conditions conducive to optimal cell growth.

For the experimental setup, the SAOS-2 cells were resuspended in culture medium and adjusted to a uniform density of 100 cells/μL. This standardized density ensured consistency across all platforms and enabled a fair comparison of cell proliferation under different conditions. The cell suspension was introduced into three separate culture environments: a PDMS-based SlipChip and two conventional polystyrene tissue culture dishes. Maintaining identical initial seeding densities across the three platforms allowed for the evaluation of how the different culture environments influenced cell adhesion, proliferation, and response to treatment.

Following cell seeding, the devices were incubated for 24 hours to allow the cells to adhere to the surfaces and establish baseline attachment prior to treatment. Ascorbic acid (AsA), a known cytotoxic compound with potential pro-apoptotic effects on various cancer cells, was prepared at a concentration of 2000μM in PBS. A volume of 100 μL of the prepared AsA solution was added to the SlipChip and to one of the tissue culture dishes. The remaining dish, which received no AsA treatment, served as the untreated control group. This setup allowed for direct comparison of cellular responses to AsA in both the SlipChip and traditional culture formats.

5.2.4 Cell Observation

Cell health, cell number, and viability were characterized. Live and Dead Cell Assay was performed using Calcein-AM (DOJINDO Co. Ltd) and PI (DOJINDO Co. Ltd) staining. Calcein-AM and PI solutions were made by diluting 15 μL of each of the chemicals in 135 μL of PBS

(Gibco, Thermo fisher Scientist Co. Ltd)). 10 μL of each of the solution was used for staining purposes. Images were obtained with a time-lapse inverted microscope (NIKON, ECLIPSE Ti-E Tokyo Japan).

5.3 Results and Discussion

5.3.1 Cell Health in SlipChip

Cells were observed after 24 hours of cell adhesion (Figure 32). Figures 32 (a) and (c) indicate cell morphologies of osteosarcoma cells before adding AsA in a SlipChip and a control tissue culture dish. Figures 32(b) and (d) show cells after 24 hours of insertion of AsA. Cell health in a SlipChip was better than that in a tissue culture dish. Cells in SlipChip were more elongated and flat and seemed to have a larger surface area. Cells in the tissue culture dish were also elongated, but the spread area at the cellular level was less than the cells in SlipChip. According to Figure 32, a total of 95 cells were found in SlipChip. 74 and 23 cells were present in the control dish and tissue culture dish with AsA. As shown in Figure 33, based on the total number of cells and total volume of cell culture under analysis, the percentage of cell proliferation was obtained. Cell proliferation data indicate that the highest cell proliferation was obtained in SlipChip before subjecting it to AsA.

This can be associated with the PDMS material properties. PDMS, being a porous and biocompatible material, allows the cells to breathe effectively, which contributes to good cell health [114]. In addition, a tissue culture dish allows 2-D cell culture, whereas PDMS-based SlipChip allows us to have a 3-D compartment. PDMS-based 3-D compartment allows the cells to adhere in multiple directions; this configuration increases cell-to-cell contact. These interactions increase cell regulatory pathways [115]. Growth factor protein signaling in the form of cytokines is enhanced, which enhances cell proliferation and differentiation [116].

Figures 32 (b) and (d) indicate the cell morphologies after subjecting the SlipChip and tissue culture device to AsA for 24 hours. Both images indicate rounded and thinner morphologies. From the shapes, it seems like the cells were busted. This type of morphology depicts cell death. This indicates that ascorbic acid is cytotoxic for osteosarcoma cells and has triggered apoptotic cell death [30].

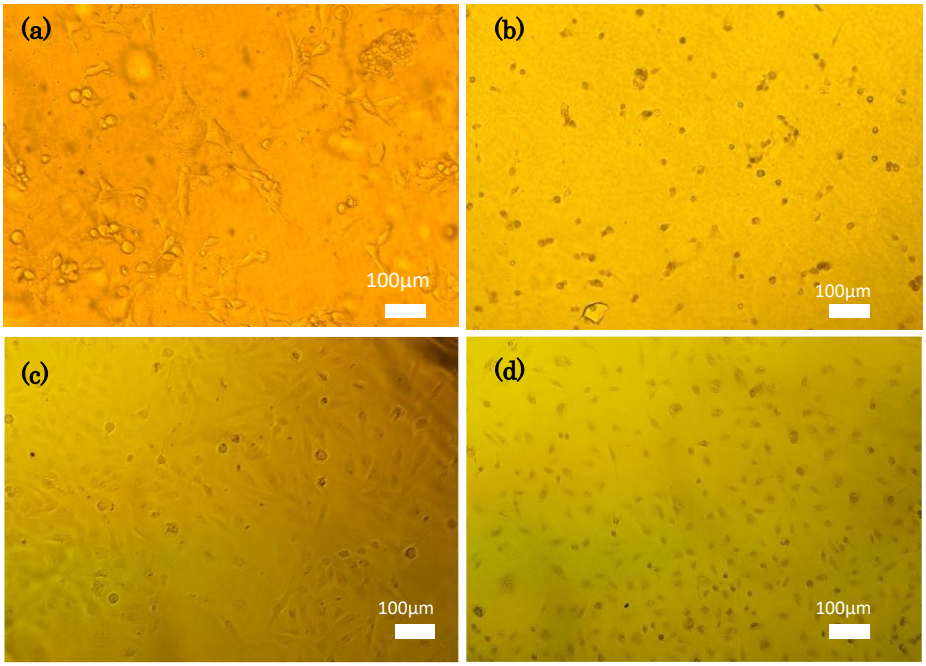

Figure 32 Cell culture in SlipChip (a) before and (b) after adding AsA. Cell culture in a tissue culture dish (c) without and (d) with AsA.

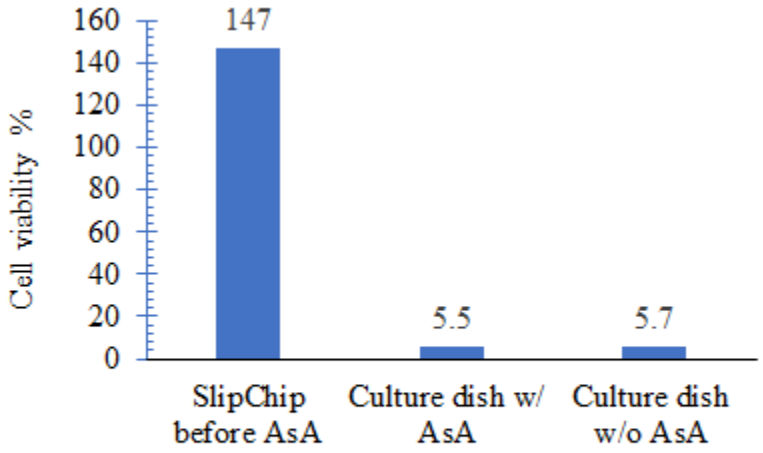

Figure 33 Comparison of cell viability in SlipChip and a cell culture dish with and without ascorbic acid.

5.3.2 Live and Dead Cell Assay

Figure 34 shows live and dead cell assays for the control dish and tissue culture dish with AsA and A SlipChip. Figures 34(a), (c), and (e) indicate live cell assay and high fluorescence for the control dish and zero fluorescence for the tissue culture dish, and SlipChip with ascorbic acid. It shows 73 live cells for the control dish, whereas no live cells were found for the SlipChip and

culture dish subjected to ascorbic acid. On the other hand, Figures 34 (b), (d), and (f) show PI-stained images indicating only one dead cell in the control dish and 95 and 23 dead cells in the SlipChip and culture dish subjected to AsA, respectively.

Figures 35 indicate the percentage of live and dead cells in each respective case. The percentage of live and dead cells was obtained by counting the number of cells in each case and dividing it by the total number of cells obtained from bright-field images. Figure 35 indicates 100% live cells in the control dish, whereas no live cells in the SlipChip and cell culture dish with AsA. Figure 35 indicates 100% cell death in the SlipChip and cell culture dish with AsA, whereas just 1.4% cell death in the control dish. This again indicates that AsA was cytotoxic for osteosarcoma cells.

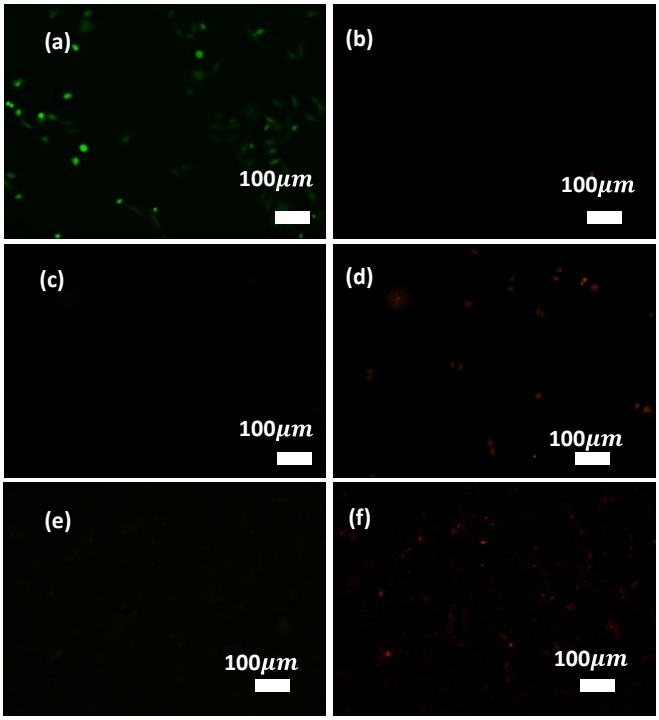

Figure 34 Fluorescent images of cells. (a) Calcein-AM stained cells in control dish. (b) PI stained cells in control dish. (c) Calcein-AM stained culture dish with AsA. (d) PI stained cells in culture dish with AsA. (e) Calcein-AM stained cells in SlipChip. (f) PI stained cells in SlipChip.

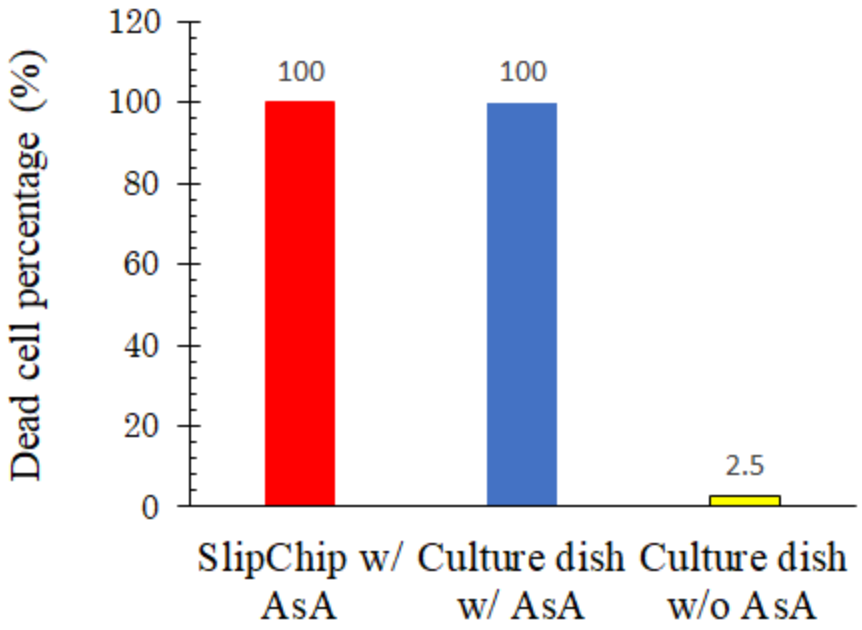

Figure 35 Percentage of dead cells in SlipChip with ascorbic acid and a cell culture dish.

5.4 Conclusions

Based on experimental observations, this study concludes that polydimethylsiloxane (PDMS)-based three-dimensional (3D) compartmentalized culture systems integrated into a SlipChip platform provide a significantly more favorable environment for osteosarcoma cell culture compared to traditional two-dimensional (2D) polystyrene tissue culture dishes. The use of PDMS for fabricating 3D microenvironments allows for the recreation of key aspects of the tumor microenvironment, offering structural and biochemical cues that more closely mimic in vivo conditions. As a result, osteosarcoma cells cultured in these 3D PDMS compartments exhibited improved cell health, increased proliferation rates, and enhanced cell-to-cell interactions, all of which are often compromised in flat, rigid 2D culture systems.

One of the major advantages of PDMS as a biomaterial lies in its gas-permeable nature, which facilitates efficient oxygen and carbon dioxide exchange—critical factors for maintaining cell viability over extended periods. Additionally, PDMS is biocompatible, optically transparent for imaging, and amenable to low-cost, reproducible fabrication techniques such as soft lithography. These properties collectively contribute to a more physiologically relevant and supportive environment for cancer cell culture. Microscopic analysis revealed that, under untreated

conditions, osteosarcoma cells adhered well to the PDMS surface, maintained their morphology, and proliferated efficiently within the 3D compartments.

To evaluate the responsiveness of cells to external therapeutic agents, ascorbic acid (AsA) was introduced into the system. AsA is known to exert cytotoxic effects on cancer cells, potentially through oxidative stress or apoptosis induction. In our experiments, cells treated with AsA displayed distinct morphological signs of apoptotic cell death, including cell shrinkage, detachment from the substrate, membrane disintegration, and overall structural collapse. These observations were further validated by live/dead fluorescence assays, which confirmed significantly higher levels of cell death in the AsA-treated groups compared to controls.

Interestingly, although PDMS-based compartments enhanced overall cell viability and growth under normal conditions, they did not provide any protective advantage against AsA-induced cytotoxicity. This finding suggests that while PDMS offers a superior culture environment, it does not interfere with the cells' intrinsic biological responses to external stimuli. In other words, the PDMS platform supports natural cellular behavior without artificially altering the effects of treatment compounds, making it an ideal medium for accurate drug screening and apoptosis studies.

The implications of these results are significant. First, they demonstrate that PDMS-based 3D culture systems are not only safe and supportive for cell proliferation but also maintain cellular integrity and functional responsiveness, which are essential for therapeutic assessment. Second, the reproducibility and adaptability of the SlipChip format allow for scalable and high-throughput experimentation, ideal for applications in drug discovery and cancer research.

In summary, the PDMS-based 3D culture platform offers clear advantages over conventional 2D systems by better replicating the tumor microenvironment, enhancing baseline cell behavior, and faithfully capturing drug response dynamics. These findings reinforce the utility of PDMS microenvironments for advanced in vitro cancer modeling, particularly for studies focused on therapeutic screening, apoptosis mechanisms, and drug resistance profiling.

While this chapter demonstrates successful 3D cell culture and drug response evaluation using ascorbic acid, the gradient generation capabilities developed in Chapters 3-4 were not utilized here. This represents a proof-of-concept for future MEC studies where the optimized WR=5 SlipChip design will enable systematic concentration gradient evaluation of clinical therapeutics like doxorubicin.

Chapter 6 Conclusions

6.1 Conclusions and Discussions

This doctoral research addresses the fundamental absence of integrated systems combining osteosarcoma microenvironment reproduction with systematic drug evaluation capabilities. Through systematic technical development across five interconnected chapters, we have created the first platform capable of:

1. Reproducing physiologically relevant tumor conditions (Chapter 2: hypoxic microenvironment simulation)
2. Ensuring reliable gradient generation sealing/lubrication optimization (Chapter 3: low-viscosity silicone oils, curing conditions).
3. Supporting diverse therapeutic modalities (biocompatible conditions for molecules ranging from 500 Da to >150 kDa)
4. Successful alignment optimization (magnetic aligner) and bubble minimization (WR=5). (Chapter 4: magnetic alignment, width ratios)
5. Enabling 3D culture validation (Chapter 5: proof-of-concept for drug response evaluation)

The integrated system overcomes the three primary technical barriers that have prevented practical implementation: device leakage, bubble formation, and misalignment. This represents the first solution capable of systematic MEC determination under tumor-relevant conditions.

We identified that the root cause of these issues lies in inadequate sealing between the PDMS layers, which leads to uneven pressure distribution and the trapping of air pockets between layers. These trapped air bubbles obstruct fluid flow, causing the medium to divert from the intended path, thereby resulting in leakage and inconsistent gradient formation. Such anomalies directly affect the quality of biological experiments, especially in studies involving cell viability, drug screening, and biochemical gradient applications.

To mitigate these issues, we explored various strategies to enhance the sealing and mechanical stability of the SlipChip. A key breakthrough came through the optimization of the curing process for the PDMS layers. We found that curing the bottom layer at 60 °C and the top layer at 80 °C strikes an ideal balance between achieving smooth slip action and ensuring sufficient

adhesion. This thermal strategy minimizes internal stresses while maintaining surface uniformity necessary for proper alignment.

Furthermore, we addressed lubrication challenges, which are critical for the sliding mechanism of SlipChip layers. Traditional lubrication methods often leave residual oil between layers, interfering with cell imaging and biochemical interaction studies. To overcome this, we implemented a spin coating technique using low-viscosity silicone oils at higher RPMs, enabling even distribution and reducing oil residue. In addition, we introduced a novel oil absorption method by leveraging the porous nature of PDMS. By soaking PDMS layers in silicone oil and subsequently cleaning the contact surfaces, we ensured that no free oil remained between layers during operation, thus preserving both functionality and biocompatibility.

We also enhanced the mechanical integrity and precision of the SlipChip using a magnetic sealing system integrated with a 3D-printed stage and micro gauges. This assembly allowed for tight sealing and accurate microwell alignment, crucial for reliable gradient generation and repeatability in assays.

After resolving sealing and mechanical concerns, we evaluated the device's biocompatibility. Due to PDMS's porous and inert properties, the device supports the creation of diverse microenvironments, such as hypoxic conditions mimicking tumor biology. It also provides a suitable substrate for mammalian cell culture. As a proof of concept, we studied the effects of ascorbic acid on SAOS-2 osteosarcoma cells and found that the PDMS-based 3D encapsulated compartments facilitated healthy cell viability and accurate biochemical assessments. We created the first integrated platform combining osteosarcoma microenvironment reproduction with systematic drug evaluation, enabling personalized therapy development through reliable MEC determination.

6.2 Future Work

Immediate future work will focus on applying the optimized integrated system for doxorubicin MEC determination using:

- WR=5 SlipChip configuration (established in Chapter 4)
- Hypoxic culture conditions (validated in Chapter 2)
- 50 cSt oil lubrication system (optimized in Chapter 3)

- Magnetic alignment system (developed in Chapter 4)

This represents the culmination of our technical development into practical clinical application for personalized osteosarcoma therapy. Advancements in the simultaneous generation of multiple gradient concentrations and the cultivation of healthy cells within a leak-free, bubble-free PDMS-based SlipChip at the microscale will support the optimization of the minimum effective dose of chemotherapeutic drugs, paving the way for future clinical studies and applications.

References

1. Hacker K. The Burden of Chronic Disease. *Mayo Clin Proc Innov Qual Outcomes*. 2024;8(1):112-119. doi:10.1016/j.mayocpiqo.2023.08.005

2. Moukengue B, Lallier M, Marchandet L, et al. Origin and Therapies of Osteosarcoma. *Cancers*. 2022;14(14):3503. doi:10.3390/cancers14143503

3. Czarnecka AM, Synoradzki K, Firlej W, et al. Molecular Biology of Osteosarcoma. *Cancers*. 2020;12(8):2130. doi:10.3390/cancers12082130

4. Espejo Valle-Inclan J, De Noon S, Trevers K, et al. Ongoing chromothripsis underpins osteosarcoma genome complexity and clonal evolution. *Cell*. 2025;188(2):352-370.e22. doi:10.1016/j.cell.2024.12.005

5. Pilavaki P, Gahanbani Ardakani A, Gikas P, Constantinidou A. Osteosarcoma: Current Concepts and Evolutions in Management Principles. *J Clin Med*. 2023;12(8):2785. doi:10.3390/jcm12082785

6. Mirabello L, Troisi RJ, Savage SA. International osteosarcoma incidence patterns in children and adolescents, middle ages and elderly persons. *Int J Cancer*. 2009;125(1):229-234. doi:10.1002/ijc.24320

7. Mehrvar A, Mehrvar N, Sadeghi Y, Tashvighi M. Outcomes and survival rates of childhood osteosarcoma in Iran, A report from MAHAK Pediatric Cancer Treatment and Research Center, from 2007 to 2020. *J Cancer Res Ther*. 2023;19(Suppl 1):S272-S277. doi:10.4103/jcrt.JCRT_1559_20

8. Tsimberidou AM, Fountzilas E, Nikanjam M, Kurzrock R. Review of precision cancer medicine: Evolution of the treatment paradigm. *Cancer Treat Rev*. 2020;86:102019. doi:10.1016/j.ctrv.2020.102019

9. Haslem DS, Van Norman SB, Fulde G, et al. A Retrospective Analysis of Precision Medicine Outcomes in Patients With Advanced Cancer Reveals Improved Progression-Free Survival Without Increased Health Care Costs. *J Oncol Pract*. 2017;13(2):e108-e119. doi:10.1200/JOP.2016.011486

10. Kästner A, Kron A, Van Den Berg N, et al. Evaluation of the effectiveness of a nationwide precision medicine program for patients with advanced non-small cell lung cancer in Germany: a historical cohort analysis. *Lancet Reg Health - Eur*. 2024;36:100788. doi:10.1016/j.lanepe.2023.100788

11. Acanda De La Rocha AM, Berlow NE, Fader M, et al. Feasibility of functional precision medicine for guiding treatment of relapsed or refractory pediatric cancers. *Nat Med*. 2024;30(4):990-1000. doi:10.1038/s41591-024-02848-4

12. Mark D, Haeberle S, Roth G, Von Stetten F, Zengerle R. Microfluidic lab-on-a-chip platforms: requirements, characteristics and applications. *Chem Soc Rev*. 2010;39(3):1153. doi:10.1039/b820557b

13. Zheng X, Wojcik R, Zhang X, et al. Coupling Front-End Separations, Ion Mobility Spectrometry, and Mass Spectrometry For Enhanced Multidimensional Biological and Environmental Analyses. *Annu Rev Anal Chem*. 2017;10(1):71-92. doi:10.1146/annurev-anchem-061516-045212

14. Sia SK, Whitesides GM. Microfluidic devices fabricated in Poly(dimethylsiloxane) for biological studies. *ELECTROPHORESIS*. 2003;24(21):3563-3576. doi:10.1002/elps.200305584

15. Faudzi, Sabzehmeidani, Suzumori. Application of Micro-Electro-Mechanical Systems (MEMS) as Sensors: A Review. *J Robot Mechatron*. 2020;32(2):281-288. doi:10.20965/jrm.2020.p0281

16. Gharib G, Bütün İ, Muganlı Z, et al. Biomedical Applications of Microfluidic Devices: A Review. *Biosensors*. 2022;12(11):1023. doi:10.3390/bios12111023

17. Narayanamurthy V, Jeroish ZE, Bhuvaneshwari KS, et al. Advances in passively driven microfluidics and lab-on-chip devices: a comprehensive literature review and patent analysis. *RSC Adv*. 2020;10(20):11652-11680. doi:10.1039/D0RA00263A

18. Ebrahimi A, Icoz K, Didarian R, et al. Molecular Separation by Using Active and Passive Microfluidic chip Designs: A Comprehensive Review. *Adv Mater Interfaces*. 2024;11(2):2300492. doi:10.1002/admi.202300492

19. Natsuhara D, Kiba Y, Saito R, et al. A sequential liquid dispensing method in a centrifugal microfluidic device operating at a constant rotational speed for the multiplexed genetic detection of foodborne pathogens. *RSC Adv*. 2024;14(31):22606-22617. doi:10.1039/D4RA04055D

20. Senel M, Dervisevic E, Sammy A, et al. Microfluidic Electrochemical Sensor for Cerebrospinal Fluid and Blood Dopamine Detection in a Mouse Model of Parkinson's Disease. *Anal Chem*. 2020;92(18):12347-12355. doi:10.1021/acs.analchem.0c02032.

21. Du W, Li L, Nichols KP, Ismagilov RF. SlipChip. *Lab Chip*. 2009;9(16):2286. doi:10.1039/b908978k

22. Yu Z, Lyu W, Yu M, et al. Self-partitioning SlipChip for slip-induced droplet formation and human papillomavirus viral load quantification with digital LAMP. *Biosens Bioelectron*. 2020;155:112107. doi:10.1016/j.bios.2020.112107

23. Inaam R, Bolontrade MF, Okamoto S, Shibata T, Santra TS, Nagai M. PDMS SlipChip: Optimizing Sealing, Slipping, and Biocompatibility Using Low-Viscosity Silicone Oils.

24. Shen C, Xu P, Huang Z, Cai D, Liu SJ, Du W. Bacterial chemotaxis on SlipChip. *Lab Chip*. 2014;14(16):3074-3080. doi:10.1039/C4LC00213J

25. Shen F, Du W, Kreutz JE, Fok A, Ismagilov RF. Digital PCR on a SlipChip. *Lab Chip*. 2010;10(20):2666-2672. doi:10.1039/C004521G

26. Cai G, Wu W, Feng S, Liu Y. Label-free *E. coli* detection based on enzyme assay and a microfluidic slipchip. *The Analyst*. 2021;146(14):4622-4629. doi:10.1039/D1AN00495F

27. Emami Nejad A, Najafgholian S, Rostami A, et al. The role of hypoxia in the tumor microenvironment and development of cancer stem cell: a novel approach to developing treatment. *Cancer Cell Int*. 2021;21(1):62. doi:10.1186/s12935-020-01719-5

28. Álvarez MV, Gutiérrez LM, Auzmendi J, Correa A, Lazarowski A, Bolontrade MF. Acquisition of stem associated-features on metastatic osteosarcoma cells and their functional effects on mesenchymal stem cells. *Biochim Biophys Acta BBA - Gen Subj*. 2020;1864(4):129522. doi:10.1016/j.bbagen.2020.129522

29. Gutiérrez LM, Valenzuela Alvarez M, Yang Y, et al. Up-regulation of pro-angiogenic molecules and events does not relate with an angiogenic switch in metastatic osteosarcoma cells but to cell survival features. *Apoptosis*. 2021;26(7-8):447-459. doi:10.1007/s10495-021-01677-x

30. Valenti MT, Zanatta M, Donatelli L, et al. Ascorbic Acid Induces either Differentiation or Apoptosis in MG-63 Osteosarcoma Lineage. *ANTICANCER Res*. Published online 2014.

31. Liao C, Liu X, Zhang C, Zhang Q. Tumor hypoxia: From basic knowledge to therapeutic implications. *Semin Cancer Biol*. 2023;88:172-186. doi:10.1016/j.semcancer.2022.12.011

32. Shahpouri M, Adili-Aghdam MA, Mahmudi H, et al. Prospects for hypoxia-based drug delivery platforms for the elimination of advanced metastatic tumors: From 3D modeling to clinical concepts. *J Controlled Release*. 2023;353:1002-1022. doi:10.1016/j.jconrel.2022.12.009

33. Uchida H, Sato A, Miyayama A, Tsukada K. Generation of an Oxygen Gradient in a Microfluidic Device and Cellular Analysis in Hypoxia. *Adv Biomed Eng*. 2013;2(0):143-149. doi:10.14326/abe.2.143

34. Zhou Zhao R, Jiang S, Yu Ru N, Jiao B, Zhi-Bin Y. Comparison of hypoxic effects induced by chemical and physical hypoxia on cardiomyocytes. *Can J Physiol Pharmacol*. 2019;97(10):980-988. doi:10.1139/cjpp-2019-0092

35. Kaida A, Miura M. Differential dependence on oxygen tension during the maturation process between monomeric Kusabira Orange 2 and monomeric Azami Green expressed in HeLa cells. *Biochem Biophys Res Commun*. 2012;421(4):855-859. doi:10.1016/j.bbrc.2012.04.102

36. Lochovsky C. Trapping and Removal of Bubbles in a Microfluidic Format.

37. Wang Y, Lee D, Zhang L, et al. Systematic prevention of bubble formation and accumulation for long-term culture of pancreatic islet cells in microfluidic device. *Biomed Microdevices*. 2012;14(2):419-426. doi:10.1007/s10544-011-9618-3

38. Xu J, Vaillant R, Attinger D. Use of a porous membrane for gas bubble removal in microfluidic channels: physical mechanisms and design criteria. *Microfluid Nanofluidics*. 2010;9(4-5):765-772. doi:10.1007/s10404-010-0592-5

39. Sapoval B, Filoche M, Weibel ER. Smaller is better—but not too small: A physical scale for the design of the mammalian pulmonary acinus. *Proc Natl Acad Sci*. 2002;99(16):10411-10416. doi:10.1073/pnas.122352499

40. Nagai M, Kato K, Soga S, Santra TS, Shibata T. Scalable Parallel Manipulation of Single Cells Using Micronozzle Array Integrated with Bidirectional Electrokinetic Pumps. *Micromachines*. 2020;11(4):442. doi:10.3390/mi11040442

41. Qin D, Xia Y, Whitesides GM. Soft lithography for micro- and nanoscale patterning. *Nat Protoc*. 2010;5(3):491-502. doi:10.1038/nprot.2009.234

42. Sadeghi S, Elitas M. A simple, bubble-free cell loading technique for culturing mammalian cells on lab-on-a-chip devices. *Chips Tips*. Published online 2017.

43. Wang R, Jin F, Zhong H. A novel experimental hypoxia chamber for cell culture.

44. Bortner CD, Cidlowski JA. Cell shrinkage and monovalent cation fluxes: role in apoptosis. *Arch Biochem Biophys*. 2007;462(2):176-188. doi:10.1016/j.abb.2007.01.020

45. Ziegler U, Groscurth P. Morphological Features of Cell Death. *Physiology*. 2004;19(3):124-128. doi:10.1152/nips.01519.2004

46. Akman M, Belisario DC, Salaroglio IC, et al. Hypoxia, endoplasmic reticulum stress and chemoresistance: dangerous liaisons. *J Exp Clin Cancer Res*. 2021;40(1):28. doi:10.1186/s13046-020-01824-3

47. Xu L, Lee H, Jetta D, Oh KW. Vacuum-driven power-free microfluidics utilizing the gas solubility or permeability of polydimethylsiloxane (PDMS). *Lab Chip*. 2015;15(20):3962-3979. doi:10.1039/C5LC00716J

48. X R, H L, J.G Z, P.L.G C, W Y, M N. Porous Polydimethylsiloxane as a Gas-Liquid Interface for Microfluidic Applications. *J Microelectromechanical Syst*. 2017;26(1):120-126. doi:10.1109/JMEMS.2016.2618395

49. The effects of short-term hypoxia on human mesenchymal stem cell proliferation, viability and p16INK4A mRNA expression: Investigation using a simple hypoxic culture system with a deoxidizing agent. *J Stem Cells Regen Med*. 2015;11(1):25-31. doi:10.46582/jsrm.1101005

50. Raj M K, Chakraborty S. PDMS microfluidics: A mini review. *J Appl Polym Sci*. 2020;137(27):48958. doi:10.1002/app.48958

51. Yang Y, Chen Y, Tang H, Zong N, Jiang X. Microfluidics for Biomedical Analysis. *Small Methods*. 2020;4(4):1900451. doi:10.1002/smtd.201900451

52. Battat S, A. Weitz D, M Whitesides G. An outlook on microfluidics: the promise and the challenge. *Lab Chip*. 2022;22(3):530-536. doi:10.1039/D1LC00731A

53. Utharala R, Grab A, Vafaizadeh V, et al. A microfluidic Braille valve platform for on-demand production, combinatorial screening and sorting of chemically distinct droplets. *Nat Protoc*. 2022;17(12):2920-2965. doi:10.1038/s41596-022-00740-4

54. Melin J, Quake SR. Microfluidic Large-Scale Integration: The Evolution of Design Rules for Biological Automation. *Annu Rev Biophys*. 2007;36(Volume 36, 2007):213-231. doi:10.1146/annurev.biophys.36.040306.132646

55. Nagai M, Ryu S, Thorsen T, Matsudaira P, Fujita H. Chemical control of Vorticella bioactuator using microfluidics. *Lab Chip*. 2010;10(12):1574-1578. doi:10.1039/c003427d

56. Minghui T, Guanghui W, Siu-Kai K, Ho-Pui H. A Review of Biomedical Centrifugal Microfluidic Platforms. *Micromachines Basel*. 2016;7(2):26. doi:10.3390/mi7020026

57. Nishat S. Paper-based microfluidics: Simplified fabrication and assay methods. *Sens Actuators*. Published online 2021.

58. Liu W, Chen D, Du W, Nichols KP, Ismagilov RF. SlipChip for Immunoassays in Nanoliter Volumes. *Anal Chem*. 2010;82(8):3276-3282. doi:10.1021/ac100044c

59. Catterton MA, Dunn AF, Pompano RR. User-defined local stimulation of live tissue through a movable microfluidic port. *Lab Chip*. 2018;18(14):2003-2012. doi:10.1039/C8LC00204E

60. Li Y, Xuan J, Hu R, Zhang P, Lou X, Yang Y. Microfluidic triple-gradient generator for efficient screening of chemical space. *Talanta*. 2019;204:569-575. doi:10.1016/j.talanta.2019.06.018

61. Lyu W, Yu M, Qu H, Yu Z, Du W, Shen F. Slip-driven microfluidic devices for nucleic acid analysis. *Biomicrofluidics*. 2019;13(4):041502. doi:10.1063/1.5109270

62. Kangning R, Jianhua Z, Hongkai W. Materials for Microfluidic Chip Fabrication. *Acc Chem Res*. 2013;46(11):2396-2406.

63. Chang CW, Peng CC, Liao WH, Tung YC. Polydimethylsiloxane SlipChip for mammalian cell culture applications. *Analyst*. 2015;140(21):7355-7365. doi:10.1039/C5AN00547G

64. Miranda I, Souza A, Sousa P, et al. Properties and Applications of PDMS for Biomedical Engineering: A Review. *J Funct Biomater*. 2021;13(1):2. doi:10.3390/jfb13010002

65. Montazerian H, Mohamed MGA, Montazeri MM, et al. Permeability and mechanical properties of gradient porous PDMS scaffolds fabricated by 3D-printed sacrificial templates designed with minimal surfaces. *Acta Biomater*. 2019;96:149-160. doi:10.1016/j.actbio.2019.06.040

66. Siyuan W, Gaozhe C, Hong D, Wuzhen Q, Jianhan L. Automatic and multi-channel detection of bacteria on a slidable centrifugal disc based on FTA card nucleic acid extraction and recombinase aided amplification. *Lab Chip*. 2021;22:80-89. doi:DOI%09https://doi.org/10.1039/D1LC00915J

67. Yang J, Deng Y, Zhang M, et al. Construction and Manipulation of Serial Gradient Dilution Array on a Microfluidic Slipchip for Screening and Characterizing Inhibitors against Human Pancreatic Lipase. *Biosensors*. 2023;13(2):274. doi:10.3390/bios13020274

68. Konku-Asase Y, Yaya A, Kan-Dapaah K. Curing Temperature Effects on the Tensile Properties and Hardness of $\gamma -Fe_2 O_3$ Reinforced PDMS Nanocomposites. Bellucci S, ed. *Adv Mater Sci Eng*. 2020;2020(1):6562373. doi:10.1155/2020/6562373

69. Wang Z, Volinsky AA, Gallant ND. Crosslinking effect on polydimethylsiloxane elastic modulus measured by custom-built compression instrument. *J Appl Polym Sci*. 2014;131(22). doi:10.1002/app.41050

70. Drebezghova V, Hakil F, Grimaud R, Gojzewski H, Vancso GJ, Nardin C. Initial bacterial retention on polydimethylsiloxane of various stiffnesses: The relevance of modulus (mis)match. *Colloids Surf B Biointerfaces*. 2022;217:112709. doi:10.1016/j.colsurfb.2022.112709

71. Yu Y, Sanchez D, Lu N. Work of adhesion/separation between soft elastomers of different mixing ratios. *J Mater Res*. 2015;30(18):2702-2712. doi:10.1557/jmr.2015.242

72. Park M, Shin J, Lee S. Controlled Tensile Behavior of Pre-Cured PDMS via Advanced Bonding Techniques. *Polymers*. 2025;17(1):103. doi:10.3390/polym17010103

73. Yi Q, Cai D, Xiao M, et al. Direct antimicrobial susceptibility testing of bloodstream infection on SlipChip. *Biosens Bioelectron*. 2019;135:200-207. doi:10.1016/j.bios.2019.04.003

74. Shen C, Xu P, Huang Z, Cai D, Liu SJ, Du W. Bacterial chemotaxis on SlipChip. *Lab Chip*. 2014;14(16):3074-3080. doi:10.1039/C4LC00213J

75. Tsaloglou MN, Watson RJ, Rushworth CM, et al. Real-time microfluidic recombinase polymerase amplification for the toxin B gene of Clostridium difficile on a SlipChip platform. *Analyst*. 2014;140(1):258-264. doi:10.1039/C4AN01683A

76. Chang CW, Peng CC, Liao WH, Tung YC. Polydimethylsiloxane SlipChip for mammalian cell culture applications. *Analyst*. 2015;140(21):7355-7365. doi:10.1039/C5AN00547G

77. Xue L, Liao M, Jianhan L. An all-in-one microfluidic SlipChip for power-free and rapid biosensing of pathogenic bacteria. *Lab Chip*. 2024;24(17):4039-4049. doi:DOI%09https://doi.org/10.1039/D4LC00366G

78. Ionescu M, Winton B, Wexler D, et al. Enhanced biocompatibility of PDMS (polydimethylsiloxane) polymer films by ion irradiation. *Nucl Instrum Methods Phys Res Sect B Beam Interact Mater At*. 2012;273:161-163. doi:10.1016/j.nimb.2011.07.065

79. Zehentbauer FM, Moretto C, Stephen R, et al. Fluorescence spectroscopy of Rhodamine 6G: Concentration and solvent effects. *Spectrochim Acta A Mol Biomol Spectrosc*. 2014;121:147-151. doi:10.1016/j.saa.2013.10.062

80. Calissendorff J, Falhammar H. Lugol's solution and other iodide preparations: perspectives and research directions in Graves' disease. *Endocrine*. 2017;58(3):467-473. doi:10.1007/s12020-017-1461-8

81. Nagai M, Oohara K, Kato K, Kawashima T, Shibata T. Development and characterization of hollow microprobe array as a potential tool for versatile and massively parallel manipulation of single cells. *Biomed Microdevices*. 17(2). doi:10.1007/s10544-015-9943-z.

82. Vudayagiri S, Junker MD, Skov AL. Factors affecting the surface and release properties of thin polydimethylsiloxane films. *Polym J*. 2013;45(8):871-878. doi:10.1038/pj.2012.227

83. Laukemper R, Becker T, Jekle M. Surface Energy of Food Contact Materials and Its Relation to Wheat Dough Adhesion. *Food Bioprocess Technol*. 2021;14(6):1142-1154. doi:10.1007/s11947-021-02625-y

84. Panneer Selvam VK, Fukunaga T, Suzuki Y, et al. Single-Cell Screening through Cell Encapsulation in Photopolymerized Gelatin Methacryloyl. *Micro*. 2024;4(2):295-304. doi:10.3390/micro4020018

85. Inaam R, Bolontrade M, Okamoto S, Shibata T, Subhra Santra T, Nagai M. Hypoxic Culture of Osteosarcoma Cells in PDMS Microfluidic Chamber and Plastic Bag. *IEEJ Trans Sens Micromachines*. 2024;144(5):94-99. doi:10.1541/ieejsmas.144.94

86. Barca F, Caporossi T, Rizzo S. Silicone Oil: Different Physical Proprieties and Clinical Applications. *BioMed Res Int*. 2014;2014(1):502143. doi:10.1155/2014/502143

87. Yang CS, Chen KH, Hsu WM, Li YS. Cytotoxicity of silicone oil on cultivated human corneal endothelium. *Eye*. 2008;22(2):282-288. doi:10.1038/sj.eye.6702962

88. Li C, Humayun M, Walker GM, et al. Under-Oil Autonomously Regulated Oxygen Microenvironments: A Goldilocks Principle-Based Approach for Microscale Cell Culture. *Adv Sci*. 2022;9(10):2104510. doi:10.1002/advs.202104510

89. Abdul Halim MS, Dyson JM, Gong MM, O'Bryan MK, Nosrati R. Fallopian tube rheology regulates epithelial cell differentiation and function to enhance cilia formation and coordination. *Nat Commun*. 2024;15(1):7411. doi:10.1038/s41467-024-51481-9

90. Inaam R, Bolontrade M, Okamoto S, Shibata T, Subhra Santra T, Nagai M. Hypoxic Culture of Osteosarcoma Cells in PDMS Microfluidic Chamber and Plastic Bag. *IEEJ Trans Sens Micromachines*. 2024;144(5):94-99. doi:10.1541/ieejsmas.144.94

91. Chang CW, Peng CC, Liao WH, Tung YC. Polydimethylsiloxane SlipChip for mammalian cell culture applications. *The Analyst*. 2015;140(21):7355-7365. doi:10.1039/C5AN00547G

92. Xue L, Liao M, Lin J. An all-in-one microfluidic SlipChip for power-free and rapid biosensing of pathogenic bacteria. *Lab Chip*. 2024;24(17):4039-4049. doi:10.1039/D4LC00366G

93. Inaam R, Bolontrade MF, Okamoto S, Shibata T, Santra TS, Nagai M. PDMS SlipChip: Optimizing Sealing, Slipping, and Biocompatibility Using Low-Viscosity Silicone Oils. *Micromachines*. 2025;16(5):525. doi:10.3390/mi16050525

94. Pompano RR, Platt CE, Karymov MA, Ismagilov RF. Control of Initiation, Rate, and Routing of Spontaneous Capillary-Driven Flow of Liquid Droplets through Microfluidic Channels on SlipChip. *Langmuir*. 2012;28(3):1931-1941. doi:10.1021/la204399m

95. Yu M, Chen X, Qu H, et al. Multistep SlipChip for the Generation of Serial Dilution Nanoliter Arrays and Hepatitis B Viral Load Quantification by Digital Loop Mediated Isothermal Amplification. *Anal Chem*. 2019;91(14):8751-8755. doi:10.1021/acs.analchem.9b01270

96. Li X, Liu X, Yu Z, et al. Combinatorial screening SlipChip for rapid phenotypic antimicrobial susceptibility testing. *Lab Chip*. 2022;22(20):3952-3960. doi:10.1039/D2LC00661H

97. Liu X, Li X, Wu N, et al. Formation and Parallel Manipulation of Gradient Droplets on a Self-Partitioning SlipChip for Phenotypic Antimicrobial Susceptibility Testing. *ACS Sens*. 2022;7(7):1977-1984. doi:10.1021/acssensors.2c00734

98. Quirós-Solano WF, Gaio N, Stassen OMJA, et al. Microfabricated tuneable and transferable porous PDMS membranes for Organs-on-Chips. *Sci Rep*. 2018;8(1):13524. doi:10.1038/s41598-018-31912-6

99. Norfatriah A, Ahmad Syamaizar AS, Zuruzi AS. Application of Porous Polydimethylsiloxane (PDMS) in oil absorption. *IOP Conf Ser Mater Sci Eng*. 2018;342:012050. doi:10.1088/1757-899X/342/1/012050

100. Yu C, Yu C, Cui L, et al. Facile Preparation of the Porous PDMS Oil-Absorbent for Oil/Water Separation. *Adv Mater Interfaces*. 2017;4(3):1600862. doi:10.1002/admi.201600862

101. Ong CC, Sundera Murthe S, Mohamed NM, Perumal V, Mohamed Saheed MS. Nanoscaled Surface Modification of Poly(dimethylsiloxane) Using Carbon Nanotubes for Enhanced Oil and Organic Solvent Absorption. *ACS Omega*. 2018;3(11):15907-15915. doi:10.1021/acsomega.8b01566

102. Peng S che, Nagarkar SP, Lowen JL, Velankar SS. Circuit model for microfluidic bubble generation under controlled pressure. *Microfluid Nanofluidics*. 2013;15(6):797-805. doi:10.1007/s10404-013-1189-6

103. Thi Phan KK, Truong T, Wang Y, Bhandari B. Nanobubbles: Fundamental characteristics and applications in food processing. *Trends Food Sci Technol*. 2020;95:118-130. doi:10.1016/j.tifs.2019.11.019

104. Vega-Sánchez C, Chiara N. Pressure Drop Measurements in Microfluidic Devices: A Review on the Accurate Quantification of Interfacial Slip. *Adv Mater Interfaces*. 2022;9(5). doi:2101641

105. Rapoport NY, Efros AL, Christensen DA, Kennedy AM, Nam KH. Microbubble generation in phase-shift nanoemulsions used as anticancer drug carriers. *Bubble Sci Eng Technol*. 2009;1(1-2):31-39. doi:10.1179/175889709X446516

106. YONEMOTO Y, YANAGISAWA H, KAWARA Z, KUNUGI T. Coalescence of Microbubble. *The Japanese Society for Experimental Mechanics*. Preprint posted online 2008. doi:10.11395/jjsem.8.38

107. Wei X, Song S, Yu T, et al. In situ microbubble-mediated strategy for highly efficient anti-crude oil-fouling membrane with parallel nanosheet structure. *Sep Purif Technol*. 2025;357:130220. doi:10.1016/j.seppur.2024.130220

108. Picci P. Osteosarcoma (Osteogenic sarcoma). *Orphanet J Rare Dis*. 2007;2(1):6. doi:10.1186/1750-1172-2-6

109. Valenti MT, Zanatta M, Donatelli L, et al. Ascorbic Acid Induces either Differentiation or Apoptosis in MG-63 Osteosarcoma Lineage. *ANTICANCER Res*. Published online 2014.

110. Fernandes G, Barone AW, Dziak R. The effect of ascorbic acid on bone cancer cells *in vitro*. Winder S, ed. *Cogent Biol*. 2017;3(1):1288335. doi:10.1080/23312025.2017.1288335

111. Influence of Vitamin C on Lymphocytes: An Overview.

112. Nicolas J, Magli S, Rabbachin L, Sampaolesi S, Nicotra F, Russo L. 3D Extracellular Matrix Mimics: Fundamental Concepts and Role of Materials Chemistry to Influence Stem Cell Fate. *Biomacromolecules*. 2020;21(6):1968-1994. doi:10.1021/acs.biomac.0c00045

113. Torino S, Corrado B, Iodice M, Coppola G. PDMS-Based Microfluidic Devices for Cell Culture. *Inventions*. 2018;3(3):65. doi:10.3390/inventions3030065

114. Meyvantsson I, J Beebe D. Cell culture models in microfluidic systems. *Annu Rev Anal Chem*. 2008;1:423-449. doi:10.1146/annurev.anchem.1.031207.113042

115. Cardoso BD, Castanheira EMS, Lanceros-Méndez S, Cardoso VF. Recent Advances on Cell Culture Platforms for In Vitro Drug Screening and Cell Therapies: From Conventional to Microfluidic Strategies. *Adv Healthc Mater*. 2023;12(18):2202936. doi:10.1002/adhm.202202936

116. Edmondson R, Jenkins Broglie J, F. Adcock A, Yang L. Three-Dimensional Cell Culture Systems and Their Applications in Drug Discovery and Cell-Based Biosensors. *ASSAY Drug Dev Technol*. 2014;12(4). doi:https://doi.org/10.1089/adt.2014.573

Publication List

List of Papers with Referee's Review

1 Inaam, R., Bolontrade, M., Okamoto, S., Shibata, T., Santra, T. S., & Nagai, M. (2024). "Hypoxic Culture of Osteosarcoma Cells in PDMS Microfluidic Chamber and Plastic Bag," IEEJ Transactions on Sensors and Micromachines, 144(5), pp. 94-99, https://doi.org/10.1541/ieejsmas.144.94.

2 Inaam, R., Bolontrade, M. F., Okamoto, S., Shibata, T., Santra, T. S., & Nagai, M. (2025). PDMS SlipChip: Optimizing Sealing, Slipping, and Biocompatibility Using Low-Viscosity Silicone Oils. *Micromachines*, *16*(5), 525, pp. 1-16, https:// 10.3390/mi16050525.

List of Papers at International Conference with Referee's Review

1 Inaam, R., Bolontrade, M., Okamoto, S., Shibata, T., & Nagai, M. (2024). Tuning Cross-Linking Conditions of PDMS for Leak-Free Slip Action in SlipChip. *The Proceedings of ICPE2024: The 20th International Conference on Precision Engineering, 23-27 October 2024*, *held by* Tohoku University (Aoba Yama Campus), Sendai, Japan *(Oral Presentation, published).*

2 Inaam, R., Nagabooshanam S., Okamoto, S., Shibata, T., & Nagai, M. (2024). Gradient Generation in Ellipsoidal Microwells with PDMS-based SlipChip for Chemical and Pharmaceutical Applications. *ICAM 2024: JSME 8th International Conference of Automation and Mechatronics, 06-08 November 2024, held by* Kyushu University, Kita-Kyushu, Japan, *(Oral Presentation).*